DOKUZ EYLÜL UNIVERSITY
GRADUATE SCHOOL OF NATURAL AND APPLIED SCIENCES

PRODUCTION AND DEVELOPMENT OF PHOTOCURABLE RESIN USED IN 3D PRINTING FOR DENTAL APPLICATIONS

by
Berk ÖZLER

January, 2023
İZMİR

PRODUCTION AND DEVELOPMENT OF PHOTOCURABLE RESIN USED IN 3D PRINTING FOR DENTAL APPLICATIONS

A Thesis Submitted to the
Graduate School of Natural and Applied Sciences of Dokuz Eylül University
In Partial Fulfillment of the Requirements for the Master's Degree in
Metallurgical and Materials Engineering

by
Berk ÖZLER

January, 2023
İZMİR

M.Sc. THESIS EXAMINATION RESULT FORM

We have read the thesis entitled **"PRODUCTION AND DEVELOPMENT OF PHOTOCURABLE RESIN USED IN 3D PRINTING FOR DENTAL APPLICATIONS"** completed by **BERK ÖZLER** under supervision of **ASSOC. PROF. DR. SERDAR YILDIRIM** and we certify that in our opinion it is fully adequate, in scope and in quality, as a thesis for the degree of Master of Science.

Assoc. Prof. Dr. Serdar YILDIRIM

Supervisor

Assoc. Prof. Dr. Hüsnügül YILMAZ ATAY	Assoc. Prof. Dr. Metin YURDDAŞKAL
Jury Member	Jury Member

Prof. Dr. Okan FISTIKOĞLU

Director

Graduate School of Natural and Applied Sciences

ACKNOWLEDGEMENTS

I would like to thank everyone for their sincere support on this stressful but enjoyable journey that I have embarked on to obtain my master's degree.

Firstly, I would like to tell my interior appreciation to my advisor, Assoc. Prof. Dr. Serdar YILDIRIM, for his constructive ideas, supervision, support, understanding, contributions, and encouragement during my thesis. I would also like to thank my committee members, Assoc. Prof. Dr. Metin YURDDAŞKAL and Assoc. Prof. Dr. Hüsnügül YILMAZ ATAY for reviewing my thesis and offering precious suggestions and sharing their visions.

I would like to present my special thanks to Dokuz Eylül University, Center of Electronic Materials Production and Application (EMUM) and its staff for the resources they enable for me. Also, I would like to thank Assoc. Prof. Dr. Mustafa EROL for their precious help and support. I would also like to thank NanoRes Co. for their material supply and analysis support.

I would like to express my gratitude to Dokuz Eylül University Scientific Research Projects Coordination Unit (DEU-BAP) for the support and opportunities they provided to my master's thesis, which was carried out within the scope of the project named "Production and development of photocurable nanocomposite resins used in 3D printers for dental applications" with the code of 2021.KB.FEN.046. I also give my thanks to The Scientific and Technological Research Council of Turkey TUBITAK-BIDEB for the student scholarship support they provided within the scope of the "2210-C Domestic Postgraduate Scholarship Program for Priority Areas" with the application number 1649B022100444.

Also, I give my thanks Erdem Tevfik ÖZDEMİR for his encouragement and emotional support during this process. I would also like to thank Helin DEMİR for her moral and emotional support, and patience during my graduate period.

Finally, and most importantly, my family's support and belief in me has always motivated me. My mother Hatice Nursun ÖZLER and my father Nevzat ÖZLER deserve the greatest thanks for their love and support, as they are always by my side.

Berk ÖZLER

PRODUCTION AND DEVELOPMENT OF PHOTOCURABLE RESIN USED IN 3D PRINTING FOR DENTAL APPLICATIONS

ABSTRACT

Photochemical 3D printers, one of the additive manufacturing methods, polymerize photo-crosslinkable resin with UV-light to fabricate well-detailed dental models without using molds. These resin contain monomers, oligomers, photoinitiators, preferably nanoparticles and color pigments. With the addition of titania nanoparticles, nanocomposite polymers may have high conversion degree and mechanical properties. However, nanoparticles tend to agglomerate. But this behavior can be prevented by the silanization process. In this thesis, the effects of different ratios of titania and silica nanoparticles used as reinforcement materials in UDMA and bis-GMA based resins on the mechanical properties and conversion degree were investigated. Spherical shaped nanoparticles with particle sizes between 40 nm and 150 nm were synthesized and silanized using the sol-gel method. Then, the optimum particle amount was determined by mixing it with the acrylate-based commercial resin. In parallel, the appropriate monomer and oligomer ratio was determined and nanocomposite resins were obtained by adding the determined amount of particles into UDMA and bis-GMA based resin. At the end of each production stage, relevant characterization methods such as FT-IR, XRD, SEM, tensile, three-point bending were applied to the materials. U1S and B1S samples showed an increase of 38.3 percent and 6.4 percent in flexural strength values, 17.9 percent and 8.3 percent in modulus of elasticity, and decrease of 14.3 percent and 12.4 percent in conversion degree, respectively. Besides the conversion degree, flexural strength and modulus of elasticity are also important in dental applications. The results are promising for the use of prepared nanocomposite resins in dental applications.

Keywords: Photopolymer, nanocomposite, dental, additive manufacturing.

DENTAL UYGULAMALAR İÇİN 3 BOYUTLU YAZICIDA KULLANILAN FOTOKÜRLENEBİLİR REÇİNENİN ÜRETİMİ VE GELİŞTİRİLMESİ

ÖZ

Eklemeli imalat yöntemlerinden biri olan fotokimyasal üç boyutlu yazıcılar, UV-ışık ile foto-çapraz bağlanabilir reçineleri polimerize ederek kalıp kullanmadan ince ayrıntılı dental modeller üretir. Bu reçineler monomerler, oligomerler, fotobaşlatıcılar, tercihen nanoparçacıklar ve renk pigmentleri içerir. Titanya ve silika nanopartiküllerinin eklenmesiyle nanokompozit polimerler yüksek dönüşüm derecesine ve mekanik özelliklere sahip olabilir. Ancak nanopartiküllerin topaklanma eğilimi yüksektir. Fakat silanizasyon işlemi ile bu davranış önlenebilmektedir. Bu tez kapsamında, UDMA ve bis-GMA bazlı reçinede takviye malzemesi olarak kullanılan farklı oranlardaki titanya ve silika nanopartiküllerinin mekanik özellikler ve dönüşüm derecesi üzerindeki etkileri araştırılmıştır. 40 nm ile 150 nm arasında partikül boyutuna sahip küresel şekilli nanopartiküller sol-jel yöntemi kullanılarak sentezlenmiş ve silanize edilmiştir. Daha sonra akrilat bazlı hazır reçine ile karıştırılarak optimum partikül miktarı belirlenmiştir. Buna paralel olarak uygun monomer ve oligomer oranı belirlenmiş ve belirlenen miktarda partiküller UDMA ve bis-GMA bazlı reçine içerisine katılarak nanokompozit reçineler elde edilmiştir. Her üretim aşamasının sonunda malzemelere FT-IR, XRD, SEM, çekme, üç noktalı eğme gibi ilgili karakterizasyon yöntemleri uygulanmıştır. U1S ve B1S numuneleri eğme mukavemeti değerlerinde sırasıyla yüzde 38,3 ve 6,4, elastisite modülünde ise sırasıyla yüzde 17,9 ve 8,3 artış göstermiştir. Dönüşüm derecesinde ise sırasıyla yüzde 14,3 ve 12,4 düşüş göstermiştir. Dental uygulamalarda dönüşüm derecesinin yanında eğme mukavemeti ve elastisite modülü de önem taşıdığından, elde edilen sonuçlar hazırlanan nanokompozit reçinelerin dental uygulamalarda kullanılabilmesi için umut vaat etmektedir.

Anahtar Kelimeler: Fotopolimer, nanokompozit, dental, eklemeli imalat.

CONTENTS

Page

M.SC. THESIS EXAMINATION RESULT FORM ii
ACKNOWLEDGEMENTS iii
ABSTRACT v
ÖZ vi
LIST OF FIGURES x
LIST OF TABLES xii

CHAPTER 1 - INTRODUCTION 1

1.1 Background 1
1.2 Organization of the Thesis 3

CHAPTER 2 – THEORETICAL BACKGROUND 5

2.1 3D Printers as Additive Manufacturing 5
2.1.1 Fused Deposition Modeling (FDM) Method 6
2.1.2 Selective Laser Sintering (SLS) Method 7
2.1.3 Direct Metal Laser Sintering (DMLS) Method 8
2.1.4 Binder Jetting Method 9
2.1.5 Material Jetting Method 10
2.1.6 Stereolithography (SLA) and Digital Light Processing (DLP) Method 11
2.2 Photosensitive Resin 12
2.2.1 Monomers and Oligomers 13
2.2.2 Photoinitiators 14
2.2.2.1 Conversion Degree 15
2.2.3 Fillers 16
2.3 Nanoparticles 17
2.3.1 Production Methods 17
2.3.1.1 Sol-Gel Process 18
2.3.2 Silanization 21

CHAPTER 3 – LITERATURE REVIEW 23

3.1 Photosensitive Nanocomposite Resins in Dental Applications 23

CHAPTER 4 – EXPERIMENTAL STUDIES 29

4.1 Purpose 29
4.2 Materials 29
4.3 Methods 30
4.4 Characterizations 35
4.4.1 X-Ray Diffraction (XRD) 35
4.4.2 Scanning Electron Microscopy (SEM) 36
4.4.3 X-Ray Photoelectron Spectroscopy (XPS) 38
4.4.4 Fourier Transform Infrared Spectroscopy (FT-IR) 39
4.4.5 Particle Size Distribution (PSD) 40
4.4.6 Viscosimetry 41
4.4.7 Thermogravimetric and Differential Thermal Analysis (TG/DTA) 41
4.4.8 Mechanical Tests 42
4.4.8.1 Tensile Test 42
4.4.8.2 Three-Point Bending Test 44

CHAPTER 5 – RESULTS AND DISCUSSION 45

5.1 Characterization of Nanoparticles 45
5.1.1 Thermal Properties 45
5.1.2 Structural Properties 47
5.1.3 Organic Bond Structures 49
5.1.4 Morphological Properties 51
5.1.5 Particle Size Properties 52
5.2 Characterization of Commercial Resin (AC) and AC-based Composites 52
5.2.1 Viscosity Properties 52
5.2.2 Morphological Properties 54
5.2.3 Organic Bond Structures 56

5.2.4 Mechanical Properties 57
5.3 Characterization of UDMA and bis-GMA Based Resins 60
5.3.1 Viscosity Properties 60
5.3.2 Organic Bond Structures 61
5.3.3 Mechanical Properties 62
5.4 Characterization of UDMA and bis-GMA Based Composites 65
5.4.1 Viscosity Properties 65
5.4.2 Morphological Properties 66
5.4.3 Organic Bond Properties 67
5.4.4 Mechanical Properties 68

CHAPTER 6 – CONCLUSION AND FUTURE WORKS 71

REFERENCES 74

LIST OF FIGURES

Page

Figure 2.1 Scheme of a FDM type printer (Mohamed et al., 2015)..... 7
Figure 2.2 Scheme of a SLS type printer (Charoo et al., 2020)..... 8
Figure 2.3 Working principle of DMLS method (Brezinová et al., 2016)..... 9
Figure 2.4 System schematic of binder jetting method (Ziaee & Crane, 2019)..... 10
Figure 2.5 Printing mechanism of material jetting method (Yang et al., 2017) 11
Figure 2.6 Scheme of stereolithography and digital light processing methods (Yu et al., 2020)..... 12
Figure 2.7 Scheme of photopolymerization process (Joseph et al., 2022)..... 14
Figure 2.8 Activation wavelengths of some radical photoinitiators 15
Figure 2.9 Nanoparticle production methods and classifications (Pal et al., 2019)... 18
Figure 2.10 The flow chart of sol-gel method with the different products (Nyamukamba et al., 2018)..... 19
Figure 3.1 Chain structure of (a) bis-GMA and (b) UDMA (Walters et al., 2016) ... 24
Figure 3.2 Chain structure of TEGDMA (Walters et al., 2016) 24
Figure 4.1 Flow chart of the production and characterization of the thesis..... 31
Figure 4.2 (a) 3D printer and (b) wash and cure machine 35
Figure 4.3 Working principle of XRD device (Callister & Rethwisch, 2018) 36
Figure 4.4 Scheme of a scanning electron microscope (Siek, 2015) 37
Figure 4.5 Working principle of XPS (Crist, 2011)..... 38
Figure 4.6 Working principle of FT-IR (Ramaiah et al., 2017)..... 40
Figure 4.7 Scheme of the tensile testing device (Callister & Rethwisch, 2018)..... 43
Figure 4.8 Scheme of the three-point bending test (Callister & Rethwisch, 2018) ... 44
Figure 5.1 TG/DTA analysis of TiO_2 nanoparticles 46
Figure 5.2 TG/DTA analysis of SiO_2 nanoparticles..... 47
Figure 5.3 XRD chart of TiO_2 nanoparticles 48
Figure 5.4 XRD chart of the SiO_2 nanoparticles..... 49
Figure 5.5 FT-IR graph of TiO_2 and TiO_2-S (a) between 4000 and 500 cm^{-1} wavenumber and (b) magnified between 2500 and 1000 cm^{-1} 49

Figure 5.6 FT-IR graph of SiO_2 and SiO_2-S (a) between 4000 and 500 cm^{-1} wavenumber and (b) magnified between 2000 and 1250 cm^{-1} 50
Figure 5.7 SEM images at 50K magnification for (a) TiO_2 and (b) SiO_2, 100K magnification for (c) TiO_2 and (d) SiO_2 51
Figure 5.8 Particle size distribution of TiO_2 and SiO_2 nanoparticles 52
Figure 5.9 Rheometer measurement chart of commercial resin and composites 53
Figure 5.10 SEM images of (a) AC1.5T, (b) AC1.5TS, (c) AC1S, (d) AC1SS and (e) AC samples at 5K magnification 55
Figure 5.11 FT-IR chart of AC sample before and after curing 56
Figure 5.12 Conversion degrees of commercial resin and composites 57
Figure 5.13 Yield strength values of commercial resin and composites 58
Figure 5.14 Modulus of elasticity values of commercial resin and composites 58
Figure 5.15 Flexural strength values of commercial resin and composites 59
Figure 5.16 Rheometer measurement chart of UDMA and bis-GMA based resins .. 60
Figure 5.17 Conversion degree values of UDMA and bis-GMA based resins 62
Figure 5.18 Yield strength of UDMA and bis-GMA based resins 63
Figure 5.19 Modulus of elasticity of UDMA and bis-GMA based resins 63
Figure 5.20 Flexural strength of UDMA and bis-GMA based resins 64
Figure 5.21 Rheometer results of UDMA and bis-GMA based composites 65
Figure 5.22 SEM images of (a) U1.5T, (b) B1.5T, (c) U1S, (d) B1S and (e) U60 and (f) B45 samples at 5K magnification 66
Figure 5.23 Conversion degrees of UDMA and bis-GMA based composites 67
Figure 5.24 Yield strength of UDMA and bis-GMA based composites 68
Figure 5.25 Modulus of elsticity of UDMA and bis-GMA based composites 69
Figure 5.26 Flexural strength of UDMA and bis-GMA based composites 69
Figure 6.1 Green products made of produced resin (Personal archive, 2022) 72
Figure 6.2 Dental model printed with produced resin (Personal archive, 2022) 72

LIST OF TABLES

Page

Table 2.1 General properties of acrylate-based resins (Schwalm, 2007b)..... 13
Table 3.1 Studies about photosensitive composite resins 27
Table 4.1 List of the chemicals used in production of nanocomposites 30
Table 4.2 Contents and naming of the prepared mixtures 32
Table 4.3 Proportions and naming of the composites made by commercial resin..... 34
Table 5.1 Crystallite size calculation of TiO_2 nanoparticles..... 48
Table 5.2 Viscosity values of commercial resin and composites..... 54
Table 5.3 Viscosity values of UDMA and bis-GMA based resins 61
Table 5.4 Viscosity values of UDMA and bis-GMA based composites..... 65

CHAPTER 1
INTRODUCTION

1.1 Background

With the development of technology, people's needs, wishes and expectations are changing day by day. With the Industry 4.0, which is the 4th Industrial Revolution, the existing industry has been digitalized and started to be equipped with high technology together with the concept of "Internet of Things (IoT)". These developments are taking place especially in the fields of robotics, additive manufacturing and nanotechnology. The production technology obtained by combining the developments with Industry 4.0 and embedded system technologies has begun to be transferred to the production chains and the industry. Additive manufacturing methods, on the other hand, are of great importance for Industry 4.0 with their potential. Thanks to this method, it has become possible to produce parts that cannot be produced with traditional production methods, and a big step has been taken in digitalization in production (Dilberoglu et al., 2017; Yuran & Yavuz, 2021).

In recent years, 3D printers, as an additive manufacturing technology, are devices that play an important role today in terms of producing shapes with complex geometry compared to traditional methods such as casting and machining. Since the 1980s, they have attracted great attention thanks to the fact that many objects can be produced at once (Chen et al., 2019). Additive manufacturing is a production technology that creates layers starting from zero point on a kind of platform, adds these layers on top of each other, and repeats this process until the target product is completed. This technology can also be summarized as a robotized version of production methods that have been carried out by humans for centuries (for example, building a brick wall). Three-dimensional printers, on the other hand, are devices that perform this production method in various ways with the help of CAD (Computer Aided Design) programs (Horvath, 2014).

Since 3D printers can shape many materials today, their usage areas have also expanded considerably. Thanks to their high efficiency, environmental friendliness and fast production, these printers, which are within the scope of Industry 4.0, operate in many fields such as aerospace, dentistry, healthcare, civil construction, food, arts, drug industry, biomaterials and tissue engineering (A. L. Silva et al., 2021; Zhang & Xiao, 2018).

3D printers are classified according to mechanical, electrical or photochemical as their production method. DLP type printers, one of the photochemical methods, produce the final product by photopolymerizing the photosensitive resins under UV-light. These resins contain monomer, oligomer, photoinitiator, optionally nanoparticle and color pigment (Zhang & Xiao, 2018). This mixture becomes a polymer by forming cross-links under UV light thanks to the photoinitiators in the structure. These cross-links are the most important factors that determine the mechanical properties and conversion degree of the polymer structure. By adding inorganic filling material into the structure, the strength and amount of cross-links can be increased, thereby improving the mechanical properties and conversion degree (Aati et al., 2021; Al-Turaif, 2010; N. Bahremandi Tolou et al., 2013; Pehlivan & Karacaer, 2014).

To improve mechanical properties and conversion degree of resin, TiO_2 and SiO_2 nanoparticles can be dispersed into the resin. TiO_2 nanoparticles come to the fore with their high UV absorbance (Pathak et al., 2017; Viana et al., 2010), antibacterial properties (Poosti et al., 2013), biocompatibility, self-cleaning properties, and photocatalytic performance (Yurddaskal et al., 2015). SiO_2 nanoparticles, on the other hand, stand out with their superior mechanical properties (Rezvani et al., 2016) and the ability to preserve the transparent appearance of the resin.

However, the disadvantage of TiO_2 and SiO_2 nanoparticles is that they agglomerate in the structure and reduce the surface area in contact with the resin, which negatively affects the mechanical properties (Pehlivan & Karacaer, 2014). In order to prevent this, the process of coating the particle surfaces with silane groups, which is called silanization, is applied. The coating of nanoparticles with silane groups contributes to

the strengthening of the bonds by ensuring that the particles do not stick to each other and bond with the matrix material (Neibloom et al., 2020; Nguyen et al., 2020; Tham et al., 2010).

1.2 Organization of the Thesis

Within the scope of this thesis, nanocomposite resins were produced with different ratios of monomer and nanoparticle mixtures and the printability of these resins was tested using a 3D printer. The aim of the thesis is to determine the producibility of tooth models used in the dental field using TiO_2 and SiO_2 nanoparticles added resin with high accuracy, high mechanical properties and conversion degree using 3D printers and to examine the effects of nanoparticles on the final product.

In Chapter 1, information about the use of three-dimensional printers in the dental field is given, and the purpose of writing the thesis is stated.

Chapter 2 presents the theoretical background of 3D printers, photosensitive resins and their properties, nanoparticles and nanocomposites. Detailed information about the production methods of nanoparticles and nanocomposites are also given in this chapter.

The literature review about nanocomposite photosensitive resins is presented in Chapter 3.

Chapter 4 consists of the synthesis and characterization methods of the TiO_2 and SiO_2 nanoparticles; production, printing and characterization of the nanocomposite resin. The names and properties of the chemicals used during nanoparticle synthesis and resin production, and information about the characterization equipment used in these products are also given in detail in this chapter.

In Chapter 5, the results of the characterizations are given and these results are interpreted. The reasons for the results have been scientifically examined and explained in this section.

In Chapter 6, which is the last part of the thesis, the conclusion of the study and future plans are presented

CHAPTER 2
THEORETICAL BACKGROUND

2.1 3D Printers as Additive Manufacturing

Additive manufacturing is a production method based on the principle of adding materials such as metal, plastic and composite to each other layer by layer to form a real 3-dimensional product. This method was first developed by 3B Systems company in the 1980s on the basis of Stereolithography (SLA) technology (Danforth & Safari, 1996). Following the development of SLA technology, methods such as Fused Deposition Modeling (FDM), Selective Laser Sintering (SLS) and Direct Metal Laser Sintering (DMLS) were developed and branded in the first half of the 1990s (Sürmen, 2019) With the diversification of additive manufacturing methods and becoming usable with desktop machines today, these machines have started to be called "Three-Dimensional (3D) Printer" among the people and this name has become widespread and has gained an important place today (Sürmen, 2019).

3D printers are, as mentioned before, an additive manufacturing technology that allows the production of three-dimensional objects by creating layers of material (eg polymers) with computer aided design (CAD) programs and adding these layers on top of each other, without the need for molds. The fact that they do not produce in a certain mold greatly increases the freedom of design and product diversity of these printers.

A three-dimensional solid model, whose design has been completed, is separated into layers by computer software. The printer then deposits each layer on top of each other to obtain the final product. Additive manufacturing, which is generally used for the rapid prototyping of the parts planned to be produced, comes into prominence with the aim of obtaining the final product day by day.

3D printers are classified according to mechanical, electrical or photochemical as their production method. To give examples of these: fused deposition method (FDM)

(Kim et al., 2019; Surange & Gharat, 2016), selective laser sintering (SLS) (Fina et al., 2017; Geng et al., 2019), direct metal laser sintering (DMLS) (Sedlak et al., 2015), laser metal deposition (LMD) (Azarniya et al., 2019; Lei et al., 2020), binder jetting (Ziaee & Crane, 2019), material jetting (Yap et al., 2017), stereolithography (SLA) (Weng et al., 2016; Yan & Peng, 2021), and digital light processing (DLP) (Alsandi et al., 2021) are the most widely used methods.

2.1.1 Fused Deposition Modeling (FDM) Method

The FDM method is a method based on the principle of heating the thermoplastic filaments, which is the starting material, to make them fluid, and then depositing the material on the table by flowing it from the tip of a nozzle. FDM type printers were developed by a company named Stratasys Inc. in the USA in 1990s (Mohamed et al., 2015). Some models have a single nozzle, while others have a double nozzle as in Figure 2.1. In double nozzle models, while the second nozzle is generally used for the support material, it can also be used for different colors of the same material.

The filaments used in this method are placed in the device as a winding. The heating process is carried out by adjusting the temperature of the nozzle according to the type of material used. If the nozzle is heated more than necessary, the material becomes too fluid and distortions occur when it is transferred to the table. Even if the temperature is set lower than necessary, the material does not soften and cannot be transferred from the tip of the nozzle to the table. As filaments, ABS (Acrylonitrile butadiene styrene), PLA (Poly lactic acid) and PC (Polycarbonate) are the most preferred materials.

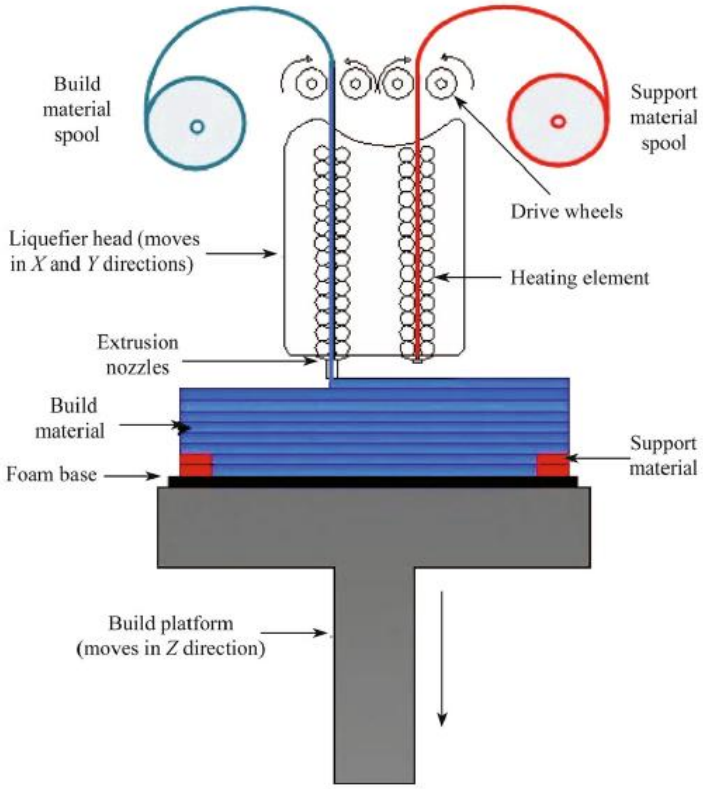


Figure 2.1 Scheme of a FDM type printer (Mohamed et al., 2015)

Printing sensitivity can be adjusted by changing the diameter of the nozzle tip and the speed of the printer tip. The printing sensitivity, the fill rate of the part, the number of layers and the part size are the parameters that affect the printing speed. It is among the most preferred printer types due to its low production cost and suitable for domestic use.

2.1.2 Selective Laser Sintering (SLS) Method

In the SLS method, all materials that can be found in powder form and tend to melt or sinter when they reach a sufficient temperature can be used as starting material. SLS sticks the powders (usually polymers or ceramics) deposited in a certain layer thickness in a pool, by pointwise sintering with the help of laser beam. The intensity of the energy used in the laser can be adjusted with the laser power and scanning speed. These parameters should be adjusted to suit the starting material used. Otherwise, the

starting material may be damaged, or the production may fail because sintering will not occur.

As can be seen in Figure 2.2, the dust pool spreads the dust on the floor as much as the adjusted layer thickness. Then this powder layer is sintered in layers by laser light. After the sintering process of the layer on which the point sintering process is performed is completed, the process is repeated and the printing process continues.

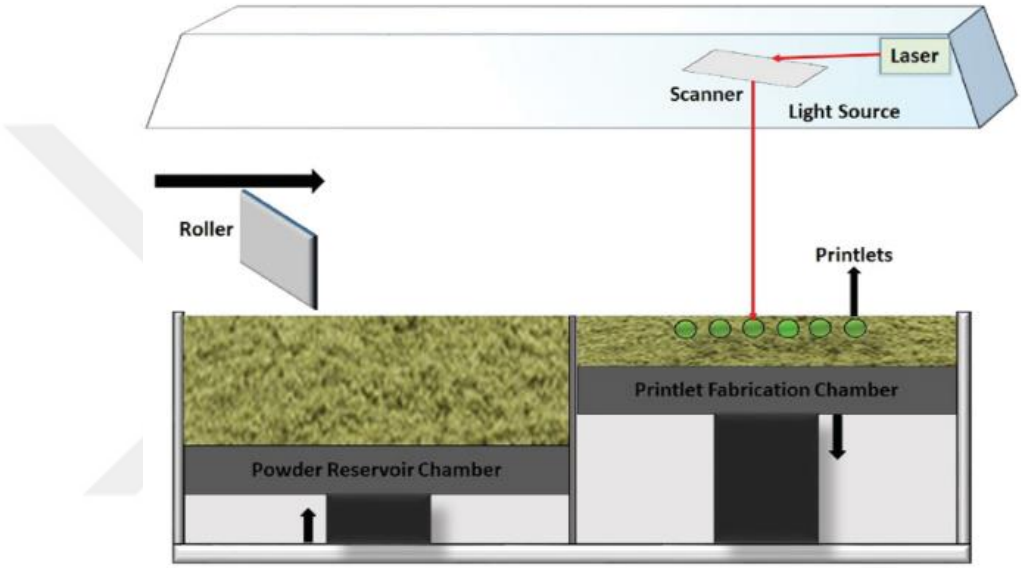


Figure 2.2 Scheme of a SLS type printer (Charoo et al., 2020)

Some of the advantages of the SLS method are that it does not require a second process such as solvent removal after production, as it does not contain any binder in the starting material, and it can produce parts with sensitive geometry for many sectors, especially the pharmaceutical industry and tissue engineering (Partee et al., 2006), thanks to its high-energy laser (Fina et al., 2017). These high-energy lasers have advantages as well as disadvantages. Since high-energy laser is used during the process, energy consumption of the process is high.

2.1.3 Direct Metal Laser Sintering (DMLS) Method

In the DMLS method, whose working principle is similar to the SLS method, high quality steels and metal alloys such as nickel and cobalt material superalloys are used

as starting materials. With this method, which has a setup as shown in Figure 2.3, it is possible to obtain rapid prototyping and final products. DMLS provides metal powders to stick together by sintering with the help of high-energy laser as in SLS method.

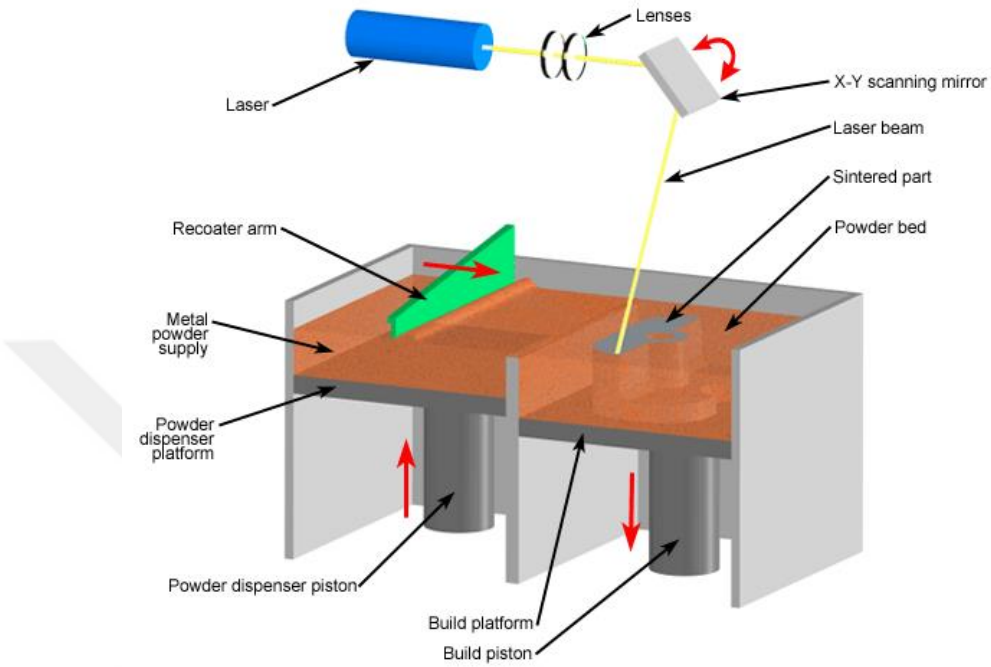


Figure 2.3 Working principle of DMLS method (Brezinová et al., 2016)

In addition to the advantages of rapid prototyping, the products produced with the DMLS method; they have poorer surface properties and more limited strength compared to conventional casting. The reason is that the density of the produced part is lower due to the micro pores it contains. These properties can be improved by optimizing printing parameters (e.g. laser power, laser-scanning speed, layer thickness, grain size of powders, material alloy).

2.1.4 Binder Jetting Method

In this method, powdered metal, ceramic and polymer materials can be used as starting materials. As in the SLS and DMLS methods, the powders are distributed on the table in the desired layer thickness with the help of a spreader as shown in Figure 2.4. Then, the liquid binder material is sprayed through the printer tip and the powders are bonded together. A new layer of powder is then laid and the process is repeated

until the piece is completed. After the green product is obtained, curing process must be applied to bind the powders permanently. Finally, post-treatment (sintering) is applied to remove residual binder and improve mechanical properties (Ziaee & Crane, 2019).

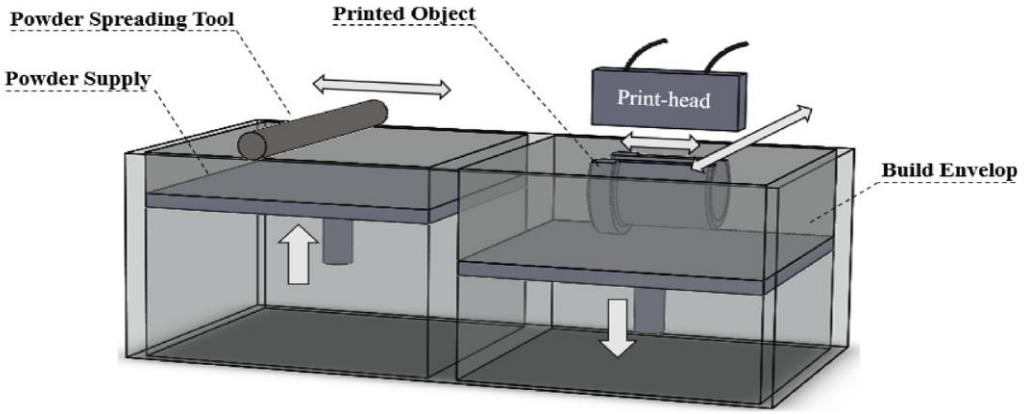


Figure 2.4 System schematic of binder jetting method (Ziaee & Crane, 2019)

The advantages of this method are that it is more economical thanks to the fact that it does not require high energy like SLS and DMLS methods. Also the raw material of this method is powders which can be prepared easier than wires, sheets or slurries and that it can be printed in color thanks to various binding materials. Its disadvantages are that it does not have as accurate printing resolution as other methods, so post-production processing may be required on parts with complex geometries (Lv et al., 2019).

2.1.5 Material Jetting Method

The material jetting method, also known as InkJet 3D printing, is a method that deposits liquid photopolymer from the print tip to the table, similar to the FDM method, and then curing the material by exposing UV light which is following the nozzle to create a final product as shown in Figure 2.5. In addition to material prototyping, it is also used in important fields such as tissue engineering (Yap et al., 2017).

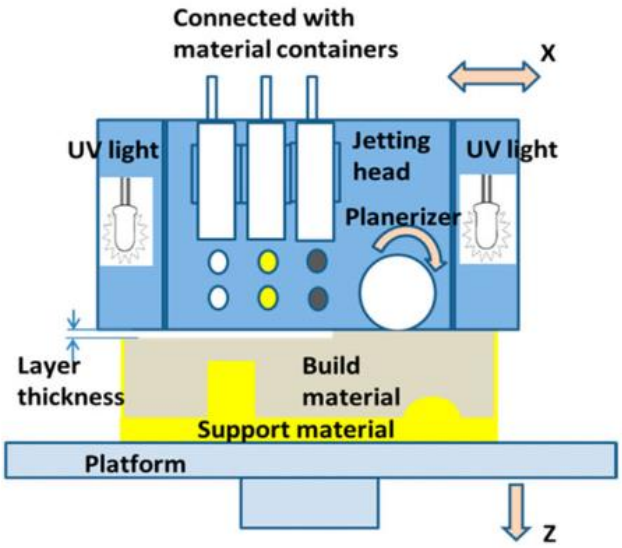


Figure 2.5 Printing mechanism of material jetting method (Yang et al., 2017)

The material jetting method has a simpler mechanism and a wider production area compared to VAT polymerization methods (SLA and DLP) which are using similar starting materials. In this way, more product output can be obtained per unit time (Dilag et al., 2019). However, more parameters have to be optimized compared to VAT polymerization methods in order to obtain optimum geometric quality (Yap et al., 2017).

2.1.6 Stereolithography (SLA) and Digital Light Processing (DLP) Method

SLA and DLP methods, which are based on photochemical methods, are systems for creating three-dimensional products with the help of UV light. Photosensitive resin is used as starting material for SLA and DLP methods. Scheme of SLA and DLP methods are shown in Figure 2.6. For SLA, the resin is filled into the vat in the device. The moving table, which is immersed in the resin vat, moves to the bottom of the pool until the distance remains as the determined layer thickness. When the set distance is reached, the resin is polymerized by giving UV laser from the light source at the top of the pool. In this way, the layers are stacked on top of each other and the final product is obtained (Manapat et al., 2017).

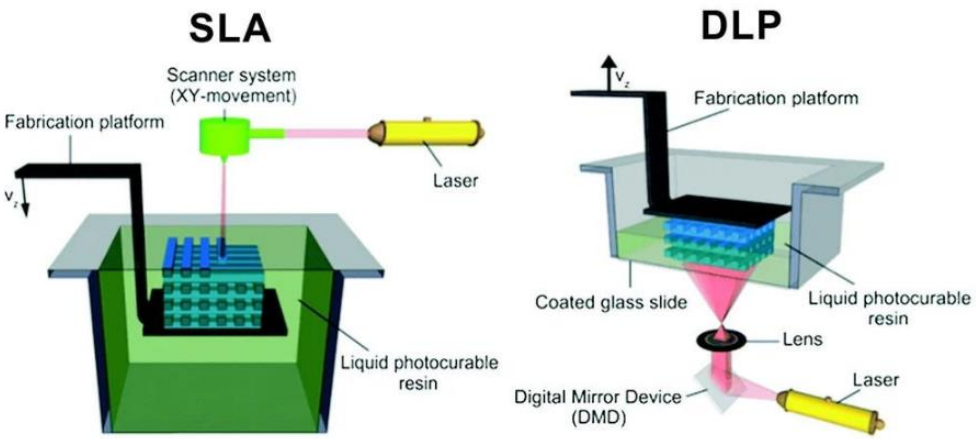


Figure 2.6 Scheme of stereolithography and digital light processing methods (Yu et al., 2020)

In DLP method, similar process is applied with SLA but there are several differences. The light is masked with a filter and shaped as a material layer and affects the entire layer in a single exposure. But in the SLA method, the light is applied pointwise and is moved by the mirrors in the source. This difference shows that the SLA method is more accurate with its high resolution but the DLP method is faster with enough resolution. In this way, DLP is become more preferable because of its printing speed, accuracy and low cost (Alsandi et al., 2021; Lin et al., 2020; Revilla-León & Özcan, 2019). Also, in the SLA method, production takes place from the bottom up, while in the DLP method, it takes place from the top down (Yu et al., 2020). DLP and SLA type printers, two of the photochemical methods, produce the final product by photopolymerizing the photosensitive resin under UV-light.

2.2 Photosensitive Resin

As mentioned in the previous topic, DLP and SLA type printers need photosensitive resin to obtain the final product with the help of UV light. This kind of resin contain monomer, oligomer, photoinitiator and fillers (Zhang & Xiao, 2018). Monomers and oligomers in this mixture become polymers by forming crosslinks under UV light, thanks to the photoinitiators in its structure. Fibers, nano and micro particles can be added to the structure as fillers. In the composite resin obtained by adding these fillers, the bonds are strengthened by filling the gaps between the polymer chains (SOURCE).

2.2.1 Monomers and Oligomers

Monomers and oligomers form the main mesh of these thermoset resins used in SLA/DLP type printers. Oligomers are low molecular weight polymers with a small number of repeats in which the physical properties are highly dependent on the chain length. Monomers are molecules with two or more binding sites that form covalent bonds with other monomer or oligomer molecules to form the polymer structure. They are often used to dilute oligomers or modify the mechanical properties of the structure.

The main types of resins that can be used for radical curing can be classified as unsaturated polyesters, epoxy acrylates, polyester acrylates, polyurethane acrylates and polyether acrylates. While radical photoinitiators can be used in acrylate-terminated monomers, UV curing can be achieved by using cationic initiators in epoxy-terminated monomers (Schwalm, 2007b). Resins terminated with acrylate group have the largest share in the resin market. General properties of acrylate-terminated resins are shown in Table 2.1.

Table 2.1 General properties of acrylate-based resins (Schwalm, 2007b)

Aromatic Epoxy Acrylates	**Aliphatic Urethane Acrylates**
Based on Bisphenol-A diglycidether	Pronounced toughness and flexibility
High viscosity	Non-yellowing
High reactivity	High weathering resistance
Diluted with reactive thinners	High viscosity
Good chemical stability	High price
Good cost/performance ratio	
Tendency to yellowing	
Polyester acrylates	**Polyether acrylates**
Good overall performance	Low viscosity
Large variety of hard or flexible resin	Applicable as resins or reactive diluent
Low residual monomers	High reactivity
Low odor	
Good compatibility with other resins	
Amine Modified Acrylates	**Acrylated Polyacrylates**
Coinitiators	Large variety of polyacrylatols available
High reactivity	High exteriour stability
Low odour, low migratables	

2.2.2 Photoinitiators

Photoinitiators become reactive by absorbing light and start polymerization by reacting with monomers and oligomers in the resin component. This process is called photopolymerization and the process scheme can be seen in Figure 2.7.

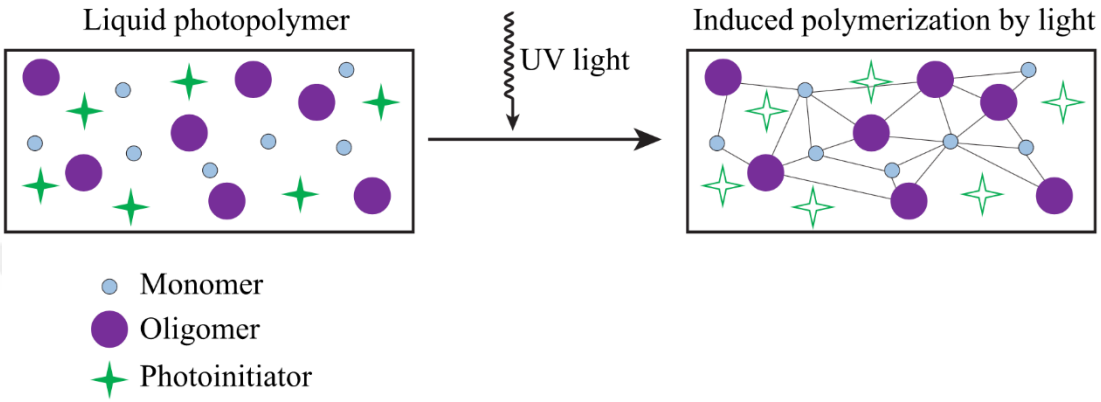


Figure 2.7 Scheme of photopolymerization process (Joseph et al., 2022)

Photoinitiators become reactive in radical, cationic or anionic state under the influence of light. The majority of UV curing processes are performed using radical-forming photoinitiators (Schwalm, 2007a). When photoinitiators are exposed to UV light, they generate free radicals with the energy of the light and bind the monomers and oligomers in the structure. Figure 2.8 shows some radical photoinitiators and their activation wavelengths. These cross-links are the most important factors that determine the mechanical properties and conversion degree of the polymer structure. By adding inorganic filling material into the structure, the strength and amount of cross-links can be increased, thereby improving the mechanical properties and conversion degree (Aati et al., 2021; Al-Turaif, 2010; N. Bahremandi Tolou et al., 2013; Pehlivan & Karacaer, 2014).

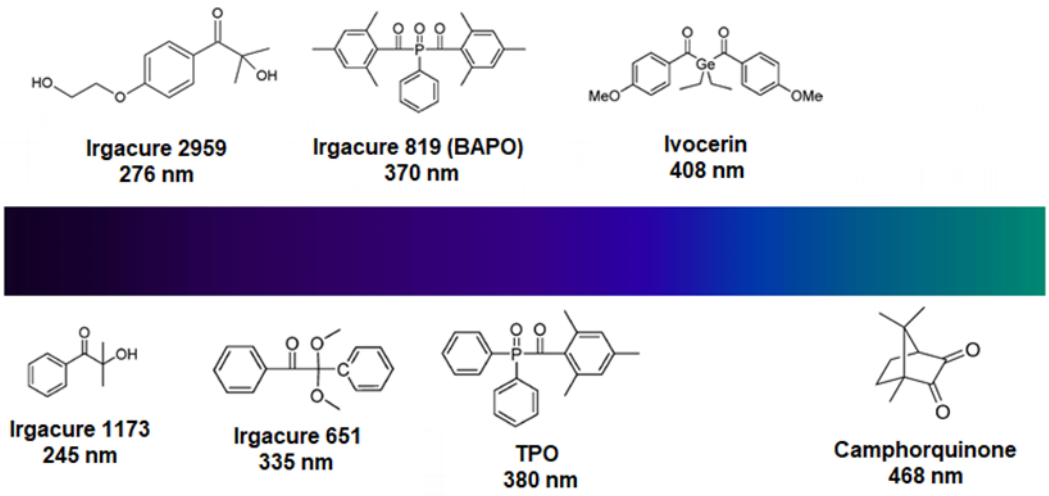


Figure 2.8 Activation wavelengths of some radical photoinitiators

2.2.2.1 Conversion Degree

Bond conversion is the conversion of C=C double bonds in the monomer structure into C-C cross-links and connecting with other monomers. Photoinitiators, which initiate this transformation, form radical groups in the structures of the monomers thanks to the light of the appropriate wavelength, allowing the monomers in the structure to form bonds. The greater the amount of this reaction, the higher the mechanical properties of the resin, such as surface hardness, fracture toughness and wear resistance. In case the reaction efficiency is not complete, monomer structures can also be found trapped in the polymer (Prasanna et al., 2007). The presence of residual monomers that are not fully polymerized, that is, uncured, in the structure also adversely affect the mechanical properties of the resin. These unreacted monomers increase the shrinkage of the polymer; It also negatively affects tensile strength, modulus of elasticity, flexural resistance, hardness and color stability. In addition, these monomers, especially with the pressure created in dental applications, can pass through the mouth to the tissue and cause an allergic reaction (Lu et al., 2005; Ulusoy & Nalçacı, 2004).

2.2.3 Fillers

Fillers play an important role in improving the performance of polymer materials. Filling materials, which can consist of a wide range of materials, are used to improve the mechanical, thermal, dimensional and water absorption properties of the polymer material they are incorporated into (Gajapriya et al., 2020). The fillers used in composites can generally be formed from inorganic materials such as glass, ceramic, metal.

Fillers can be composed of fibers, nano or microparticles. If the size of the filling material added to the structure has an order of micron and above, the material is composite; If it is under micron, that is, in nano size, it is called a nanocomposite. Composites are obtained by combining at least two kinds of materials, namely matrix and filler (reinforcement) material. The matrix material is the main material that surrounds the filler material and forms the main shape of the material. Filler materials, on the other hand, are materials added to the matrix material in order to improve the mechanical, thermal, optical and electrical properties of the matrix material in accordance with the targeted working condition.

Nanocomposites, on the other hand, are composite materials obtained on the condition that at least one dimension of the reinforcement material consists of particles, fibers or layers in the order of nanometers. When the size of the additives is reduced to the nano scale, better mechanical, thermal, optical and electrical properties can be obtained compared to the macro and micro scale (Alexandre & Dubois, 2000). These superior properties of nanoparticles are due to their higher surface area in contact with the matrix material compared to macro and micro scales. In this case, polymer nanocomposites can be defined as polymer matrix materials containing nano-sized filler material.

2.3 Nanoparticles

According to the common definition, materials that have at least one dimension less than 100 nm or that are formed by the combination of these small materials are called nanomaterials. In some areas such as health and environment, this range can vary between 0.3 nm and 300 nm. If all three dimensions of a material are less than 100 nm, such materials may be called as nanoparticle, quantum dot, nanoshell, or nanoring. If their only two dimensions are less than 100 nm, they can be called as nanotube, nanowire, or nanofiber. If only one dimension is less than 100 nm, they are called as thin film, layer or coating (Işıtan, 2018). In this study, nanoparticles were used as additive material.

Nanoparticles often exhibit improved nanocomposite performance in the matrix material compared to conventional composites, thanks to their unique phases, morphologies, and improved interfacial properties (Yurddaşkal, 2017). Optical, mechanical, electrical and color properties of the same material in macro, micro and nano dimensions may differ, even the opposite. Some features that do not occur in the macro dimension may occur in the nano dimension. The main reason for this is that the dimensions are continuous in the macro and micro world but not continuous in the nano world, and the ratio of surface areas to volumes increases as the size of the material decreases (Işıtan, 2018). Thanks to these properties, nanoparticles, which have become very popular today, can be produced by many alternative methods.

2.3.1 Production Methods

There are two general approaches to nanomaterial production: top-down and bottom-up manufacturing. In the top-down approach, the material is split into small pieces from the bulk state. In this approach, the structural dimensions of microscopic elements are reduced to nanometer scale with special processing and chemical etching techniques.

In the bottom-up production approach, the material is synthesized as a result of the growth of atoms and molecules in size through chemical reactions. Figure 2.9 shows nanoparticle production methods and classifications.

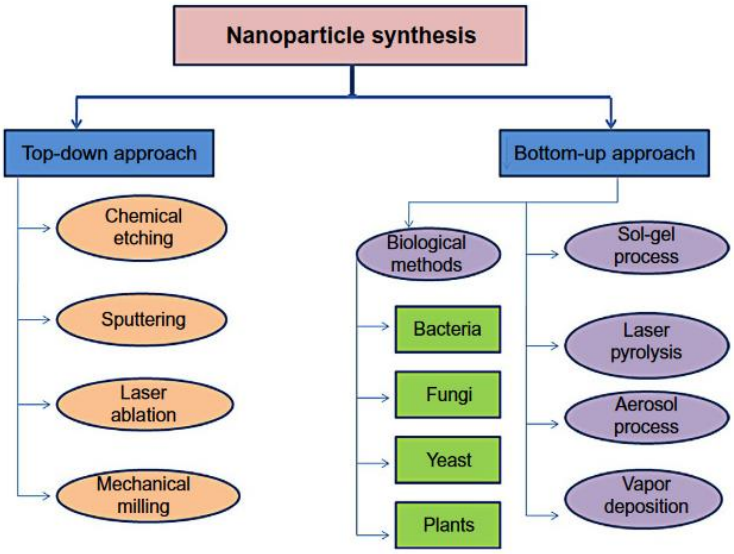


Figure 2.9 Nanoparticle production methods and classifications (Pal et al., 2019)

2.3.1.1 Sol-Gel Process

Since the sol-gel method, which is one of the aforementioned production methods, is a production method that can be carried out in laboratory environment and room temperature conditions. Based on this, the production of nanoparticles to be used in the scope of the thesis was carried out by sol-gel method. Sol-gel method is a very popular method in scientific and engineering fields due to its advantages such as its effortless application environment and the ability to produce materials of various sizes, shapes and types (Toygun et al., 2013). The flow chart of the different products that can be obtained by sol-gel production is shown in Figure 2.10.

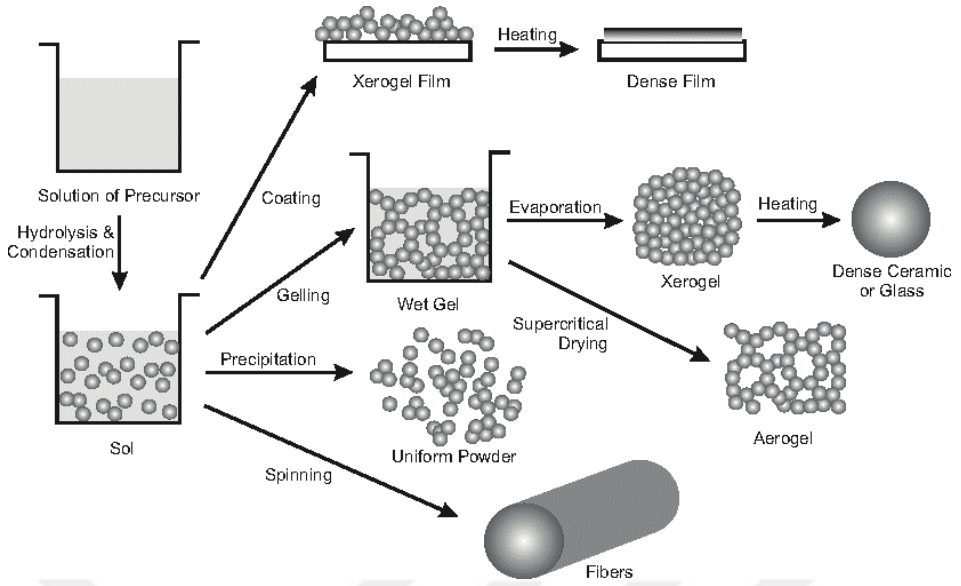


Figure 2.10 The flow chart of sol-gel method with the different products (Nyamukamba et al., 2018)

Although the sol-gel method has advantages such as being able to be carried out in laboratory conditions, not needing extra heat other than calcination, producing high-purity material and controlling every step, it also has some disadvantages. The precursors used in the productions carried out by the sol-gel method are quite costly compared to other methods, and since they are carried out in a laboratory environment, they are not suitable for large-scale production in terms of both physical and financial opportunities. Likewise, it is a time-consuming technique since every step can be controlled and the production process is multi-step (Onar, 2018).

This method, which is formed by abbreviating the words solution and gelation as sol-gel; It consists of the steps of forming a stable suspension of colloidal solid particles denser than the liquid, that is, the formation of "sol" and the precipitation of colloidal particles, forming a precipitate type structure containing plenty of water, that is, obtaining "gel". The most important criterion in gel formation is the bonds between the organic solvent and the dispersed particles. Sol-gel process can also be explained simply as the process of synthesizing gel from alkoxides.

Sol-gel process consists of steps called hydrolysis, condensation, gelation, aging, drying and sintering. In the sol-gel process, sol is obtained as a result of hydrolysis of the mixture obtained by mixing the starting metal organics (metal alkoxides or metal

salts) with organic solvents as showed in Equation 2.1. In the hydrolysis reaction, metal organic compounds are removed from organic groups by providing metal hydroxide with organic solvents.

$$M(OR)_n + nH_2O \rightarrow M(OH)_n + nROH \quad (2.1)$$

Where "R" represents organic group (alkoxide or salt), "M" metal and "ROH" released alcohol groups. After the hydrolysis reaction, a condensation reaction occurs so that the complex gel structure between two metal atoms can be formed. As can be seen in Equations 2.2 and 2.3, the condensation reaction can occur in two ways as olation or oxolation, respectively (Yıldırım, 2017).

$$2M(OR)_{n-1}(OH) \rightarrow M_2O(OR)_{2n-3}OH + ROH \quad (2.2)$$

In the olation process, the H atom bonds with the OR group and turns into an alcohol and leaves the structure.

$$2M(OR)_{n-1}(OH) \rightarrow M_2O(OR)_{2n-3} + H_2O \quad (2.3)$$

In the oxolation process, the H atom bonds with the OH group and leaves the structure as water. The resulting colloidal sol takes the form of a gel as a result of the condensation reaction, when the particles in it form a network structure and gelation process is completed. In order to accelerate the condensation reaction, acidic or basic solutions can be added to the structure as a catalyst, or the solution can be heated. The gel obtained as a result of condensation is aged by waiting for a certain period of time for precipitation of residual colloidal particles and homogenization of particle size distribution (Pierre, 1998). Finally, by applying various heat treatments, the gel is dried and the remaining organic solvents in the structure are removed. As a result of all these processes, nanoparticles are obtained as the final product (Toygun et al., 2013).

2.3.2 Silanization

The silanization process is a type of surface modification process that can be defined as the coating of particle surfaces with organofunctional alkoxysilane molecules. It is an effective coating method used to modify material surfaces rich in hydroxyl groups (-OH) such as titanium dioxide, hydroxyapatite and many other metal oxide surfaces. It happens because silicon-based molecules can easily form covalent bonds with hydroxyl groups on the inorganic metal oxide surface (Boccafoschi et al., 2018). Silane coating agents are silicon-based materials with the general chemical formula $R'(CH_2)_nSi(OR)_3$. Here, "R'" represents the organofunctional group and "R" represents the hydrolyzable alkoxy group (Liu et al., 2013). When silane agents are mixed with organic solution (water or alcohol derivatives), hydrolysis reaction (Equation 2.4) occurs and alkoxy groups are converted to silanol groups (SiOH) (Tosi et al., 2022).

$$R'(CH_2)_nSi(OR)_3 + 3H_2O \rightarrow R'(CH_2)_nSi(OH)_3 + 3ROH \qquad (2.4)$$

Later, in the condensation stage (Equation 2.5), silanol groups form hydrogen bonds with surface hydroxyl groups, while the excess silanol groups form siloxane networks (Si–O–Si).

$$2R'(CH_2)_nSi(OR)_2(OH) \rightarrow (R'(CH_2)_nSi)_2O(OR)_3OH + ROH \qquad (2.5)$$

This network is chemically stable and resists corrosion. In this way, since the particles become stable, agglomeration is prevented and a homogeneous distribution is achieved (Tosi et al., 2022).

The purpose of silanization is to modify the particle surfaces, preventing them from bonding with each other, and increasing their compatibility with the matrix material. The amount of silane agent used in the silanization process is one of the most important factors affecting the success of the process. The presence of excessive silane agent concentration between the filler material and the matrix material creates a plasticizing

effect in the material due to increased silane molecules and has a negative effect on the mechanical properties (Aati et al., 2021). Similarly, insufficient silane agents cannot prevent agglomeration, causing agglomeration of particles and insufficient adhesive force with the matrix material. In this context, the amount of silane agent to be used differs according to the type of filler and silane agent and has a mathematical formula. The amount of silane to be used in the silanization process is shown in Equation 2.6 (Aati et al., 2021).

$$x = \left(\frac{a}{w}\right) * f \tag{2.6}$$

Where; “x” indicates the amount of silane material, “a” indicates the surface area of the filler material, “w” indicates the minimum surface area that the silane group to be used can cover, and “f” indicates the amount of filler material used.

CHAPTER 3
LITERATURE REVIEW

3.1 Photosensitive Nanocomposite Resins in Dental Applications

When the literature studies on this subject were examined, it was seen that Lu et al. (Lu et al., 2005) produced new photocurable resins by combining the mono methacrylate-based diluents they synthesized with bis-GMA (bisphenol A-glycidyl dimethacrylate). These produced resins were compared with bis-GMA/TEGDMA (triethylene glycol dimethacrylate) resin, which is one of the most commonly used resins in the dental field. Although the diluents produced in the laboratory are superior to TEGDMA in terms of polymerization shrinkage and conversion degree, TEGDMA has been found to be superior in terms of mechanical properties. In a similar study, Chung et al. (Chung et al., 2002) produced TEMA/TEGDMA photocurable resin, which will be an alternative to bis-GMA/TEGDMA for use in the dental field. They synthesized TEMA (tris[4-(2'-hydroxy-3'-methacryloyloxypropoxy) phenyl]methane) monomer in vitro. In the results obtained, lower polymerization shrinkage of the TEMA-based photocurable resin was observed compared to the bis-GMA-based one, but it was found to be more costly to manufacture than the bis-GMA-based resin.

As a result of these studies, it is observed that bis-GMA (Bisphenol-A Glycidyl Dimethacrylate) and UDMA (Urethane Dimethacrylate) are the most preferred oligomer types in the dental field (Lu et al., 2005). Figure 3.1 shows the chain structure of bis-GMA and UDMA.

Bis-GMA, with a molecular weight of 512.6 g/mol, has a highly viscous structure and becomes very hard after curing. After curing, it exhibits a relatively low polymerization shrinkage of 4.7% by volume compared to other monomers. However, due to its extremely high viscosity, it should be diluted at least 25% by weight with a diluent with a lower viscosity (Lu et al., 2005).

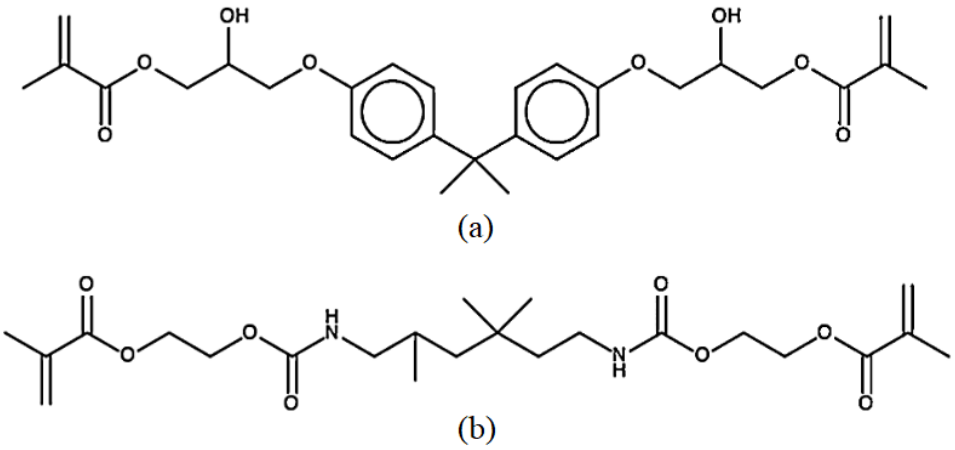


Figure 3.1 Chain structure of (a) bis-GMA and (b) UDMA (Walters et al., 2016)

UDMA, on the other hand, is a monomer with a molecular weight of 470 g/mol and a lower viscosity and higher flexibility than bis-GMA (Asmussen & Peutzfeldt, 1998). After curing, they have high flexural strength, modulus of elasticity and hardness (Gajewski et al., 2012). Since these two monomers have high viscosity, they must be diluted with a low molecular weight comonomer such as styrene, vinyl toluene or methyl methacrylate with lower viscosity (Hari Sankar et al., 2015). The most commonly used diluent in this area, together with bis-GMA and UDMA, is a methacrylate called TEGDMA (Triethyleneglycol Dimethacrylate), with a molecular weight of 286.32 g/mol which is shown in Figure 3.2 (Ulusoy & Nalçacı, 2004).

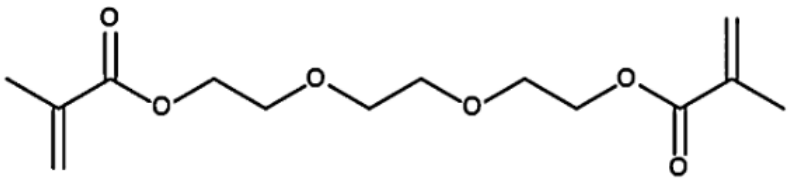


Figure 3.2 Chain structure of TEGDMA (Walters et al., 2016)

Bis-GMA/TEGDMA duo is a resin often used in coatings and dental filling materials. Advantages of bis-GMA monomer; It has a high modulus of elasticity, high glass transition temperature, low volatility and relatively low polymerization shrinkage. In the bis-GMA/TEGDMA pair, bis-GMA creates the original form, while TEGDMA provides the fluidity. The UDMA/TEGDMA duo is another mixture most commonly used in dental composite resins. Composites with this mixture show

superior mechanical properties such as high toughness thanks to the bonds formed by the urethane groups (Asmussen & Peutzfeldt, 1998). Although the addition of TEGDMA into the resin increases the degree of conversion in the structure, it also has some negative effects. The addition of TEGDMA to the structure causes an increase in polymerization shrinkage and water absorption (Walters et al., 2016).

Gajewski et al., in their study, calculated the degree of conversion of UDMA, TEGDMA and bis-GMA monomers used in dental composite resins according to the curing time in the range of 10 minutes to 24 hours. As a result of their study, the conversion degree is listed as bis-GMA (21-34%), UDMA (59-72%), and TEGDMA (74-82%) (Gajewski et al., 2012). Similarly, Gonçalves et al. investigated how the conversion degree and flexural strength were affected as the amount of TEGDMA in bis-GMA increased. Consistent with the result found by Gajewski et al., they observed that as the amount of TEGDMA in the structure increased, the conversion degree increased, but the bending strength decreased inversely (Gonçalves et al., 2009).

Barszczewska-Rybarek mentioned the methods of calculating the conversion degrees of photosensitive resins with various monomers via Fourier Transform InfraRed in their study (Barszczewska-Rybarek, 2012). According to Barszczewska-Rybarek, the degree of conversion according to the type of bonds in the monomers can be calculated with three different formulas. Monomers containing aromatic rings can be calculated as shown in Equation 3.1.

$$DC = 1 - \left(\frac{A_{C=C(t)} / A_{Ar(t)}}{A_{C=C(0)} / A_{Ar(0)}} \right) \tag{3.1}$$

Where "DC" indicates conversion degree, "$A_{C=C}$" absorption peak of C=C bond at 1637 cm^{-1} wavenumber, "A_{Ar}" absorption peak of aromatic ring at 1598 cm^{-1}, "t" after polymerization and "0" before polymerization. The conversion degree can be calculated according to the C=O bond in the monomers as in Equation 3.2.

$$DC = 1 - \left(\frac{A_{C=C(t)} / A_{C=O(t)}}{A_{C=C(0)} / A_{C=O(0)}} \right) \tag{3.2}$$

In addition to Equation 3.1, here "$A_{C=O}$" indicates absorption peak of C=O bond at 1718 cm^{-1}. For general resins that do not contain specific bonds, the degree of conversion can be calculated from decrease of absorption peak of C=C bond as seen in Equation 3.3.

$$DC = 1 - \left(\frac{A_{C=C(t)}}{A_{C=C(0)}}\right) \tag{3.3}$$

When the studies on the viscosity values of these resins are examined, it is seen that Tanimoto et al. proved that the viscosity decreases as the amount of TEGDMA in the structure increases in the resin containing UDMA/TEGDMA mixture (Tanimoto et al., 2005). Beun et al. also investigated the viscosity behavior of the bis-GMA/TEGDMA mixture and concluded that the viscosity decreased as the amount of TEGDMA increased. However, in the detailed viscosity analysis by Beun et al., it was observed that the increase in the amount of TEGDMA affected the decrease in viscosity exponentially (Beun et al., 2009). Since it is known that UDMA has 28 Pa.s, bis-GMA 1369 Pa.s and TEGDMA 0.05 Pa.s viscosity values, these are expected results that the viscosity decreases as the amount of TEGDMA in the structure increases (Sideridou & Achilias, 2005).

In a study by Lemon et al., it was observed that monomers containing aromatic rings such as bis-GMA exhibited higher strength than linear chain monomers. The reason for this was confirmed by Lemon et al. that the aromatic rings in the chain form hydrogen bonds with other chains (Lemon et al., 2007).

In the research carried out in the field of nanocomposite resin, it is seen that nanoparticles can be successfully incorporated into such resins. In a study by Szaloki et al. (Szaloki et al., 2013), they aimed to increase the bending strength of the resin by adding reactive polymeric nanoparticles consisting of a mixture of self-synthesized MMA (methyl methacrylate) and TMPTMA (trimethylol propane trimethacrylate) into the bis-GMA-based photocurable resin used in the dental field. In their study, the optimum amount of nanoparticles added into the structure significantly increased the

targeted mechanical properties of the photocurable resins, while negatively increasing the viscosity. Table 3.1 shows some studies on nanocomposite photosensitive resins.

Table 3.1 Studies about photosensitive composite resins

Resin Content	Filler Material	Reference
Bis-GMA/TEGDMA	TiO_2 nanoparticles	(Sun et al., 2011)
Bis-GMA/Cl-bis-GMA/TEGDMA	(none)	(Al-Odayni et al., 2019)
UDMA/SR833s and bis-GMA/TEGDMA	$BaAlSiO_2$ microparticles	(Ding et al., 2016)
UDMA/bis-EMA/TEGDMA	TiO_2 and Fe_3O_4 nanoparticles, SiO_2 microparticles	(Lin et al., 2020)
Bis-GMA/TEGDMA and UDMA/TEGDMA	(none)	(Floyd & Dickens, 2006)
UDMA/DMAEA	Au and SiO_2 nanoparticles	(Burunkova et al., 2013)
UDMA/TEGDMA	SiO_2 nanoparticles silanized with γ-MPS	(Du & Zheng, 2007)
Bis-GMA/HEMA/TEGDMA	Nb_2O_5 microparticles	(Leitune et al., 2013)

In the study of Tolou et al. (N. Bahremandi Tolou et al., 2013), it was seen that TiO_2 nanoparticles in amalgam filling materials increased the antibacterial properties of the structure. In another study (Al-Turaif, 2010), it was observed that the composite material obtained with TiO_2 nanoparticles added to polymers significantly increased the mechanical properties. However, TiO_2 nanoparticles have a tendency to aggregate in the material. This aggregation reduces the surface area of the reinforcement material in the structure in contact with the resin, causing a decrease in the mechanical properties of the material after polymerization. Various surface treatments can be applied to TiO_2 nanoparticles in order to prevent aggregation in these materials. For example, Sun et al. (Sun et al., 2011) aimed to achieve controlled aggregation by coating the surfaces of TiO_2 nanoparticles used as reinforcement material in the polymer matrix with acrylic acid. As a result of their studies, they have seen that the aggregation of nanoparticles can be carried out in a controlled manner.

Gad et al. (M. M. Gad et al., 2019) have seen in their study that the surfaces of nano ZrO_2 particles can be coated with TMSPM (3-(Trimethoxysilyl)propyl methacrylate) for better bonding with the resin matrix. These studies have proven the usability of micro and nano materials as additives in dental applications.

In another study by Gad et al., the effect of SiO_2 nanoparticles on flexural strength was discussed. In the study, it was investigated whether the SiO_2 nanoparticles added to the dental resin had a positive effect on the repaired part, and it was concluded that the homogeneously dispersed particles in the structure made the structure more durable before and after the repair (M. M. A. Gad et al., 2020). Sodagar et al., on the other hand, showed that the SiO_2 and TiO_2 nanoparticles added separately into the structure have a positive effect on the flexural strength, but the addition of SiO_2 and TiO_2 nanoparticles together may have a negative effect as the amount of particles increases (Sodagar et al., 2013).

CHAPTER 4
EXPERIMENTAL STUDIES

4.1 Purpose

As mentioned in the previous sections, 3D printers are highly developed and still developing devices. Among these devices, photochemical-based ones are used in many sectors, especially in dental areas. However, photosensitive resins, which are the starting material of these printers, still need to be developed for use in the dental field. As a result of the literature review, it was determined that the photosensitive resins used in the dental field can be used in 3D printers, but the use of nanocomposite resins with nanoparticle addition in 3D printers has not been found. Based on this, within the scope of this thesis, a matrix material is prepared from bis-GMA, UDMA and TEGDMA monomers, which are frequently preferred in the dental field, and nanocomposite resins are produced for printing in 3D printers by adding TiO_2 and SiO_2 nanoparticles into them. The monomers used in the matrix material were taken ready and the added nanoparticles were produced by sol-gel method using high purity starting materials. In order to examine the behavior of nanoparticles in the matrix material before and after the silanization process, commercial resin, which is similar to the target material, was used to reduce the cost. Finally, the structural, chemical, morphological, organic bond and mechanical properties of the obtained samples were characterized.

4.2 Materials

In this section, monomers, photoinitiators and commercial resin used in the matrix material of nanocomposites, and chemicals used in nanoparticle production and coating are listed. The names, chemical formulas, purity, CAS numbers and suppliers of the materials are shown in Table 4.1. The supplied chemicals were used as purchased, without further purification.

Table 4.1 List of the chemicals used in production of nanocomposites

Materials	Chemical Formula	Purity	CAS Number	Supplier
Bis-GMA	$C_{29}H_{36}O_8$	NA	1565-94-2	Sigma Aldrich
UDMA	$C_{23}H_{38}N_2O_8$	NA	72869-86-4	Sigma Aldrich
TEGDMA	$C_{14}H_{22}O_6$	NA	109-16-0	Sigma Aldrich
TPO	$C_{22}H_{21}O_2P$	NA	75980-60-8	Sigma Aldrich
Commercial Resin	NA	NA	NA	AnyCubic Co.
Titanium (IV) Isopropoxide (TTIP)	$C_{12}H_{28}O_4Ti$	$\geq$99.9%	546-68-9	Sigma Aldrich
Tetraethyl Orthosilicate (TEOS)	$C_8H_{20}O_4Si$	$\geq$97.5%	78-10-4	Sigma Aldrich
3-(Trimethoxysilyl) propyl methacrylate (MPS)	$C_{10}H_{20}O_5Si$	$\geq$98%	2530-85-0	Sigma Aldrich
Triethanol Amine (TEA)	$C_6H_{15}NO_3$	≥99%	102-71-6	Sigma Aldrich
Ethanol (EtOH)	C_2H_5OH	$\geq$99.9%	64-17-5	ISOLAB
Isopropanol (IPA)	$(CH_3)_2CHOH$	$\geq$99.9%	67-63-0	ISOLAB
Ammonia	NH_4OH	$\geq$31.5%	1336-21-6	Sigma Aldrich

4.3 Methods

The studies carried out within the scope of this thesis are, respectively, the production of matrix materials, the production of nanoparticles, the production of composites prepared with commercial resin and the production of final composite resins. The flow chart of the experimental studies carried out within the scope of the thesis is shown in Figure 4.1. The characterization tests shown in the diagram were applied to each produced sample.

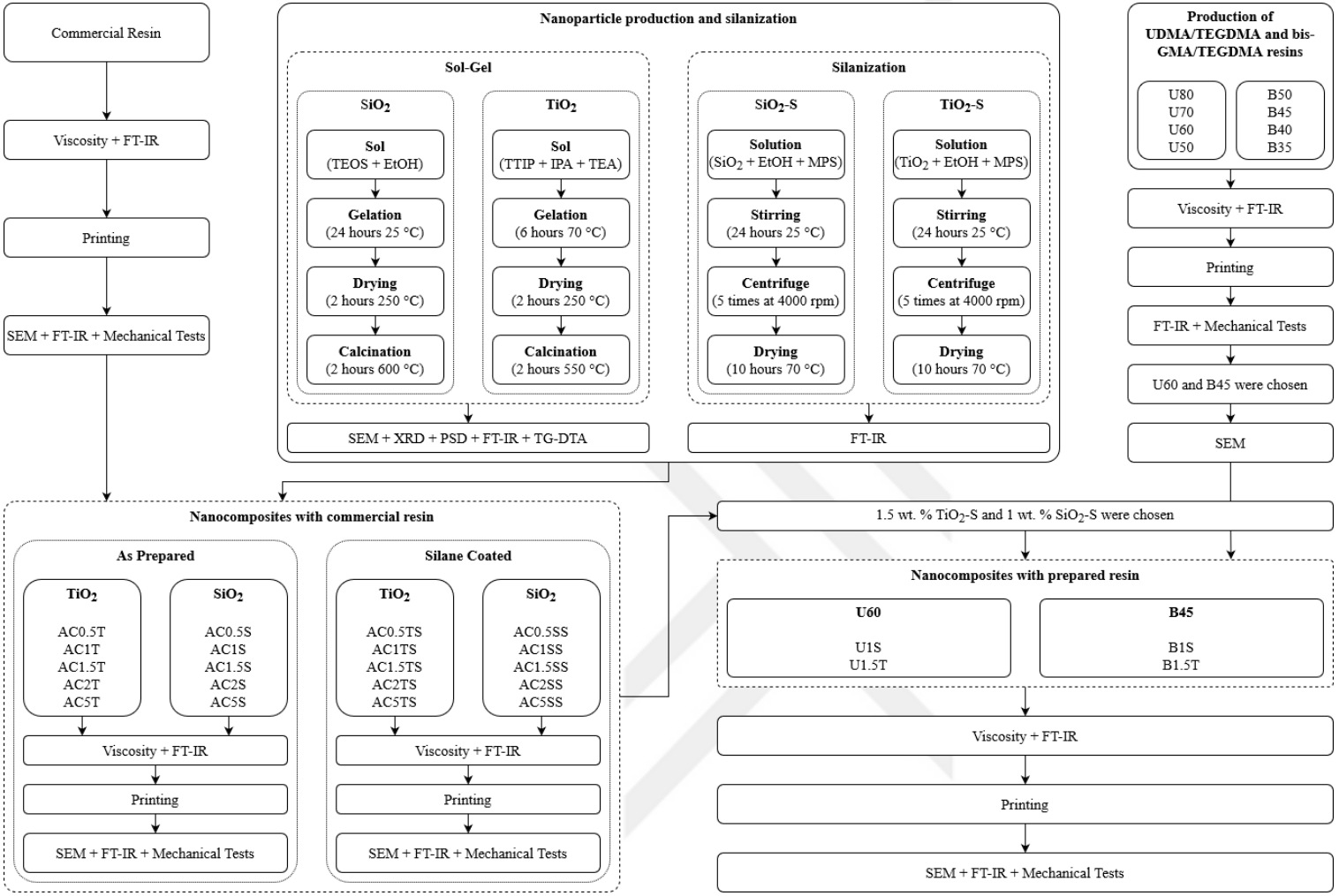


Figure 4.1 Flow chart of the production and characterization of the thesis

Different ratios of UDMA (Urethane dimethacrylate), bis-GMA (Bisphenol-A glycidyl dimethacrylate) and TEGDMA (Triethylene glycol dimethacrylate) mixtures were used as matrix material. Since the printer used in printing processes has a light source that emits light at a wavelength of 405 nm, TPO (2,4,6-trimethylbenzoyl diphenyl phosphine oxide) which has a wide photosensitivity in the UV-A region (380 – 420 nm) was used as a photoinitiator. The amount of photoinitiator used in the structure can have a negative effect during printing. In a study by Cheng et al., it was determined that as the amount of TPO in the resin increased above 2%, the layer thickness of the resin that could be cured in single exposure decreased (Cheng et al., 2020). In order not to adversely affect the curing depth and increase the cost during printing, 2% TPO by weight was used as the photoinitiator to add photosensitivity to the resins. The contents and naming of the prepared resins are shown in Table 4.2. Nanoparticles were added to the mixtures that showed optimum strength and conversion degree from the obtained resins at the determined rates.

Table 4.2 Contents and naming of the prepared mixtures

Name	UDMA (wt. %)	Bis-GMA (wt. %)	TEGDMA (wt. %)	TPO (wt. %)
U80	80	0	20	2
U70	70	0	30	2
U60	60	0	40	2
U50	50	0	50	2
B50	0	50	50	2
B45	0	45	55	2
B40	0	40	60	2
B35	0	35	65	2

The production of TiO_2 nanoparticles was carried out by the sol-gel method. First of all, 15 ml of TTIP (Titanium (IV) isopropoxide) as TiO_2 starting material was added into 100 ml of IPA (isopropyl alcohol) in order to form a homogeneous solution, in a way that it would not come into contact with air in order to prevent oxidation. Then, in order to control the particle size, 7.5 ml of TEA (Triethanolamine) was added and mixed in a magnetic stirrer for 2 hours in order to completely disperse the particles and obtain a transparent mixture. Turbidimeter measurement was made to control the

transparency of the solutions. After obtaining a transparent solution with a turbidity value of 1.44 NTU, distilled water was added until the pH value was 9.5 in order to accelerate the gelation process and stirred for another half an hour. It was then left to age at 70 °C for 6 hours to complete gelation. After gelation, TG/DTA analysis was performed to determine the heat treatment parameters. The gel obtained as a result of TG/DTA analysis was dried at 250 °C for 2 hours and calcined at 550 °C for 2 hours. After these processes, nanoparticles were produced successfully.

The production of SiO_2 nanoparticles was also done by the sol-gel method. Sol was prepared using TEOS (Tetraethyl Orthosilicate) and EtOH (Ethanol). 4.5 ml of TEOS was added slowly into 40 ml of EtOH without contacting with air. The solution was stirred on a magnetic stirrer for 2 hours to obtain a transparent solution. The turbidity value of the prepared solution was measured with a turbidimeter. 3 ml of 25% ammonia solution was added to the solution, which had a turbidity value of 1.39 NTU. The solution with a pH value of 9 was stirred for an additional 2 hours on a magnetic stirrer for homogenizing and then aged at room temperature overnight. The resulting gel was then analyzed in DTA/TG to determine the calcination temperature. The thermally analyzed gel was dried at 250 °C for 2 hours and calcined at 600 °C for 2 hours. Finally, nanoparticles were successfully produced.

MPS (3-(trimethoxysilyl)propylmethacrylate) was used for the silanization of the produced TiO_2 and SiO_2 nanoparticles. For TiO_2, 5 g of TiO_2 was dispersed in 150 ml of EtOH. 3.2 ml of MPS adjusted according to the formula in Equation 2.4 was added to the dispersant (Aati et al., 2021). In order to accelerate the adhesion of the silane agent to the particle surface, 25% ammonia solution was added to the solution until the pH value was 9. For SiO_2, 5 g of SiO_2 was dispersed in 150 ml of EtOH. It was added to 5 ml of MPS dispersant, the amount of which was adjusted with the help of Equation 2.4 in the same way as TiO_2 (Aati et al., 2021). A 25% ammonia solution was added to the solution until the pH value was 9. The resulting mixtures were stirred at room temperature overnight. The powders in the mixtures were then washed with ethanol and centrifuged 5 times at 4000 rpm. With this process, silane-coated powders

(named TiO_2-S and SiO_2-S) were purified from residual MPS and other organic solvents. Finally, the powders were dried in an oven at 70 °C for 10 hours.

In order to reduce the cost, the effect of the nanoparticles on the resins and their behavior in the resin were investigated using a commercial resin (abbreviated as AC later in the thesis) prepared by AnyCubic Co., China. The proportions and naming of the powders added to the commercial resin are given in Table 4.3.

Table 4.3 Proportions and naming of the composites made by commercial resin

Name	TiO_2 (wt. %)	TiO_2-S (wt. %)	Name	SiO_2 (wt. %)	SiO_2-S (wt. %)
AC0.5T	0,5	0	**AC0.5S**	0,5	0
AC1T	1	0	**AC1S**	1	0
AC1.5T	1,5	0	**AC1.5S**	1,5	0
AC2T	2	0	**AC2S**	2	0
AC5T	5	0	**AC5S**	5	0
AC0.5TS	0	0,5	**AC0.5SS**	0	0,5
AC1TS	0	1	**AC1SS**	0	1
AC1.5TS	0	1,5	**AC1.5SS**	0	1,5
AC2TS	0	2	**AC2SS**	0	2
AC5TS	0	5	**AC5SS**	0	5

With the prepared composites, the effect of the silane coating process on the distribution of the powders in the matrix material was investigated, and the amount of powder that provides the optimum strength and conversion degree was determined. Then, the contribution of the determined amount of powders to the structure was investigated by mixing with a predetermined ratio of UDMA and bis-GMA containing matrix material.

Creality Halot-Sky CL89 brand DLP type 3D printer with 405 nm UV-light source (Figure 4.2a) was used for printing. During the printing process, the layer thickness was set to 50 µm, the exposure time for the first 4 layers was 60 seconds, and the exposure time for the other layers was 5 seconds. Each completed sample was washed for 10 minutes in IPA using the Creality UW-02 Washing/Curing Machine (Figure 4.2b) and post-cured for 60 minutes. Thanks to the applied washing and post-curing

processes, the residual monomers remaining on the sample were removed and the bonding of the unbonded groups in the structure was ensured.



(a) (b)

Figure 4.2 (a) 3D printer and (b) wash and cure machine

4.4 Characterizations

4.4.1 X-Ray Diffraction (XRD)

X-ray diffraction (XRD) is one of the most common techniques used to determine the crystal structures and phases of powder and solid materials. The XRD device characterizes the material according to the diffraction of this beam by sending an X-ray onto the sample placed inside. The transmitted beam hits the sample and is refracted and scattered. The diffraction angles of the scattered rays are associated with Bragg's law (Equation 4.1) to obtain a diffraction graph.

$$n * \lambda = 2 * d * \sin\theta \tag{4.1}$$

Where “n” is an integer, “λ” is the wavelength of X-ray, “d” is the distance between planes and “θ” is the angle between plane and incoming X-ray. Bragg's law (Equation 4.X) is the formulation of the diffraction behavior of a wave sent to the plane at

different lattice parameters. The obtained diffraction graph represents the crystal lattice structure of the material and phase analysis is performed according to these lattice structures. Accordingly, the working principle of the XRD device can be schematized as in Figure 4.3.

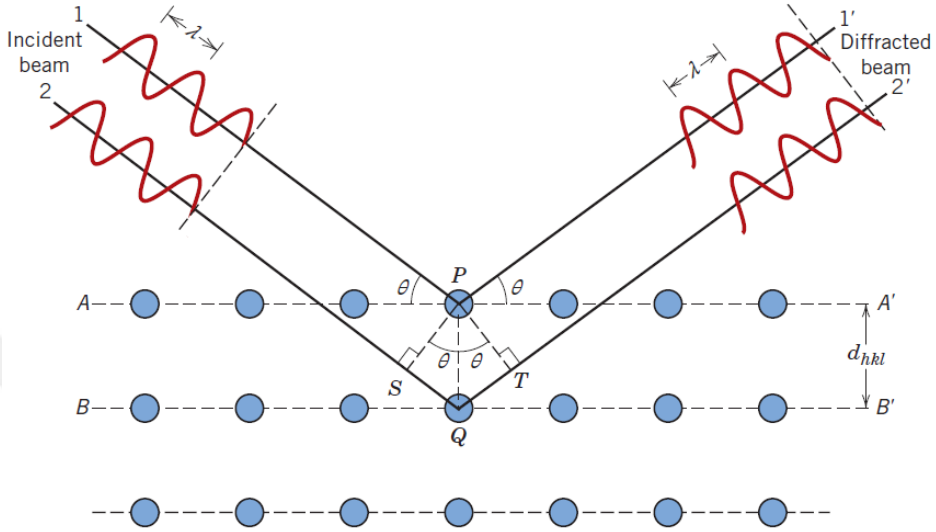


Figure 4.3 Working principle of XRD device (Callister & Rethwisch, 2018)

Within the scope of this thesis, the phase and crystal structures of composites, TiO_2 and SiO_2 nanoparticles were determined by an X-ray diffractometer (Thermo Scientific ARL X'TRA). The XRD measurement was performed using Cu-Kα radiation (1.5406 Å) to obtain diffraction patterns for 2θ value. XRD data was recorded at a scan rate of 2 °/min in the range of $20° \leq 2\theta \leq 80°$ for all samples.

4.4.2 Scanning Electron Microscopy (SEM)

Scanning electron microscope is a method used to examine the surface morphology of solid bulk and powder materials. As can be seen in Figure 4.4, the material surface is scanned with a high-energy electron beam sent to the sample surface with the help of lenses and coils inside. As a result of this scanning, two different data are obtained according to the interaction of the electrons sent to the material surface. These are secondary electrons (SE) and backscattered electrons (BSE). Each resulting data gives information about a different property of the material.

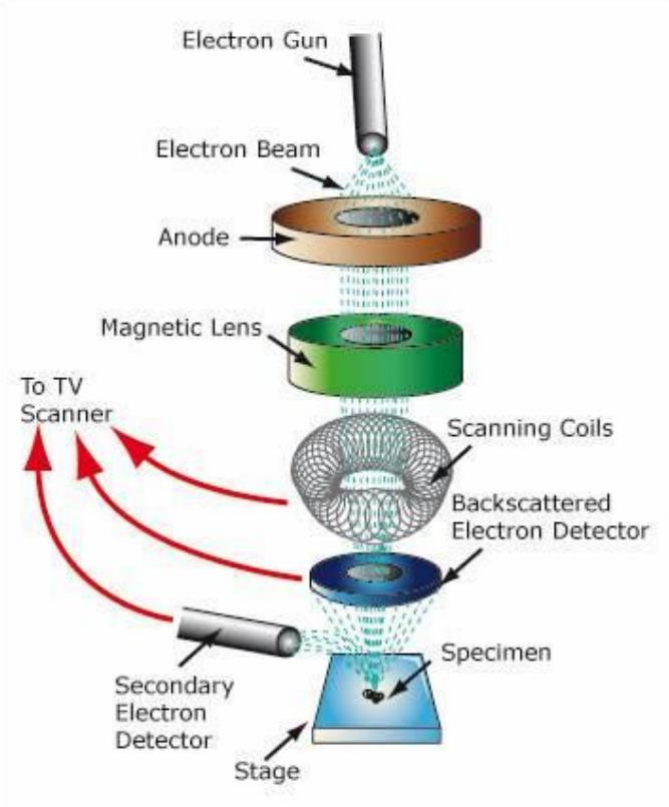


Figure 4.4 Scheme of a scanning electron microscope (Siek, 2015)

Secondary electrons are electrons that are detached from the material surface as a result of primary electrons sent from the gun to the material surface. These electrons are used to obtain a high resolution morphological image of the material surface. Back-scattered electrons are electrons that are sent from the electron gun to the surface of the material and bounce back from the surface. By using the bounce intensity values of these electrons from the material surface, information about the existence of different phases on the material surface can be obtained. According to the intensity of the backscattered electrons, a contrast difference occurs between the images of different phases and the distribution of the phases is obtained.

In this thesis, surface morphology and particle distribution of composites and nanoparticles were examined by Scanning Electron Microscopy (Zeiss, Gemini). Secondary electron (SE) mode was used at 5 kV voltage for surface morphology of nanoparticles, and back-scattered electron (BSE) mode was used at 15 kV voltage for

particle distribution of composites. Analyzes were performed at 5K, 10K, 25K, 50K and 100K magnifications.

4.4.3 X-Ray Photoelectron Spectroscopy (XPS)

X-ray photoelectron spectroscopy (XPS) is a characterization method that provides information about the element content, electronic and chemical structure of the material. As seen in Figure 4.5, X-rays sent to the material surface penetrate up to 10 nm depth of the material surface and cause the electrons in that region to spread with the photoelectric effect. With the emitted electrons, the number of electrons and the amount of kinetic energy are determined. Generally, Al-Kα (1486.6 eV) or Mg-Kα (1253.6 eV) rays are used (Moulder et al., 1992). XPS analysis is performed in an ultra-high vacuum (UHV) environment to avoid environmental pollution and noise.

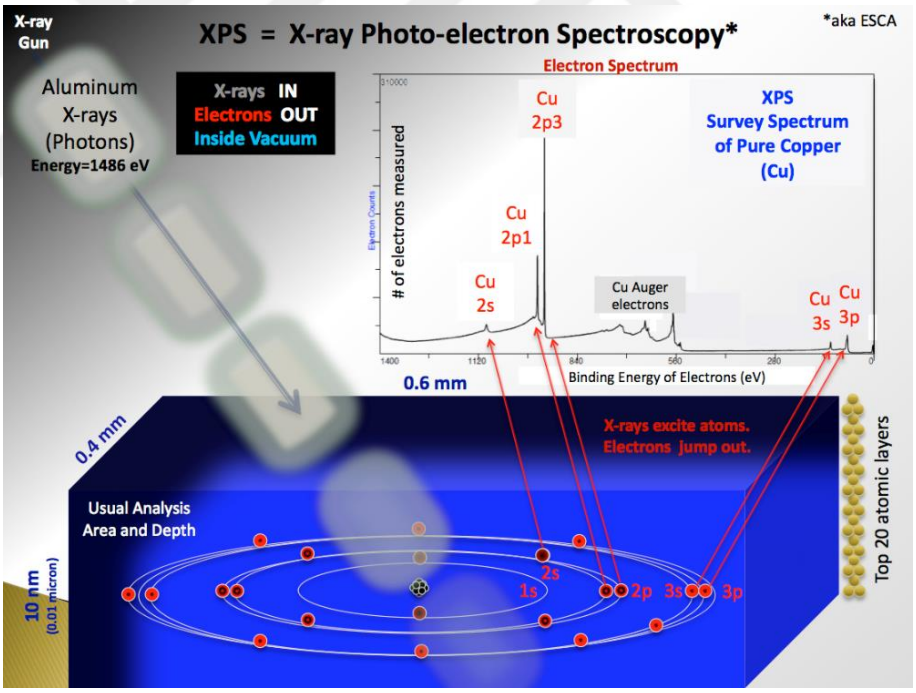


Figure 4.5 Working principle of XPS (Crist, 2011)

In XPS analysis, elements with atomic number 3 (Lithium, Li) and above can be analyzed. Hydrogen (H) and Helium (He) elements, whose atomic numbers are 1 and 2, respectively, cannot be detected by the XPS device because the diameters of their orbitals are very low (Moulder et al., 1992).

Elemental composition of composites were performed by X-ray photoelectron spectroscopy (Thermo Scientific K-Alpha). Since the sent X-rays interact with the electrons on the surface, the XPS device only gives information about the elemental structure, chemical state, empirical formula and electronic state on the surface. The XPS measurement was performed with a monochromatic Al-Kα (1486.7 eV) X-ray source and a beam size of 400 µm in diameter. XPS scanning was performed with a scanning rate of 1 eV between -10 and 1350 eV by applying of 150 eV pass energy for survey data. Elemental scan was performed with a scanning rate of 0.1 eV by applying of 30 eV pass energy. Each sample was scanned from a single point 15 times and 10 times for survey data and element data, respectively.

4.4.4 Fourier Transform Infrared Spectroscopy (FT-IR)

In Fourier transform infrared spectroscopy, infrared rays are sent on the material and various data are obtained according to the reactions of the chemical bonds in the material (Figure 4.6). FT-IR works on the principle of the Fourier transform. The interferogram is determined by collecting the beam transmitted to the sample in FT-IR spectroscopy. The spectrum is plotted according to the wave number corresponding to the transmittance or absorbance values. This conversion is performed automatically and the spectrum is displayed. The size of the peaks in the spectrum is a direct indication of the amount of material present (Ramaiah et al., 2017).

Chemical bonds in the material absorb some of the transmitted light, giving reactions such as stretching, vibration and bending. Depending on the severity of these reactions, a characteristic spectrum is obtained for each material. Since each bond between atoms is triggered in a different type and intensity, the type of chemical bonds in the material and the elements they belong to can be determined by FT-IR analysis.

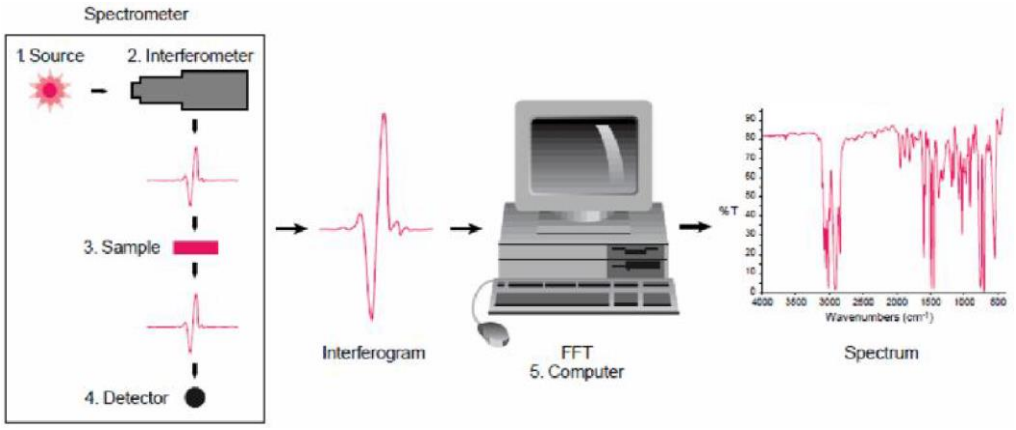


Figure 4.6 Working principle of FT-IR (Ramaiah et al., 2017)

Fourier Transform Infrared Spectroscopy (Thermo Scientific NICOLET iS10) was applied to determine the organic bond structures and conversion degrees of the samples and to control the silanization process of the nanoparticles. FT-IR was performed with 32 scans for each sample in the wavenumber range of 4000 to 500 cm^{-1} with absorption spectrum.

4.4.5 Particle Size Distribution (PSD)

Particle size distribution analysis is used to determine the size of the particles produced and to what size the particles are concentrated. Powders dispersed in a suitable dispersant are analyzed in a permeable tube. Quantitative data are obtained according to the diffraction by passing rays through the prepared sample.

Particle size distribution measurement (Malvern, Zeta Sizer Nano ZS90) was performed to observe the particle size and distribution of nanoparticles by dynamic light scattering technique. For the measurement, the powders were dispersed in IPA by ultrasonic bath for 30 minutes and placed in the device and the measurement was carried out at room temperature. The obtained data are presented by taking the average of 10 measurements.

4.4.6 Viscosimetry

Rheometer is a laboratory device used to measure the fluidity of liquids under certain forces. It is generally used when a single viscosity value is insufficient to explain the rheological properties of the liquid. However, it can also act as a viscometer in liquids with unknown properties. The viscometer is used to measure the viscosity of the liquid. Whether a liquid exhibits thixotropic or non-Newtonian property can be determined by this analysis method.

Viscosities of the resins were measured with a rheometer (Bohlin Instruments CVO Rheometer System) to determine whether they could be used with a 3D printer. Cone and plane method was used in the measurements. The angle of the cone used in the analysis was 2° and the distance between two planes was set to 100 µm. Shear rate range was set between 0 - 1000 (1/s), and the measurement was continued for 120 seconds by taking one measurement per second at room temperature.

4.4.7 Thermogravimetric and Differential Thermal Analysis (TG/DTA)

As a result of thermal analysis, the behaviors of materials such as decomposition, combustion and phase transformation at different temperatures are determined. As a result of these events, the heat exchange in the environment and the mass loss data in the material are collected and information about the thermal properties of the material is obtained. These analyzes are also carried out by differential thermal analysis (DTA) and thermogravimetry (TG) methods. The DTA method is a characterization method that measures the heat exchange of the material with the environment with changing temperature. In the TG analysis, the mass loss of the material with increasing temperature is examined. When these data are examined together, the types of reactions that occur in the material as a result of heat exchanges and mass losses are determined and how the material has undergone a change is interpreted.

In this thesis, thermogravimetric and differential thermal analysis (PerkinElmer, STA8000) were carried out to determine the heat treatment parameters of the

nanoparticles. The test was carried out in a nitrogen atmosphere, the temperature range was set 0 – 1000 °C and the rate of increase was determined as 5 °C/min.

4.4.8 Mechanical Tests

Mechanical tests are applied to determine the behavior of materials under the forces that they may be exposed to in areas of use. As a result of the tensile and bending tests, the yield, tensile, flexural and fracture strengths of the materials, the modulus of elasticity, the amount of elongation under a certain amount of load and the amount of energy it can absorb (toughness and resilience) under these loads can be calculated. In this thesis, tensile and three-point bending tests of the composite samples were carried out to determine the yield and flexural strengths and modulus of elasticity of the materials.

4.4.8.1 Tensile Test

As can be seen in Figure 4.7, the tensile test is applied according to the procedure of drawing cylindrical or rectangular specimens clamped between two holding grips at the speeds specified in the standards. While one of the grips is stationary, the other grip moves in the Z-axis in the direction of pulling the material. During this movement, the load cell connected to one of the grips records the force generated by the specimen resisting the movement. With the extensometer, the deformation of the material during this movement is recorded.

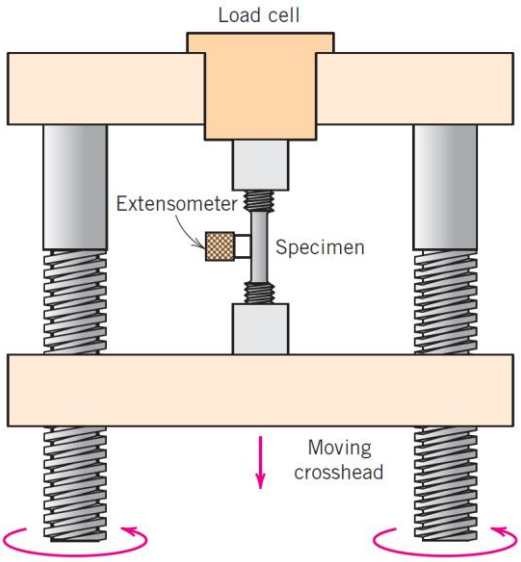


Figure 4.7 Scheme of the tensile testing device (Callister & Rethwisch, 2018)

The tests of the samples placed in the grips of the tensile device (Shimadzu AG-IS) were carried out at a speed of 1 mm/min, and the yield strength and modulus of elasticity of the samples were determined. The applied load and the amount of elongation during the test were recorded by the load cell and video extensometer, respectively. The engineering stress of the samples was calculated as formula given in Equation 4.2.

$$\sigma = \frac{F}{A_0} \tag{4.2}$$

Where "σ" is the instantaneous stress, "F" is the instantaneous load, and "A_0" is the cross-sectional area just before the test of the specimen. The unit of the stress in SI unit system is megapascals (MPa). The strain of the samples was also calculated as follows (Equation 4.3).

$$\varepsilon = \frac{l - l_0}{l_0} \tag{4.3}$$

Where "ε" is the engineering strain, "l" is the instantaneous length and l_0 is the length just before the test of the specimen.

4.4.8.2 Three-Point Bending Test

The three-point bending test is performed by subjecting cylindrical or rectangular specimens placed on two supports to force from a point opposite the supports, as shown in Figure 4.8. The point where the force is applied must be equidistant from both supports. Similar to the tensile test, the point applying force is moved towards the material at the speed specified in the standards and the resistance applied by the material is recorded with the load cell.

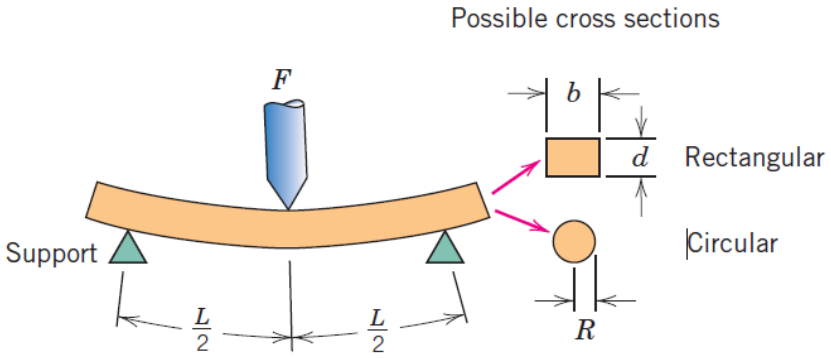


Figure 4.8 Scheme of the three-point bending test (Callister & Rethwisch, 2018)

The three-point bending test was carried out to determine the flexural strength of the composite specimens. The bending process was carried out at a speed of 2 mm/min. Cylindrical supports are used at the bending device (Shimadzu AG-50kNG), which is based on the same working principle as the tensile device. The span distance was set as 50 mm. The applied load until the fracture was recorded by the load cell and the flexural strength was calculated as Equation 4.2 (Al-Turaif, 2010).

$$\sigma_f = \frac{3*F*L}{2*b*d^2} \tag{4.4}$$

Where "σ_f" is the flexural strength, "P" is the load at fracture, "L" is the span distance, "b" is the width and "d" is the thickness of the specimen. Three samples were used for each composition.

CHAPTER 5
RESULTS AND DISCUSSION

The characterization results and comments of the intermediate products produced in this part of the thesis were arranged separately, and the comments were given in the order described in method section and shown in Figure 4.1.

5.1 Characterization of Nanoparticles

5.1.1 Thermal Properties

The heat treatment parameters of the produced nanoparticles were determined by TG/DTA analysis. Nanoparticles were taken into the analysis in gel form and according to the results of this analysis, they were subjected to drying and calcination processes.

The graph of weight loss and heat flow, depending on the temperature obtained as a result of the TG/DTA analysis of TiO_2 nanoparticles, is shown in Figure 5.1. The endotermic peak around 70 °C shows us that the water in the structure is moving away. The wide exothermic peak between 160 °C and 360 °C indicates that the organics in the structure are burned away. In reference to study of Chang et al., it was determined that the endothermic peak at 620 °C symbolizes the transition of TiO_2 from the amorphous structure to the crystalline anatase phase (Chang et al., 2017). Subramani et al. suggested in their study that the sharp endothermic peak at 820 °C symbolizes the anatase-to-rutile transition. (Subramani et al., 2020). Based on this, it was decided to carry out the calcination process at 550 °C in order to prevent the formation of the rutile phase in the powders and to completely remove the impurities in the structure.

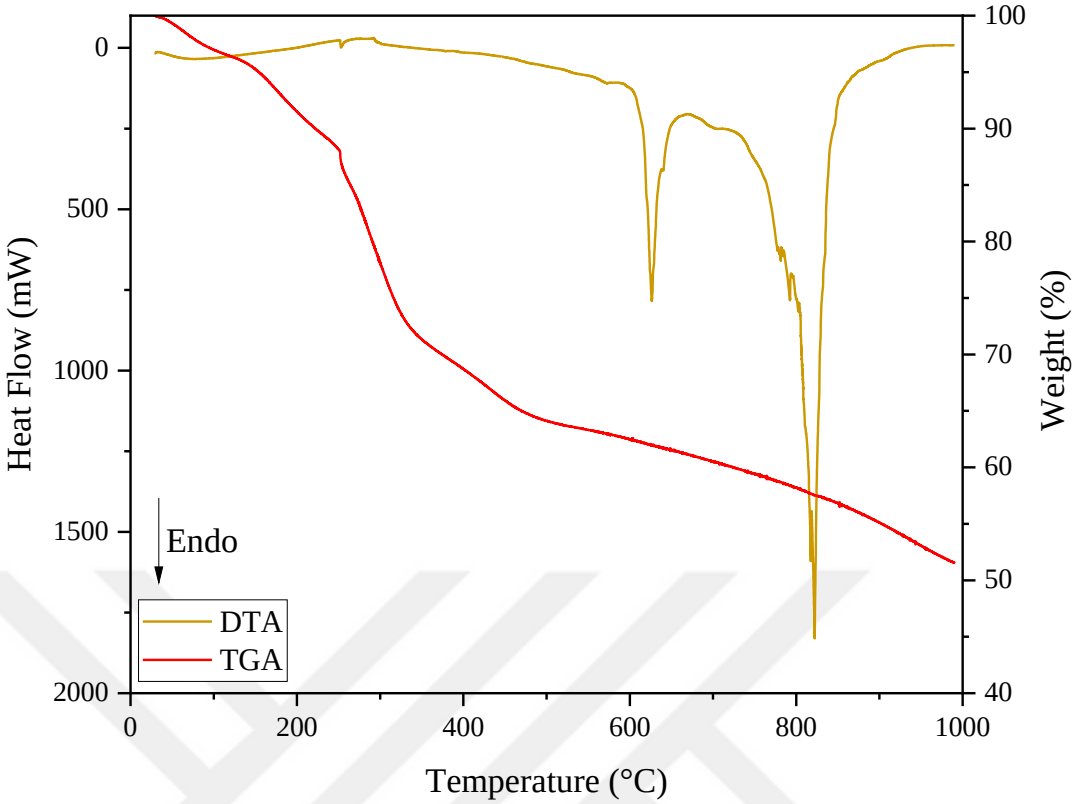


Figure 5.1 TG/DTA analysis of TiO_2 nanoparticles

The temperature-dependent weight loss and heat flow graph of the produced SiO_2 nanoparticles are given in Figure 5.2. When the graph is examined, as in Figure 5.1, the endothermic peak around 70 °C means dehydration and the wide exothermic peak between 160 °C and 360 °C burning organic components. Zornoza-Indart and Lopez-Arce is mentioned that the wide endothermic peak around 600 °C indicates that the OH groups in silanol (SiOH) are removed (Zornoza-Indart & López-Arce, 2015). Since there is no phase transition in the structure and the weight loss starts to become linear from 600 °C, it was approved to carry out the calcination process of the produced particles at 600 °C.

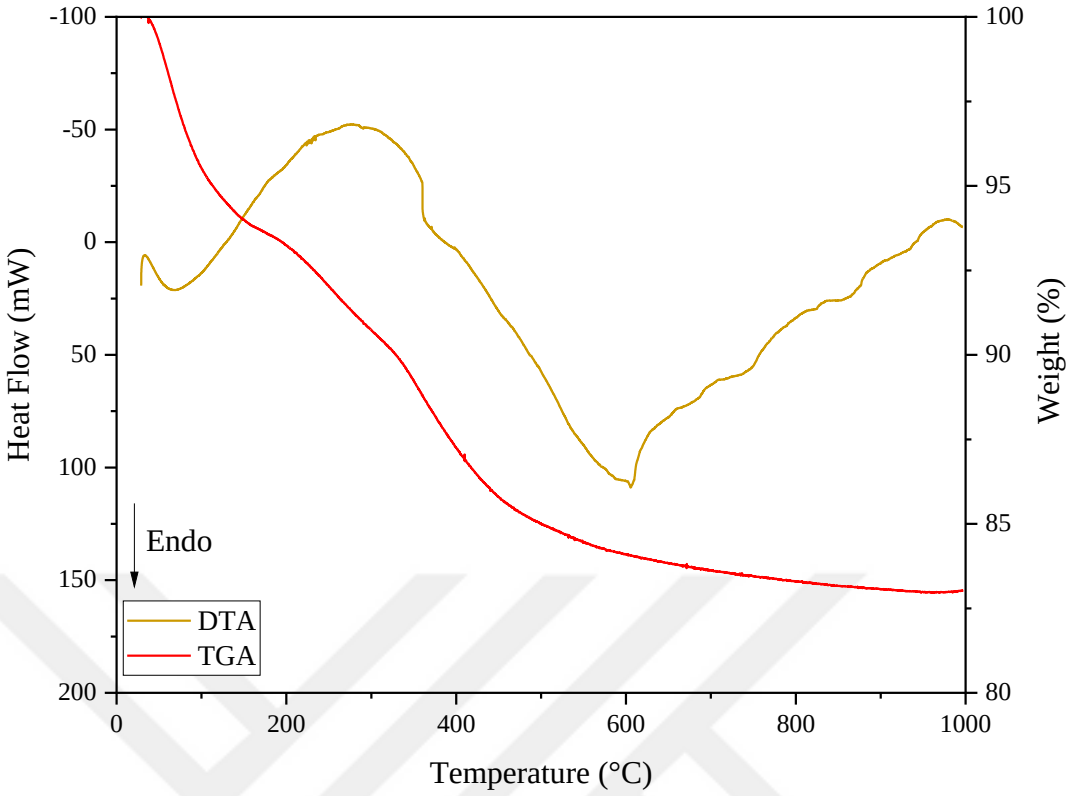


Figure 5.2 TG/DTA analysis of SiO_2 nanoparticles

5.1.2 Structural Properties

The XRD results of the produced TiO_2 nanoparticles are shown in Figure 5.3. When the graph is examined, it is seen that the produced nanoparticles consist of anatase and rutile phases with tetragonal crystal structure. As compared with JCPDS cards, peaks marked with a black heart indicate the anatase phase (JCPDS: 21-1272), and those with a red diamond indicate the rutile phase (JCPDS: 21-1276). The results obtained are found to be similar when compared with the literature (Al-Amin et al., 2016; N. Bahremandi Tolou et al., 2013).

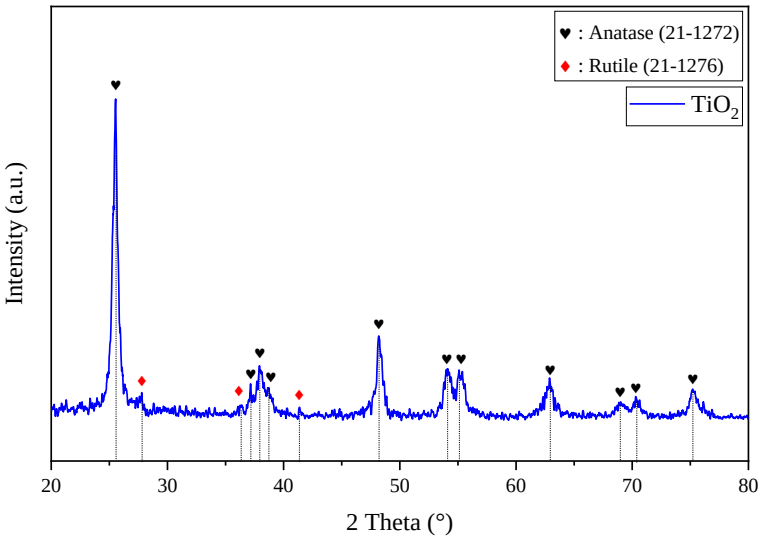


Figure 5.3 XRD chart of TiO_2 nanoparticles

The average crystallite size of the obtained nanoparticles is calculated based on the highest peak (101) of the anatase phase, using the Debye-Scherrer formula given in Equation 5.1 (Kasapoğlu et al., 2007).

$$D = \frac{K*\lambda}{\beta*cos\ \theta} \tag{5.1}$$

Where "D" is the crystallite size, "K" is the Scherrer constant (0.9), "θ" is diffraction angle in radians, "β" is the full-width at half-maximum (FWHM) of the peak in radians and "λ" is the wavelength of the X-Ray (Cu Kα = 0.15406 nm). The crystallite size of the obtained particles is calculated as 13.28 nm, while details are presented at Table 5.1.

Table 5.1 Crystallite size calculation of TiO_2 nanoparticles

2θ of (101) peak	**FWHM (rad)**	**Crystallite Size (nm)**
25.54	0.0107052	13.28

The XRD graph of the produced SiO_2 nanoparticles is shown in Figure 5.4. The large peak seen as a result of the analysis shows that the SiO_2 particles obtained do not form a crystal structure, that is, they are in an amorphous structure (Varshney et al., 2022). Likewise, the absence of other peaks in the graph indicates that there are no

organics and salts remaining from the production process in the structure (Dubey et al., 2015).

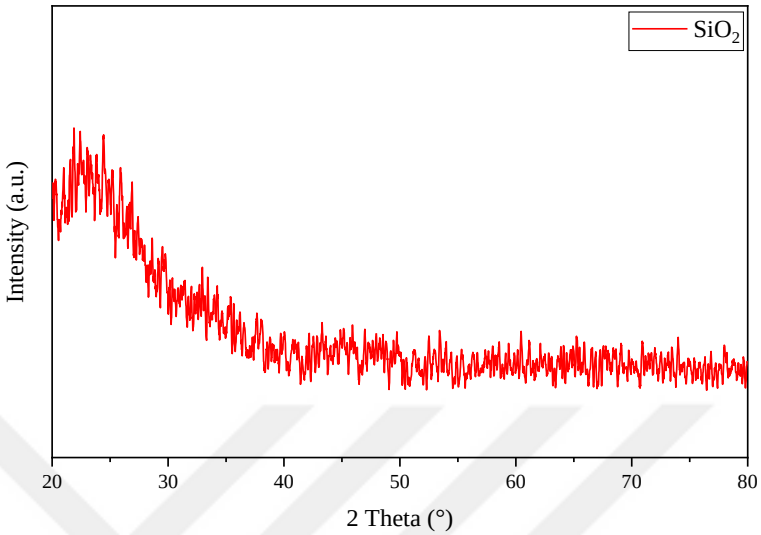


Figure 5.4 XRD chart of the SiO_2 nanoparticles

5.1.3 Organic Bond Structures

With FT-IR analysis, the silanization process of TiO_2 and SiO_2 nanoparticles were confirmed. The results of the FT-IR analysis performed to examine the organic bonds of TiO_2 and SiO_2 nanoparticles before and after silanization are shown in Figure 5.5 and 5.6, respectively.

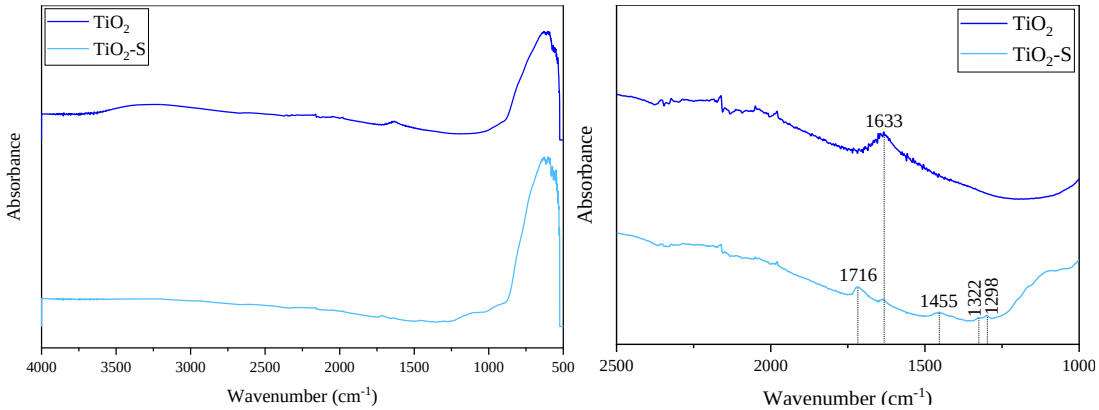


Figure 5.5 FT-IR graph of TiO_2 and TiO_2-S (a) between 4000 and 500 cm^{-1} wavenumber and (b) magnified between 2500 and 1000 cm^{-1}

When the analysis of TiO_2 is examined, it is observed that apart from the common peak in wave number of 1633 cm^{-1}, peaks are also obtained in wave numbers of 1716 cm^{-1}, 1455 cm^{-1}, 1322 cm^{-1} and 1298 cm^{-1} in the silane-coated (TiO_2-S) sample. It is determined that the peak at the common wave number of 1633 cm^{-1} belongs to the water trapped in the TiO_2 structure (Siddiquey et al., 2007). The 1716 cm^{-1} peak in the graph belongs to the TiO_2-S is caused by the C=O vibration in the methacrylate group in the MPS. In the same way, it was determined that the C=C vibration in the methacrylate group may overlap with the peak of 1633 cm^{-1} wave number of water (Rong et al., 2005; Siddiquey et al., 2007). It is confirmed that the other 1455 cm^{-1} peak in the structure belonged to C-H stretching in MPS, while 1322 and 1298 cm^{-1} peaks belonged to C-O and C-C stretching, respectively (Nguyen et al., 2020). The determination of these bonds as a result of the FT-IR analysis proves that the silanization process is successful.

When the FT-IR graph of SiO_2 nanoparticles is examined, peaks are seen in the wave number of 795 and 1046 cm^{-1}, which are also common in both graphs. Since these peaks belong to O-Si-O bending and Si-O-Si stretch bond, respectively, as it is expected for both samples (Moncada et al., 2007). It is observed that peaks at wave numbers of 1716, 1633 and 1455 cm^{-1} are obtained in the silane coated sample (SiO_2-S), as in the TiO_2-S sample. Likewise, as mentioned above, these peaks show us that the silanization process is also successful for SiO_2 nanoparticles.

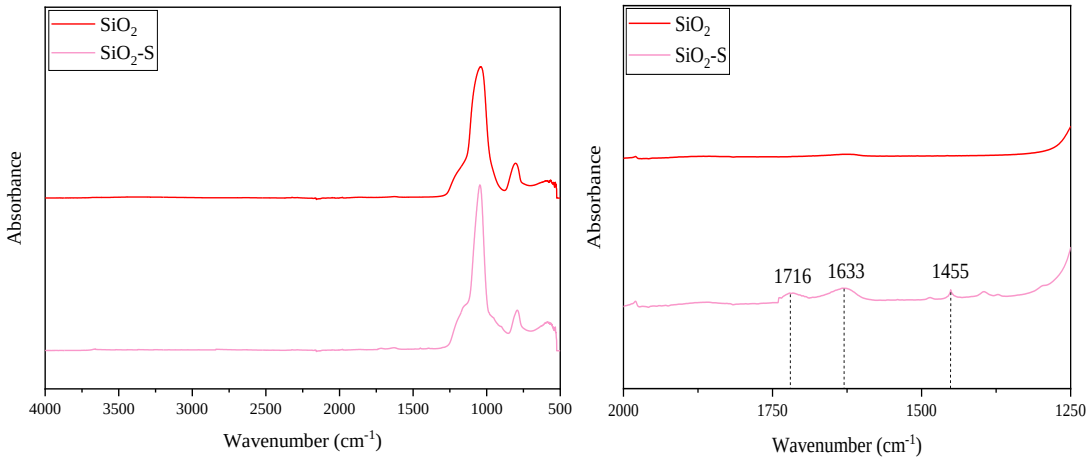


Figure 5.6 FT-IR graph of SiO_2 and SiO_2-S (a) between 4000 and 500 cm^{-1} wavenumber and (b) magnified between 2000 and 1250 cm^{-1}

5.1.4 Morphological Properties

A scanning electron microscope (SEM) was used for the morphological examination of the powders, and the topographic images of the powders were examined in the secondary electron mode. The resulting images are shown in Figure 5.7. The SEM analysis of the nanoparticles was run before the silanization process to see actual shape and size. When the images are examined, it is seen that the large particles are actually agglomerated nanoparticles. The presence of randomly dispersed particles in the 100 – 200 nm size range for TiO_2 and 40 – 100 nm size range for SiO_2 in the images shows that nano-sized and spherical-shaped particles are produced.

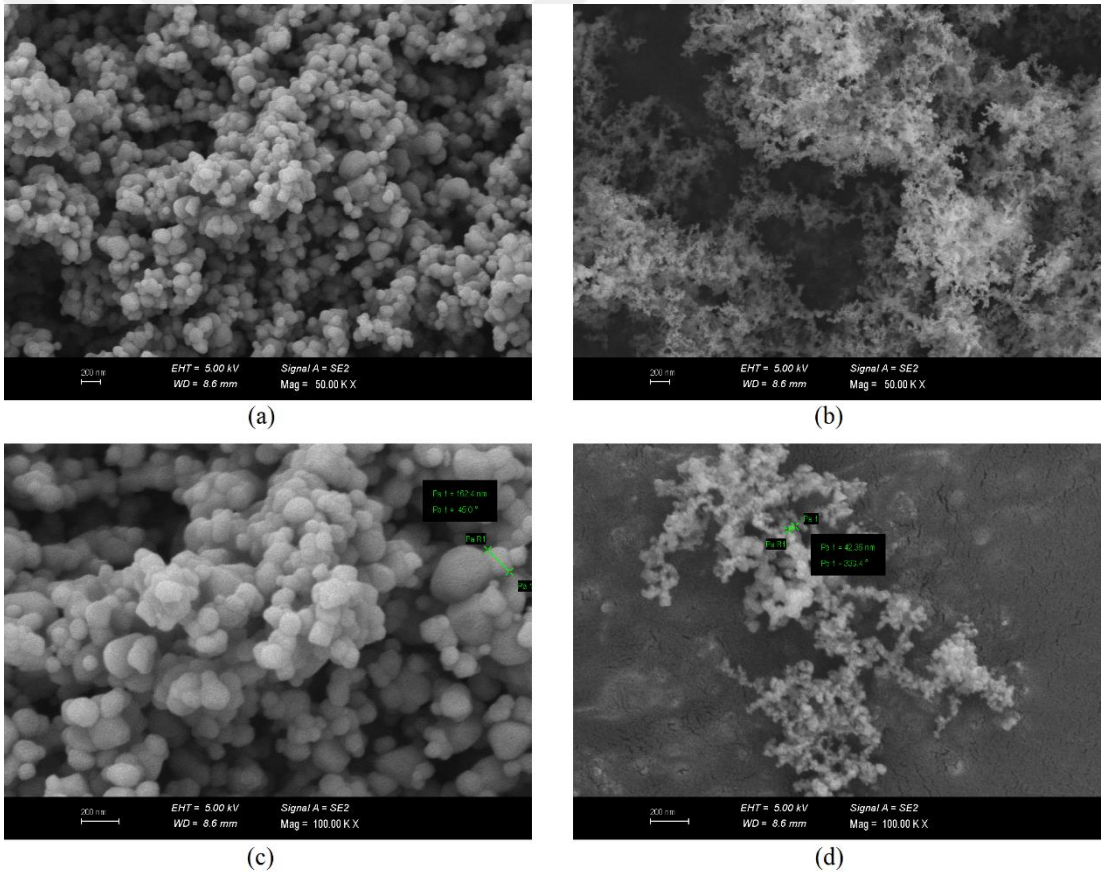


Figure 5.7 SEM images at 50K magnification for (a) TiO_2 and (b) SiO_2, 100K magnification for (c) TiO_2 and (d) SiO_2

5.1.5 Particle Size Properties

Particle size distribution graphs of TiO_2 and SiO_2 nanoparticles dispersed in IPA are shown in Figure 5.8. When the graphs are examined, it is seen that the particles are in nano size. It is seen that the PdI values of TiO_2 and SiO_2 nanoparticles are 0.495 and 0.198, respectively. Since these values are higher than the threshold value of 0.1, it is seen that the particles have polydisperse behavior (Raval et al., 2019). When the particle sizes obtained are compared with the SEM images, it is seen that the TiO_2 sizes are consistent, but the SiO_2 sizes are larger than the SEM images (Figure 5.7). It was concluded that this difference between the two analyzes was due to the fact that the SiO_2 powders in the dispersant continued to agglomerate and were not dispersed homogeneously during the PSD analysis. Peter et al. (Peters et al., 2014) confirmed this situation by showing that small-dimensional nanoparticles can also agglomerate in the dispersant in their study.

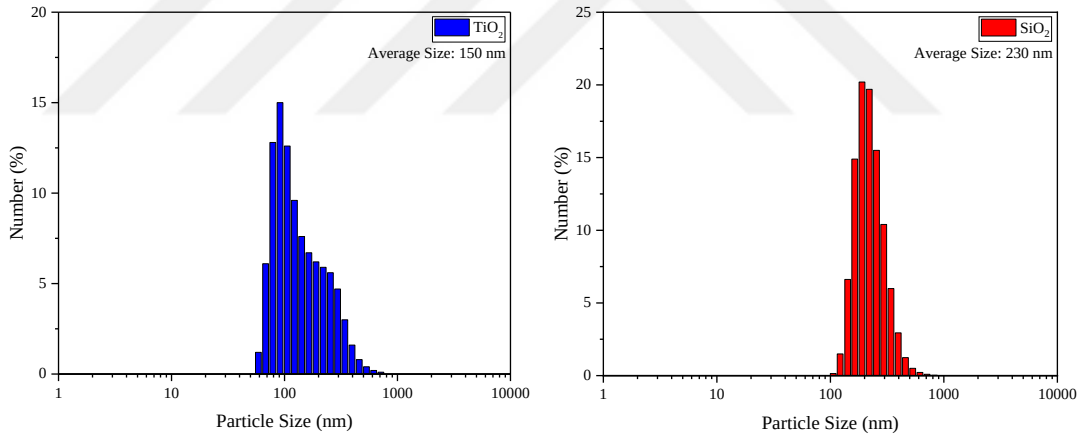


Figure 5.8 Particle size distribution of TiO_2 and SiO_2 nanoparticles

5.2 Characterization of Commercial Resin (AC) and AC-based Composites

5.2.1 Viscosity Properties

The viscosity properties of the commercial resin and composites were determined by rheometer measurement. Bao et al. (Bao et al., 2022) argued that the viscosity value is a limitation in SLA and DLP type printers and emphasized the importance of this

situation in terms of dimensional accuracy of the material. Based on this research, it was determined by the preliminary studies carried out before the thesis that the upper viscosity limit for the resins to be used successfully in our printer was 0.8 Pa.s. Resins with a viscosity higher than the specified value force the movement of the printer in the Z-axis during printing and cause errors with the pressure they create on the part. The viscosity values of the composites and commercial resin prepared considering this data are shown in Figure 5.9 and Table 5.2.

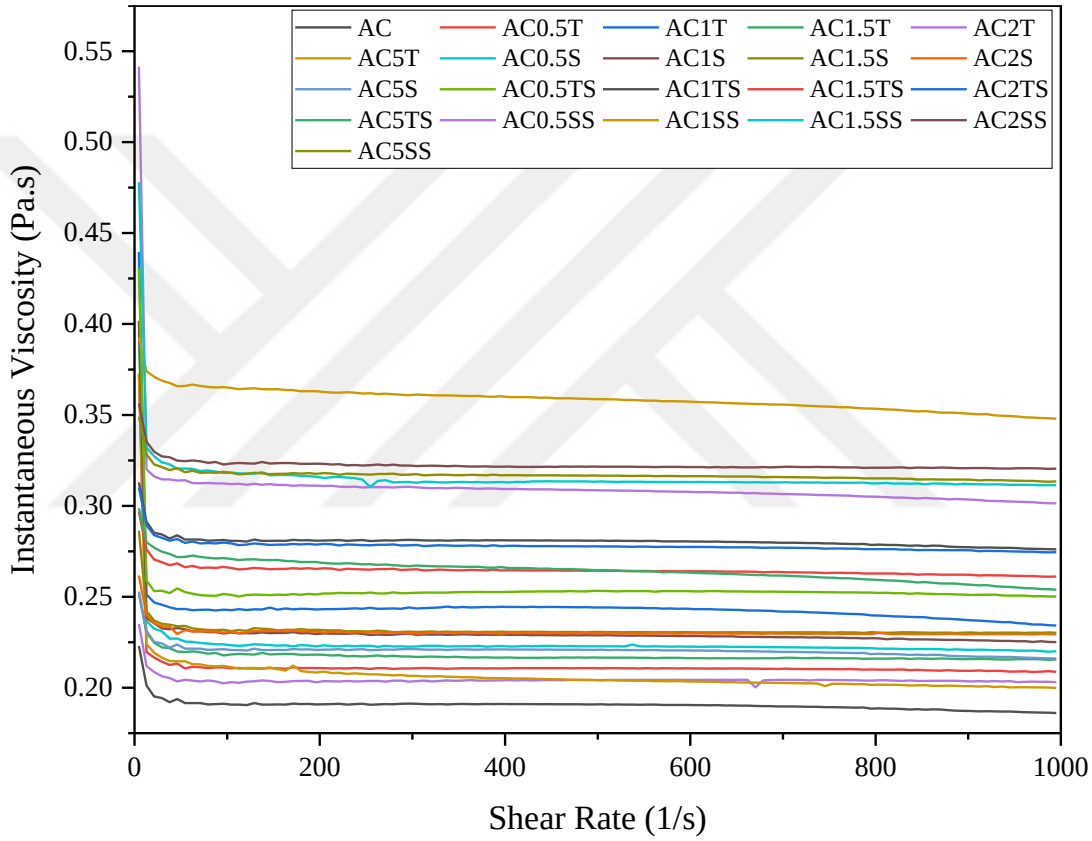


Figure 5.9 Rheometer measurement chart of commercial resin and composites

Table 5.2 Viscosity values of commercial resin and composites

Name	Viscosity (Pa.s)	Name	Viscosity (Pa.s)
AC	0.19	**AC0.5S**	0.22
AC0.5T	0.21	**AC1S**	0.23
AC1T	0.23	**AC1.5S**	0.23
AC1.5T	0.22	**AC2S**	0.23
AC2T	0.2	**AC5S**	0.22
AC5T	0.2	**AC0.5SS**	0.3
AC0.5TS	0.25	**AC1SS**	0.35
AC1TS	0.28	**AC1.5SS**	0.31
AC1.5TS	0.26	**AC2SS**	0.32
AC2TS	0.28	**AC5SS**	0.31
AC5TS	0.25		

As seen in the graph in Figure 5.9 and the data in Table 5.2, it is determined that the obtained composite resins were suitable for use in the printer. As seen in the study by Mohsen and Craig, the higher viscosity values of silane-coated samples compared to non-silane-coated samples indicate that the powders adhere better to the matrix material with the silanization effect (Mohsen & Craig, 1995). Also any thixotropic or non-Newtonian behavior is not observed according to their constant viscosity values at measured shear rate.

5.2.2 Morphological Properties

A scanning electron microscope was used in the morphological examination of commercial resin and composites, and topographic images of AC, AC1.5T, AC1.5TS, AC1S and AC1SS coded samples were examined in back-scattered electron mode. As a result of the analysis, the distribution of the powders in the structure, the agglomerations that occurred and the effect of silanization were examined. The resulting images are shown in Figure 5.10.

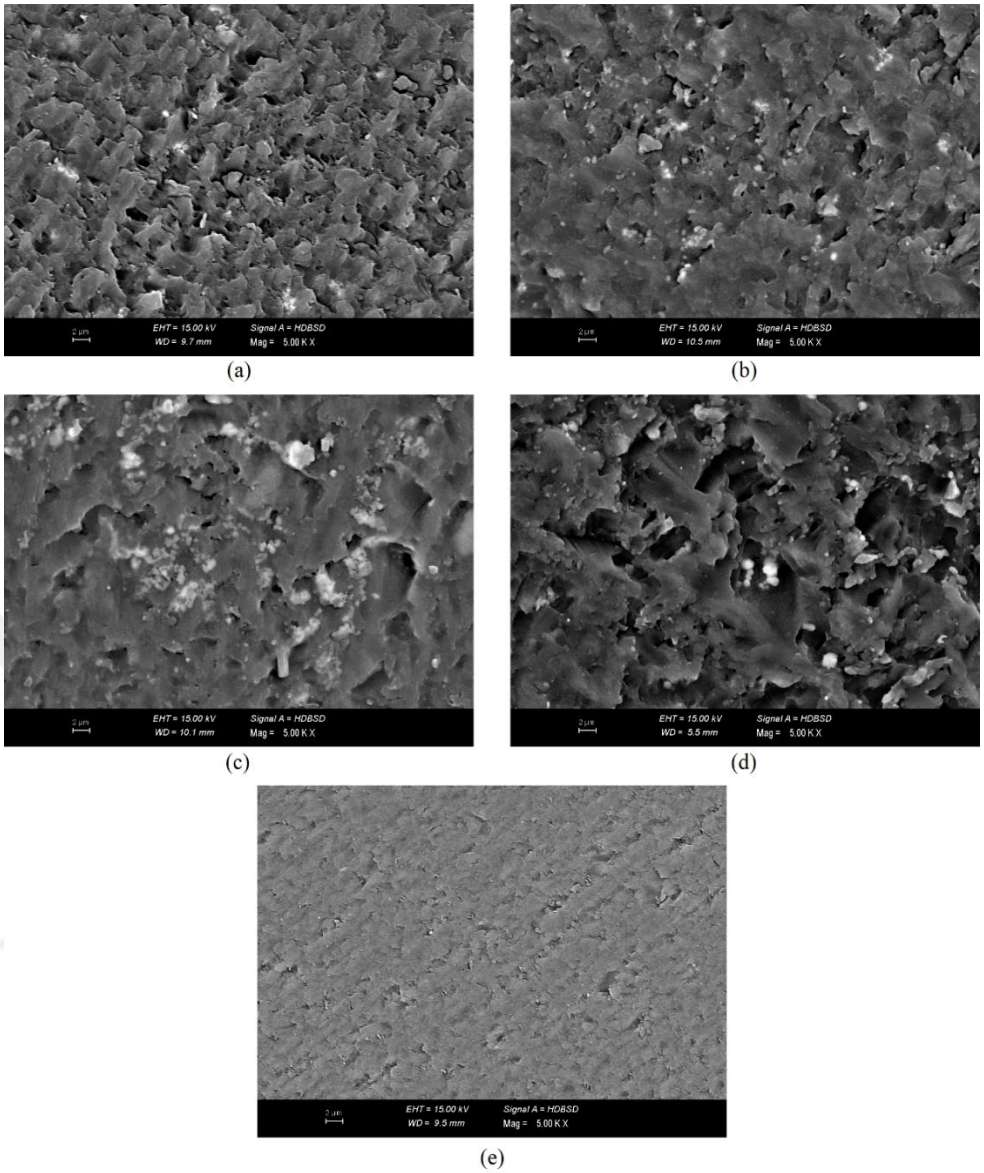


Figure 5.10 SEM images of (a) AC1.5T, (b) AC1.5TS, (c) AC1S, (d) AC1SS and (e) AC samples at 5K magnification

When the images are examined, agglomeration of non-silanized powders in the structure is seen (AC1.5T and AC1S samples). Since the images were taken in the back-scattered electron mode, the bright white colored dots show the filler material (TiO_2 and SiO_2) in the structure. After silanization, it is confirmed that the powders have more homogeneous distribution, as a result of comparing the obtained SEM images with similar studies in the literature (Mussatto et al., 2020; Rossi Canuto de Menezes et al., 2021).

5.2.3 Organic Bond Structures

Organic bond structures and conversion degrees of commercial resin and composites were determined by Fourier Transform InfraRed spectrum. FT-IR analysis was applied to the prepared samples before and after printing. In this way, the conversion rate of C=C bonds in the structure to C-C bonds, that is, the conversion degrees of the samples were determined. The following equation (5.2) is used to calculate the conversion degree (Barszczewska-Rybarek, 2012).

$$DC = 1 - \left(\frac{A_{C=C(t)}}{A_{C=C(0)}}\right) \tag{5.2}$$

Where $A_{C=C(t)}$ is the intensity of the peak belonging to the C=C bond at the wavenumber of 1637 cm^{-1} after polymerization; and $A_{C=C(0)}$ represents the strength of the same bond before polymerization. Figure 5.11 shows the FT-IR analysis graph of the AC sample before and after polymerization as an example. Conversion degrees of all samples are shown in Figure 5.12. All values were calculated as average of 3 measurements.

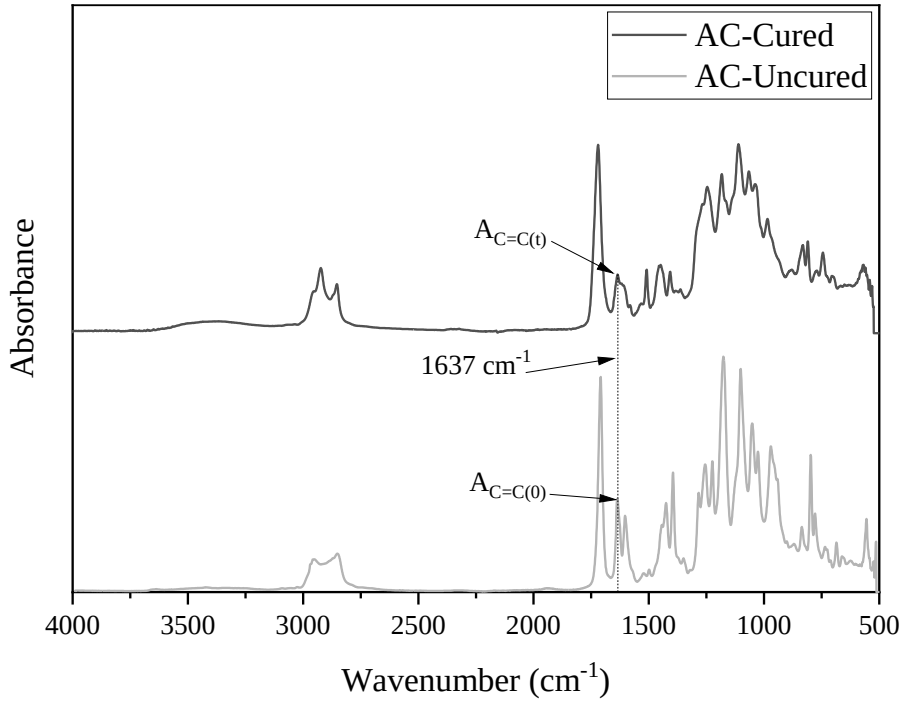


Figure 5.11 FT-IR chart of AC sample before and after curing

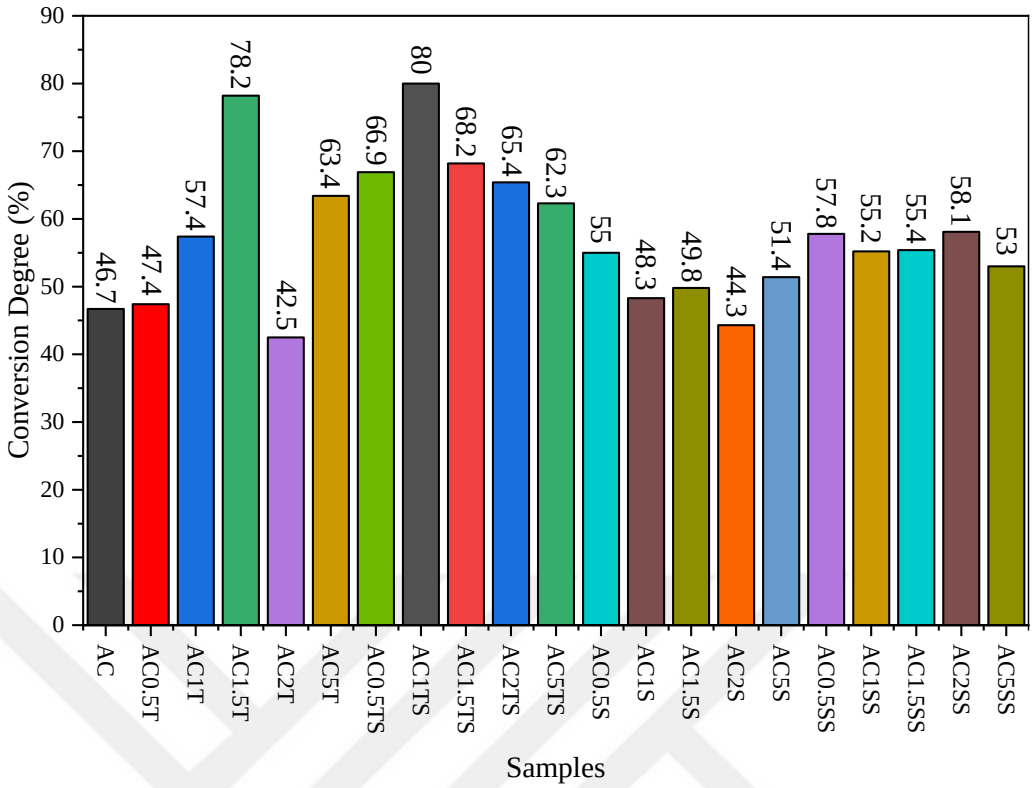


Figure 5.12 Conversion degrees of commercial resin and composites

As can be seen in Figure 5.12, TiO_2 and SiO_2 nanoparticle contribution to the structure generally increased the degree of conversion. The effect of the silanization process on the conversion degree was neither positive nor negative (Ferracane et al., 1998). AC1TS and AC2SS are showed the best conversion degree results for TiO_2 and SiO_2 reinforced materials, respectively. It is thought that the lowest conversion degree of the AC2T sample is due to the agglomeration of the powders in the structure which might be preventing polymerization (Sodagar et al., 2013).

5.2.4 Mechanical Properties

Mechanical properties of commercial resin and composite materials were determined by tensile and three-point bending tests. As a result of the tests, yield strength, flexural strength and modulus of elasticity values were determined. Mechanical test results are shown in Figure 5.13, 5.14 and 5.15.

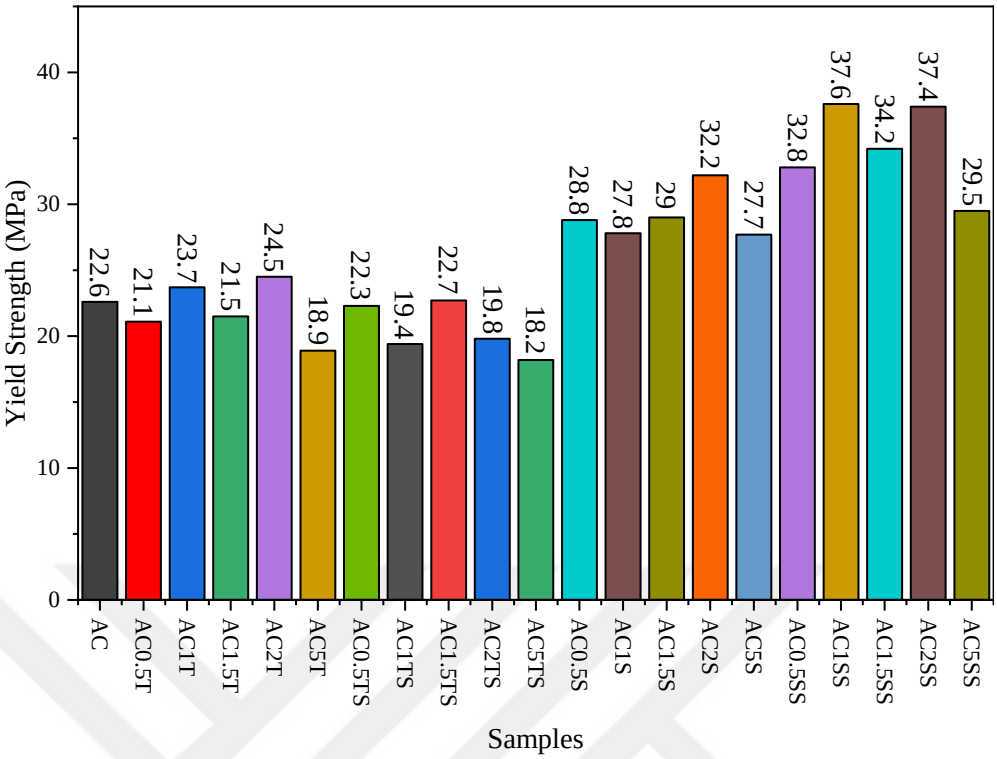


Figure 5.13 Yield strength values of commercial resin and composites

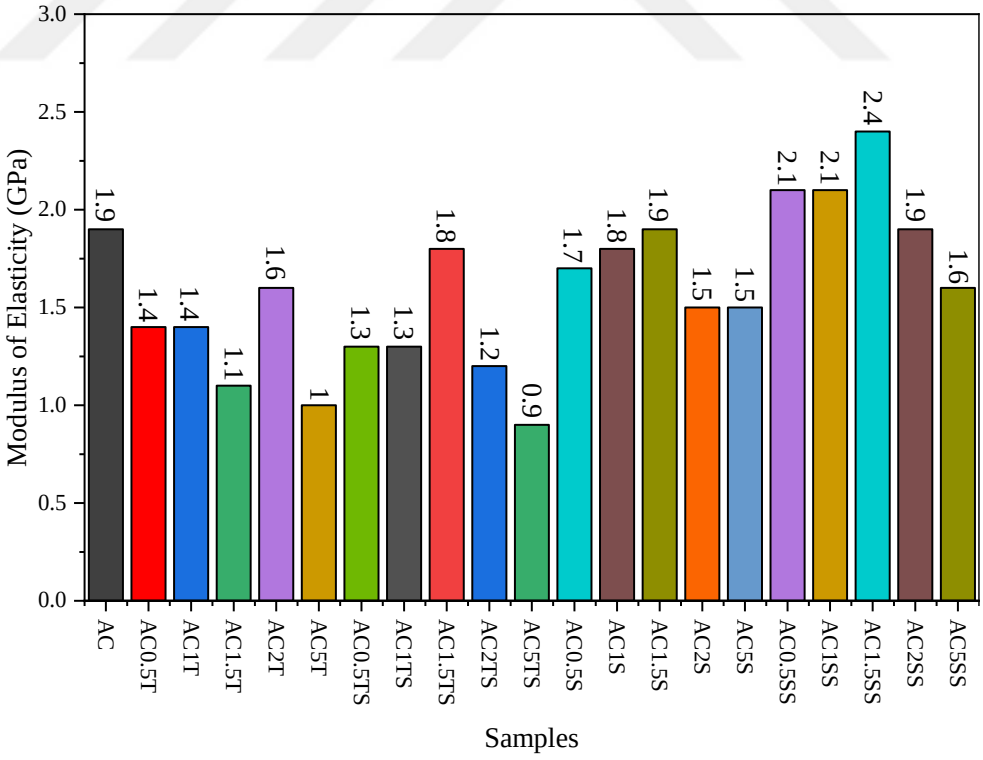


Figure 5.14 Modulus of elasticity values of commercial resin and composites

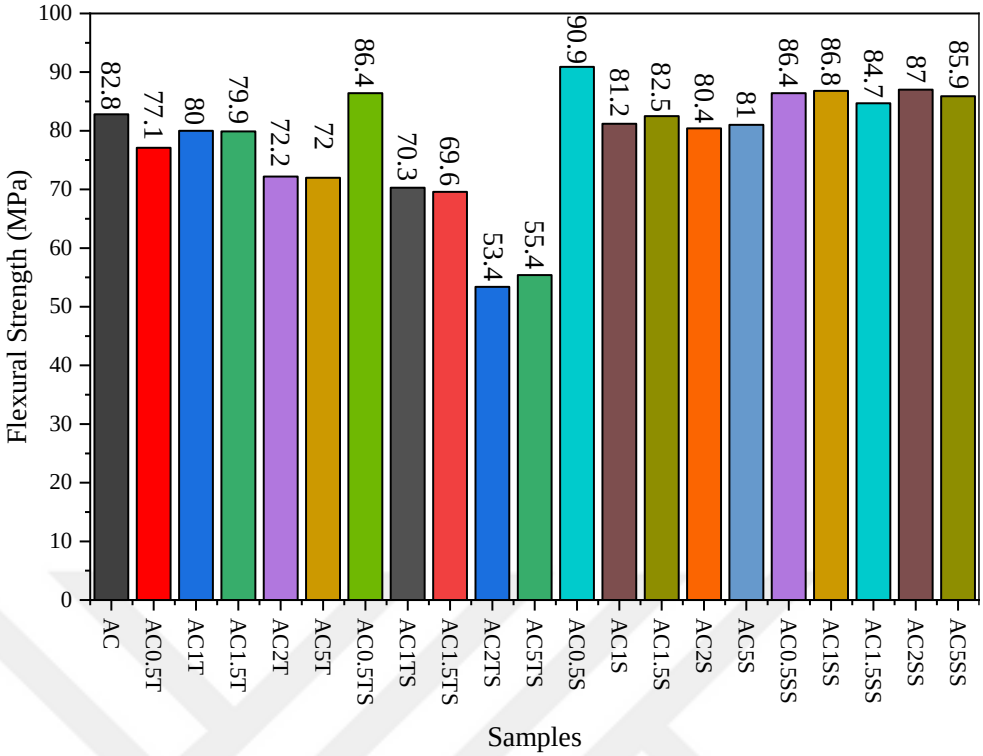


Figure 5.15 Flexural strength values of commercial resin and composites

When the elasticity modulus, yield and flexural strength values are examined, it is seen that the addition of TiO_2 has a negative effect on the mechanical properties. The reason of this situation is that TiO_2 nanoparticles added to the structure behave like impurities in the structure due to the inability to form proper bonds with the acrylate groups, thus negatively affecting the strength due to the stress concentration formed at the point where the particles are located (Merad et al., 2014; Sodagar et al., 2013). It is seen that the addition of SiO_2 contributes positively to both modulus of elasticity and yield and flexural strengths. When similar studies are examined, it is observed that the presence of SiO_2 nanoparticles in the structure has a positive effect on the mechanical properties(L. H. da Silva et al., 2012). Likewise, silane-coated SiO_2 added samples exhibit better results in mechanical tests, by reducing agglomeration by the silanization process of SiO_2 nanoparticles and preventing stress concentration which occurs in TiO_2 addition (M. M. A. Gad et al., 2020).

As conversion degree, modulus of elasticity, yield and flexural strength is the most important mechanical properties for dental application, AC1.5TS and AC1SS are

showed the optimum results for TiO_2 and SiO_2 reinforced materials, respectively. This means that addition of 1.5% TiO_2-S and 1% SiO_2-S gave the most optimum results in acrylate-based resin. Based on this, samples reinforced with the specified amount of additives are examined in elemental, morphological and thermal properties.

5.3 Characterization of UDMA and bis-GMA Based Resins

5.3.1 Viscosity Properties

The viscosity properties of the UDMA and bis-GMA based resins were determined by rheometer measurement. The viscosity values of the resins prepared are shown in Figure 5.16 and Table 5.3.

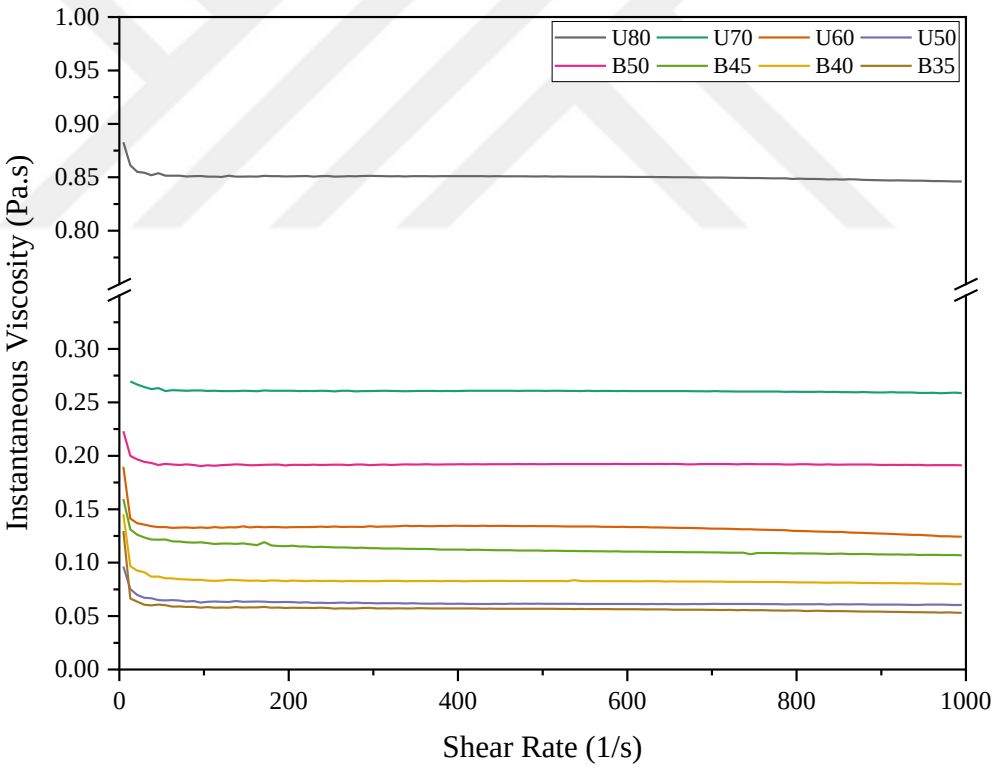


Figure 5.16 Rheometer measurement chart of UDMA and bis-GMA based resins

Table 5.3 Viscosity values of UDMA and bis-GMA based resins

Name	Viscosity (Pa.s)	Name	Viscosity (Pa.s)
U80	0.85	B50	0.19
U70	0.26	B45	0.11
U60	0.13	B40	0.08
U50	0.06	B35	0.05

When the values in Figure 5.16 and Table 5.3 are examined, it is seen that all samples are Newtonian and except for the U80 sample, at printable level. At the same time, it is seen that the viscosity value decreases as the amount of TEGDMA in the mixtures increases. Since UDMA and bis-GMA monomers have relatively high viscosity values such as 1369 and 28 Pa.s, respectively, the decrease in viscosity values when diluted with diluents with high fluidity such as TEGDMA (0.05 Pa.s) is also supported by the literature (Beun et al., 2009; Sideridou & Achilias, 2005; Tanimoto et al., 2005). According to these results, the remaining analyzes were applied to other samples except U80.

5.3.2 Organic Bond Structures

Organic bond structures and conversion degrees of UDMA and bis-GMA based resins were determined by Fourier Transform InfraRed spectrum. FT-IR analysis was applied to the prepared samples before and after printing. Conversion degrees were calculated as Equation 5.2 which mentioned in Organic Bond Structures of commercial resin. Conversion degrees of all samples are shown in Figure 5.17. All values were calculated as average of 3 measurements.

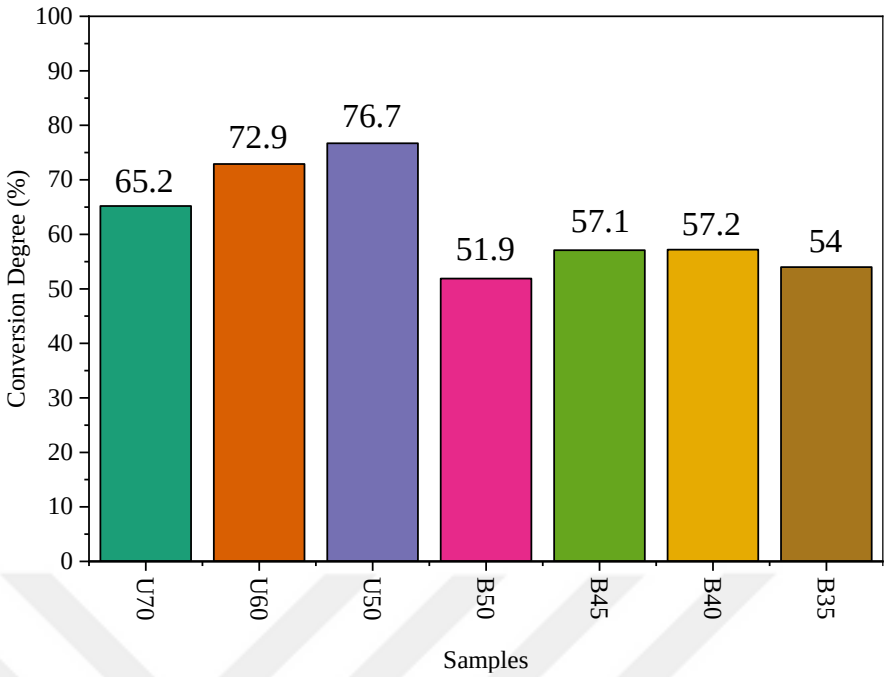


Figure 5.17 Conversion degree values of UDMA and bis-GMA based resins

When the conversion degree values are examined, it is seen that the UDMA-based samples give a higher conversion degree than the bis-GMA-based ones. It is seen that the U50 sample gives the highest result. In the graph, it is observed that the degree of transformation increases as the amount of TEGDMA in the structure increases. When the monomers are cured alone, the conversion rates are ordered from small to large as bis-GMA (21-34%), UDMA (59-72%), and TEGDMA (74-82%) (Gajewski et al., 2012). Based on these conversion degrees, it is confirmed by the literature that the conversion degree increases as the amount of TEGDMA in the bis-GMA and UDMA mixtures increases (Gonçalves et al., 2009).

5.3.3 Mechanical Properties

Mechanical properties of UDMA and bis-GMA based resins were determined by tensile and three-point bending tests. Mechanical test results are shown in Figure 5.18, 5.19 and 5.20.

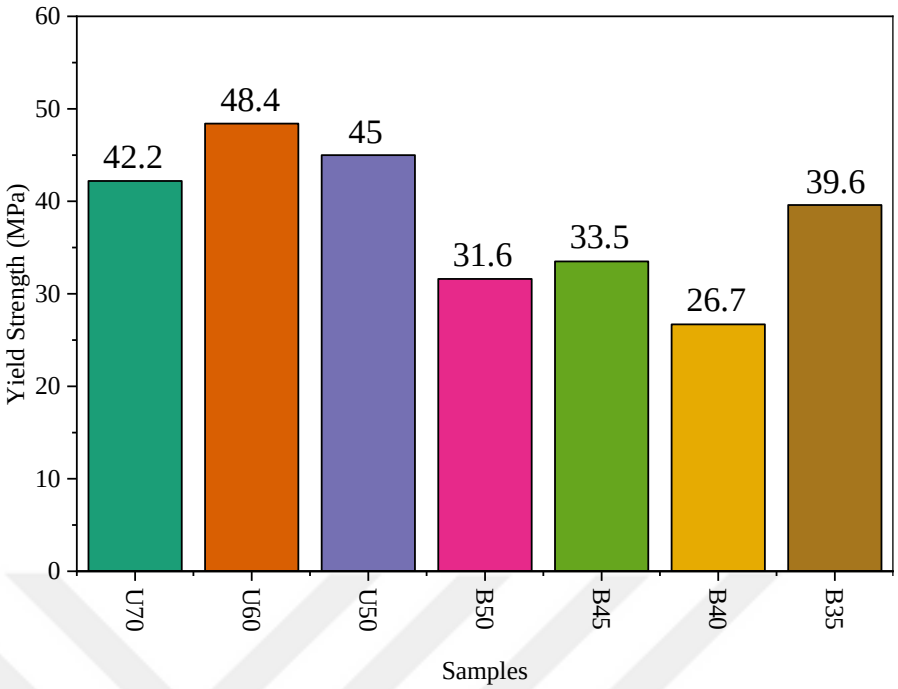


Figure 5.18 Yield strength of UDMA and bis-GMA based resins

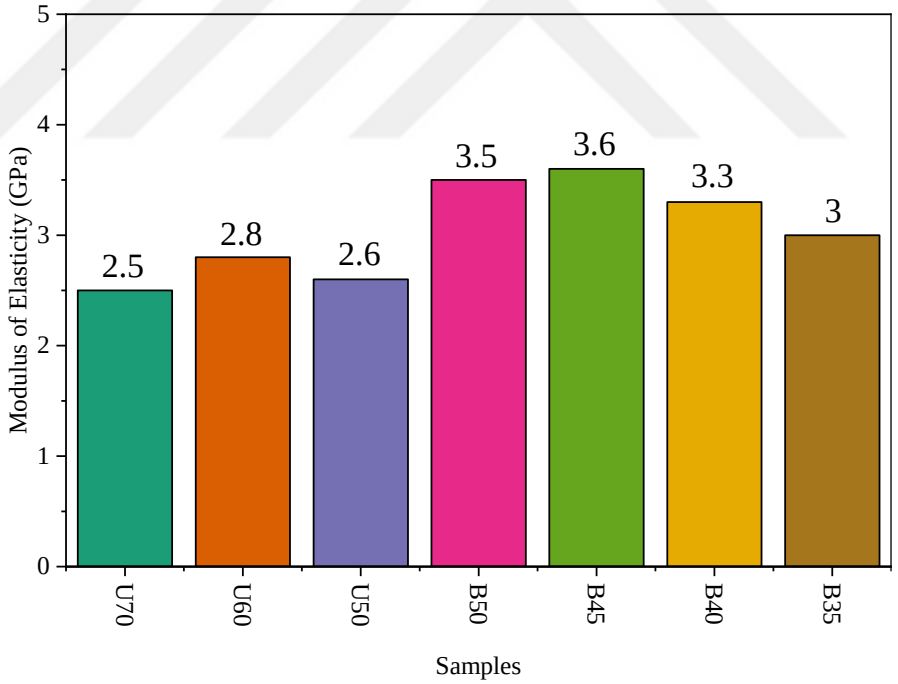


Figure 5.19 Modulus of elasticity of UDMA and bis-GMA based resins

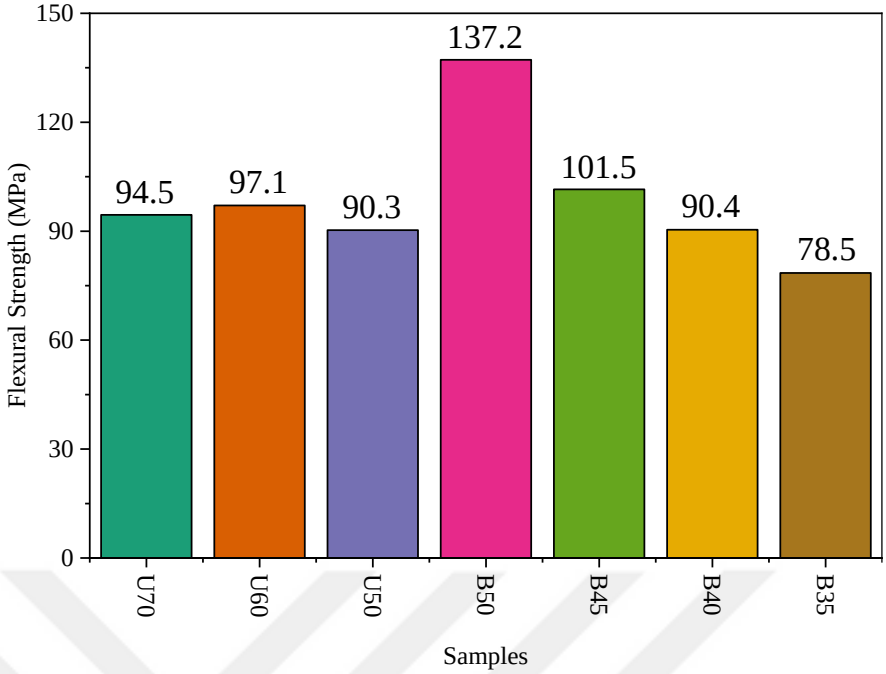


Figure 5.20 Flexural strength of UDMA and bis-GMA based resins

When the modulus of elasticity, yield and flexural strengths were examined, it was observed that UDMA based samples had better yield strength, while bis-GMA based samples had higher modulus of elasticity and flexural strength. It is estimated that UDMA has higher yield strength due to its higher toughness than bis-GMA monomer thanks to the urethane groups in it (Schwalm, 2007b). Likewise, bis-GMA, on the other hand, has a higher modulus of elasticity and bending strength thanks to the aromatic groups it contains and its ability to form hydrogen bonds with other monomers (Lemon et al., 2007).

Considering the results obtained, U60 and B45 samples showed the most optimum results in terms of conversion degree and mechanical properties. Based on these inferences, analyzes were carried out by making additions to these samples at a predetermined rate in the later parts of the thesis.

5.4 Characterization of UDMA and bis-GMA Based Composites

5.4.1 Viscosity Properties

The viscosity properties of the UDMA and bis-GMA based composites were determined by rheometer measurement. Composite resins were obtained by adding 1% SiO_2 and 1.5% TiO_2 nanoparticles by weight into resins containing UDMA and bis-GMA according to the results of AC-based composites. The viscosity values of the composite resins prepared are shown in Figure 5.21 and Table 5.4.

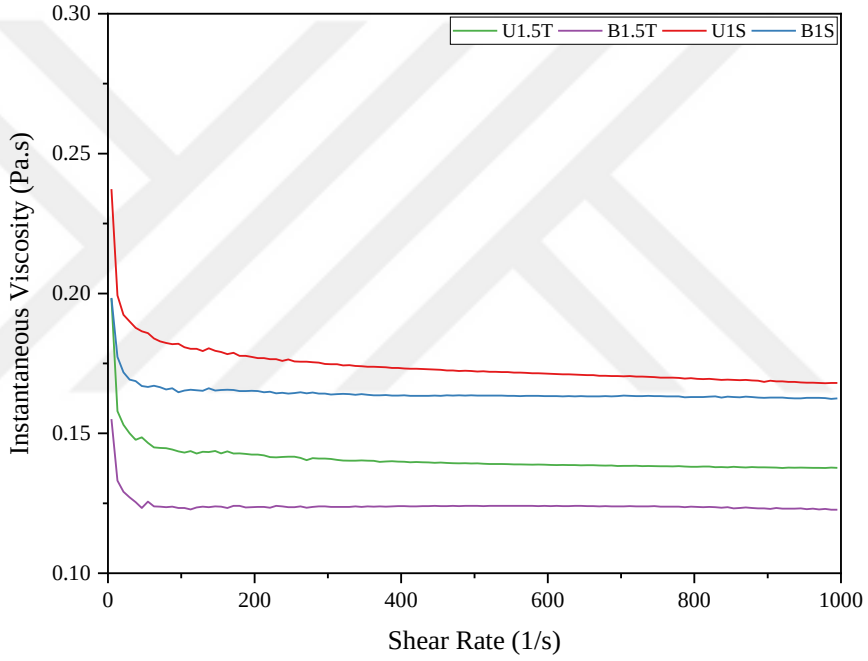


Figure 5.21 Rheometer results of UDMA and bis-GMA based composites

Table 5.4 Viscosity values of UDMA and bis-GMA based composites

Name	Viscosity (Pa.s)	Name	Viscosity (Pa.s)
U1.5T	0.14	**B1.5T**	0.12
U1S	0.17	**B1S**	0.16

As given in the graph in Figure 5.21 and the data in Table 5.4, it is seen that the viscosity values of the obtained composites are within the printable limits. As with AC-based composites and acrylate-based resins, UDMA and bis-GMA-based composites also exhibit Newtonian behavior. Similar to what is seen in AC-based

composites, SiO_2 added samples are seen to reach higher viscosity values. Based on the study done by Mohsen and Craig, it can be interpreted that this behavior increases the viscosity more due to the larger surface area in contact with the resin due to the finer grains of SiO_2 (Mohsen & Craig, 1995).

5.4.2 Morphological Properties

A scanning electron microscope was used in the morphological examination of U60, U1S, U1.5T, B45, B1S and B1.5T samples and images were obtained in back-scattered electron mode. As a result of the analysis, distribution of powders in composites were examined. The resulting images are shown in Figure 5.22.

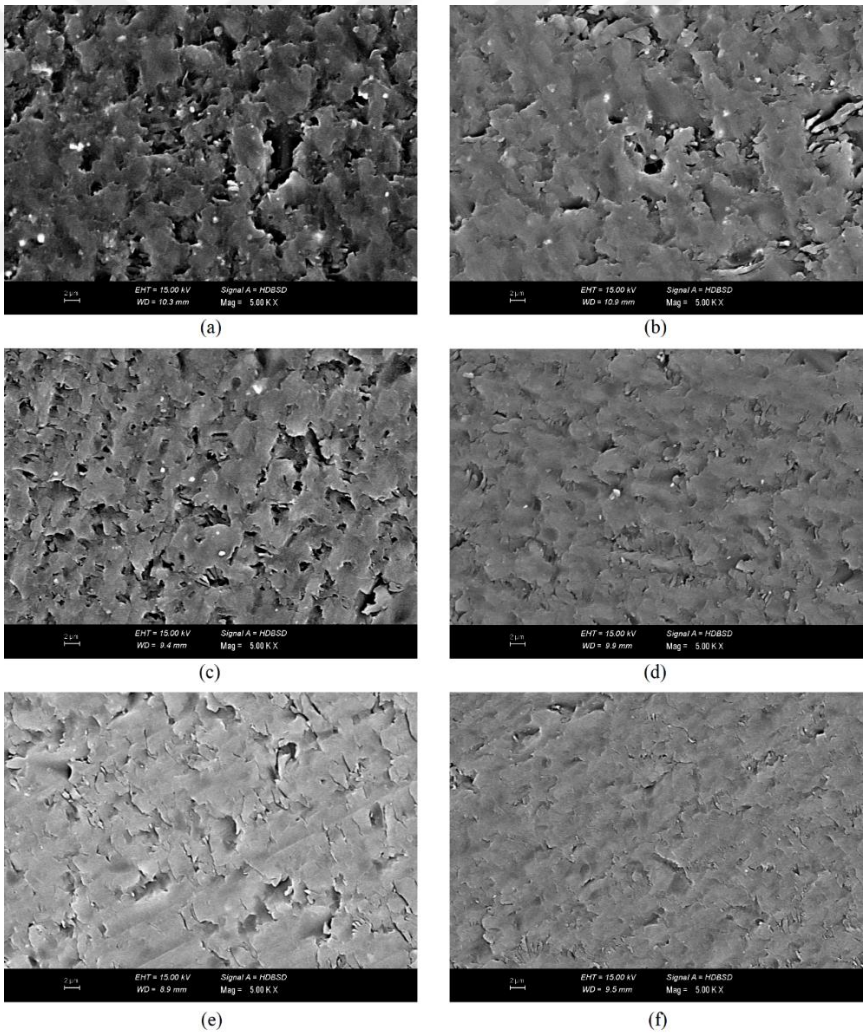


Figure 5.22 SEM images of (a) U1.5T, (b) B1.5T, (c) U1S, (d) B1S and (e) U60 and (f) B45 samples at 5K magnification

Since the images were taken in the backscattered electron mode, the bright white colored dots show the filling material in the structure. It is seen that the particles in the structure are homogeneously dispersed as in the AC-based composite samples. When the images are compared with the studies in the literature, it can be interpreted that the behavior of silane-coated powders in resins terminated with similar acrylate group is the same (Mussatto et al., 2020).

5.4.3 Organic Bond Properties

Organic bond structures and conversion degrees of UDMA and bis-GMA based composites were determined by Fourier Transform InfraRed spectrum. FT-IR analysis was applied to the prepared samples before and after printing. Conversion degrees were calculated as Equation 5.2 which mentioned in Organic Bond Structures of commercial resin. Conversion degrees of all samples are shown in Figure 5.23. All values were calculated as average of 3 measurements.

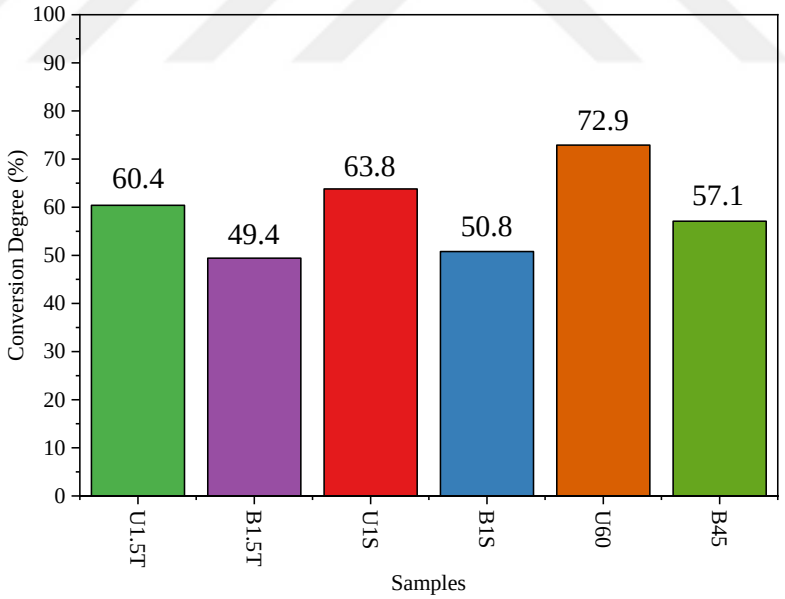


Figure 5.23 Conversion degrees of UDMA and bis-GMA based composites

When the conversion degree values are examined, it is seen that UDMA-based samples have a higher conversion degree compared to bis-GMA-based ones in composites as in pure resins. However, in general, it is seen that the nanoparticle

additive has a negative effect on the degree of conversion. When compared with each other, it is seen that SiO_2 additive provides relatively higher conversion than TiO_2 additive. In the studies conducted on AC based composites, it was concluded that both additives increased the conversion, and it was seen that the samples with TiO_2 additives showed the highest conversion degree.

It is thought that this opposite behavior in the degree of conversion occurs due to the incompatibility between the particles and the monomers in the structure. Although AC resin is a resin that terminates with an acrylate group, the types of monomers and oligomers used in it are unknown. As a result of the viscosity test, although it was observed that the particles could adhere to the resin surface, it was observed that the particles in the structure restricted chain formation during polymerization. It is estimated that the higher size of the TiO_2 particles and the lower homogeneity in the structure compared to the SiO_2 particles affect the polymerization negatively.

5.4.4 Mechanical Properties

Mechanical properties of UDMA and bis-GMA based composites were determined by tensile and three-point bending tests. Mechanical test results are shown in Figure 5.24, 5.25 and 5.26.

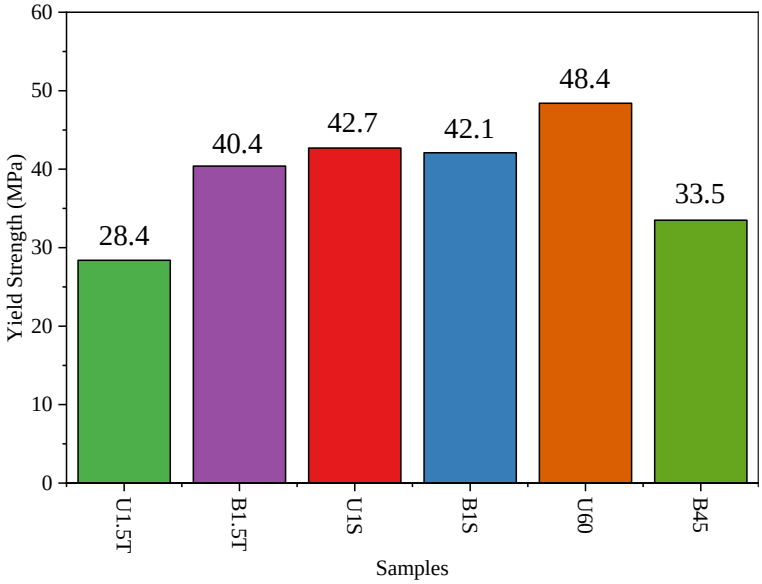


Figure 5.24 Yield strength of UDMA and bis-GMA based composites

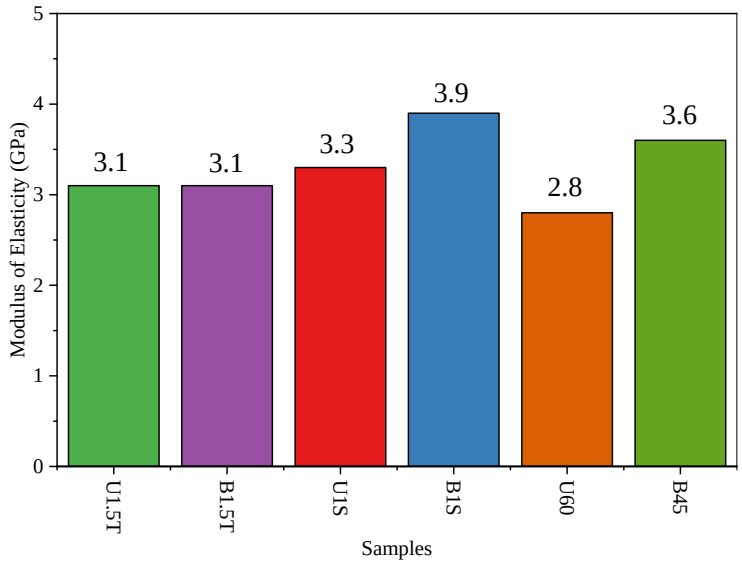


Figure 5.25 Modulus of elsticity of UDMA and bis-GMA based composites

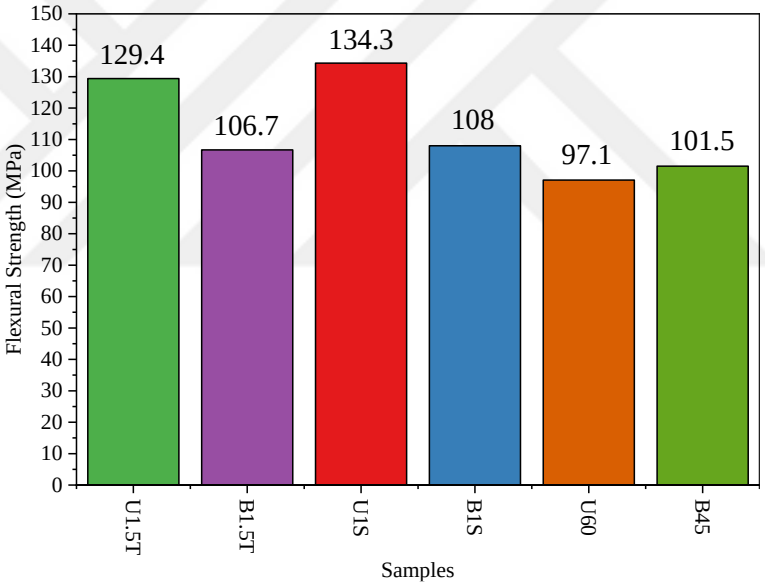


Figure 5.26 Flexural strength of UDMA and bis-GMA based composites

When the graphs are examined, it is seen that generally SiO_2 reinforced samples have higher mechanical properties compared to TiO_2 reinforced ones. Likewise, when the mechanical properties are interpreted together with the SEM images, it is seen that the SiO_2 nanoparticles are in a finer grained structure and more homogeneously dispersed compared to the TiO_2 nanoparticles. In this case, since the surface of SiO_2 nanoparticles in contact with the resin is more, it was determined that the mechanical properties increased more than TiO_2 nanoparticles. In the study of Da Silva et al., it is

seen that the addition of SiO_2 contributes positively to the mechanical properties (L. H. da Silva et al., 2012). Moreover, Gad et al. determined as a result of their study that the homogeneous distribution of the particles in the structure contributes positively to the mechanical properties by reducing the stress concentration effect (M. M. A. Gad et al., 2020).

CHAPTER 6
CONCLUSION AND FUTURE WORKS

The production and printing of TiO_2 and SiO_2 reinforced nanocomposite resins was carried out successfully. The results obtained as a result of the characterizations carried out during the production process are concluded at this chapter.

The production of nanoparticles by sol-gel method and silanization process were carried out, and the obtained TiO_2 nanoparticles had an anatase phase and an average particle size of 150 nm; It was determined that SiO_2 nanoparticles had amorphous quartz phase and an average particle size of 50 nm.

Composite samples were obtained by adding the powders obtained into the ready-made resin in certain proportions. The conversion rates and mechanical properties of the samples obtained were examined, and the particle ratios in the AC1.5TS and AC1SS samples, which gave the optimum results in these analyzes, were noted.

Samples were prepared by mixing UDMA, bis-GMA and TEGDMA monomers in various ratios, the conversion rates and mechanical properties of these samples were investigated. The proportions of U60 and B45 samples with optimum mechanical properties and degree of transformation were noted for use as matrix material.

The final nanocomposite resins were prepared by adding TiO_2 and SiO_2 powders in the determined proportions into the U60 and B45 samples, and their conversion degrees and mechanical properties were examined. The products targeted for use in dental areas are expected to have high flexural strengths and modulus of elasticity. As a result of the analyzes made, the usability of U1S and B1S specimens in dental fields emerged with the significant increase in flexural strength and modulus of elasticity.

Various color pigments were added to the product obtained as a result of the studies carried out within the scope of the thesis, and it was made ready to be presented to the market. As can be seen in Figures 6.1 and 6.2, it is seen that the product can

successfully create details even in finely detailed models with various dental model trials. In Figure 6.1, the state of the products immediately after printing on the printer table is seen. These products, which do not go through any post-processing, are called green products. After the products are taken from the table and cleaned of the excess called support, they are made ready for use by applying the post-curing process.



Figure 6.1 Green products made of produced resin (Personal archive, 2022)

The product that has been removed from the printer table and made ready for use is shown in Figure 6.2. After cleaning and post-curing, unwanted monomers on the structure were removed and made ready for use.



Figure 6.2 Dental model printed with produced resin (Personal archive, 2022)

In future studies on this subject, the synergistic effects of TiO_2 and SiO_2 nanoparticles can be examined together, and changes in their behavior in the structure can be observed with different silanization materials. As a different approach, optimization can be performed by changing the printing parameters without changing the materials.

REFERENCES

Aati, S., Akram, Z., Ngo, H., & Fawzy, A. S. (2021). Development of 3D printed resin reinforced with modified ZrO2 nanoparticles for long-term provisional dental restorations. *Dental Materials*, *37*(6), e360–e374. https://doi.org/10.1016/j.dental.2021.02.010

Al-Amin, M., Chandra Dey, S., Rashid, T. U., Ashaduzzaman, M., & Shamsuddin, S. M. (2016). Solar Assisted Photocatalytic Degradation of Reactive Azo Dyes in Presence of Anatase Titanium Dioxide. *International Journal of Latest Research in Engineering and Technology (IJLRET*, *2*(March), 14–21. www.ijlret.com‖www.ijlret.com

Alexandre, M., & Dubois, P. (2000). Polymer-layered silicate nanocomposites: preparation, properties and uses of a new class of materials. *Materials Science and Engineering: R: Reports*, *28*(1), 1–63. https://doi.org/https://doi.org/10.1016/S0927-796X(00)00012-7

Al-Odayni, A.-B., Alfotawi, R., Khan, R., Sharaf Saeed, W., Al-Kahtani, A., Aouak, T., & Alrahlah, A. (2019). Synthesis of chemically modified BisGMA analog with low viscosity and potential physical and biological properties for dental resin composite. *Dental Materials*, *35*(11), 1532–1544. https://doi.org/https://doi.org/10.1016/j.dental.2019.07.013

Alsandi, Q., Ikeda, M., Arisaka, Y., Nikaido, T., Tsuchida, Y., Sadr, A., Yui, N., & Tagami, J. (2021). Evaluation of mechanical and physical properties of light and heat polymerized udma for dlp 3d printer. *Sensors*, *21*(10). https://doi.org/10.3390/s21103331

Al-Turaif, H. A. (2010). Effect of nano TiO2 particle size on mechanical properties of cured epoxy resin. *Progress in Organic Coatings*, *69*(3), 241–246. https://doi.org/https://doi.org/10.1016/j.porgcoat.2010.05.011

Asmussen, E., & Peutzfeldt, A. (1998). Influence of UEDMA, BisGMA and TEGDMA on selected mechanical properties of experimental resin composites. In *Dent Mater* (Vol. 14).

Azarniya, A., Colera, X. G., Mirzaali, M. J., Sovizi, S., Bartolomeu, F., St Weglowski, M. k., Wits, W. W., Yap, C. Y., Ahn, J., Miranda, G., Silva, F. S., Madaah Hosseini, H. R., Ramakrishna, S., & Zadpoor, A. A. (2019). Additive manufacturing of Ti–6Al–4V parts through laser metal deposition (LMD): Process, microstructure, and mechanical properties. In *Journal of Alloys and Compounds* (Vol. 804, pp. 163–191). Elsevier Ltd. https://doi.org/10.1016/j.jallcom.2019.04.255

Bao, Y., Paunović, N., & Leroux, J.-C. (2022). Challenges and Opportunities in 3D Printing of Biodegradable Medical Devices by Emerging Photopolymerization Techniques. *Advanced Functional Materials*, *32*(15), 2109864. https://doi.org/https://doi.org/10.1002/adfm.202109864

Barszczewska-Rybarek, I. M. (2012). Quantitative determination of degree of conversion in photocured poly(urethane-dimethacrylate)s by Fourier transform infrared spectroscopy. *Journal of Applied Polymer Science*, *123*(3), 1604–1611. https://doi.org/https://doi.org/10.1002/app.34553

Beun, S., Bailly, C., Dabin, A., Vreven, J., Devaux, J., & Leloup, G. (2009). Rheological properties of experimental Bis-GMA/TEGDMA flowable resin composites with various macrofiller/microfiller ratio. *Dental Materials*, *25*(2), 198–205. https://doi.org/10.1016/j.dental.2008.06.001

Boccafoschi, F., Fusaro, L., & Cannas, M. (2018). 15 - Immobilization of peptides on cardiovascular stent. In J. G. Wall, H. Podbielska, & M. Wawrzyńska (Eds.), *Functionalised Cardiovascular Stents* (pp. 305–318). Woodhead Publishing. https://doi.org/https://doi.org/10.1016/B978-0-08-100496-8.00016-0

Brezinová, J., Hudák, R., Guzanová, A., Draganovská, D., Ižaríková, G., & Koncz, J. (2016). Direct metal laser sintering of Ti6Al4V for biomedical applications: Microstructure, corrosion properties, and mechanical treatment of implants. *Metals*, *6*(7). https://doi.org/10.3390/met6070171

Burunkova, J., Denisiuk, I., Vorzobova, N., Daroczi, L., Hegedus, Cs., Charnovych, S., & Kokenyesi, S. (2013). Fabrication and characterization of gold/acrylic polymer nanocomposites. *European Polymer Journal*, *49*(10), 3072–3077. https://doi.org/https://doi.org/10.1016/j.eurpolymj.2013.05.024

Callister, W. D., & Rethwisch, D. G. (2018). *Materials science and engineering: an introduction* (10th edition.). John Wiley & Sons, Inc.

Chang, Y., Wu, C., Wang, H., Xiong, Y., Chen, Y., Ke, K., He, Y., & 董仕节 S. (2017). Effect of post-heat treatment on the photocatalytic activity of titanium dioxide nanowire membranes deposited on a Ti substrate. *RSC Adv.*, *7*, 21422–21429. https://doi.org/10.1039/C7RA02092A

Charoo, N. A., Barakh Ali, S. F., Mohamed, E. M., Kuttolamadom, M. A., Ozkan, T., Khan, M. A., & Rahman, Z. (2020). Selective laser sintering 3D printing–an overview of the technology and pharmaceutical applications. In *Drug Development and Industrial Pharmacy* (Vol. 46, Issue 6, pp. 869–877). Taylor and Francis Ltd. https://doi.org/10.1080/03639045.2020.1764027

Chen, Z., Li, Z., Li, J., Liu, C., Lao, C., Fu, Y., Liu, C., Li, Y., Wang, P., & He, Y. (2019). 3D printing of ceramics: A review. In *Journal of the European Ceramic Society* (Vol. 39, Issue 4, pp. 661–687). Elsevier Ltd. https://doi.org/10.1016/j.jeurceramsoc.2018.11.013

Cheng, Q., Zheng, Y., Wang, T., Sun, D., & Lin, R. (2020). Yellow resistant photosensitive resin for digital light processing 3D printing. *Journal of Applied*

Polymer Science, *137*(7), 48369. https://doi.org/https://doi.org/10.1002/app.48369

Chung, C.-M., Kim, J.-G., Kim, M.-S., Kim, K.-M., & Kim, K.-N. (2002). Development of a new photocurable composite resin with reduced curing shrinkage. *Dental Materials*, *18*(2), 174–178. https://doi.org/https://doi.org/10.1016/S0109-5641(01)00039-2

Crist, V. B. (2011, November 7). *X-ray Photoelectron Spectroscopy*. Wikipedia. https://en.wikipedia.org/wiki/X-ray_photoelectron_spectroscopy

da Silva, L. H., Feitosa, S. A., Valera, M. C., de Araujo, M. A. M., & Tango, R. N. (2012). Effect of the addition of silanated silica on the mechanical properties of microwave heat-cured acrylic resin. *Gerodontology*, *29*(2), e1019–e1023. https://doi.org/https://doi.org/10.1111/j.1741-2358.2011.00604.x

Danforth, S. C., & Safari, A. (1996). Solid freeform fabrication: novel manufacturing opportunities for electronic ceramics. *ISAF '96. Proceedings of the Tenth IEEE International Symposium on Applications of Ferroelectrics*, *1*, 183–188 vol.1. https://doi.org/10.1109/ISAF.1996.602732

Dilag, J., Chen, T., Li, S., & Bateman, S. A. (2019). Design and direct additive manufacturing of three-dimensional surface micro-structures using material jetting technologies. *Additive Manufacturing*, *27*, 167–174. https://doi.org/10.1016/j.addma.2019.01.009

Dilberoglu, U. M., Gharehpapagh, B., Yaman, U., & Dolen, M. (2017). The Role of Additive Manufacturing in the Era of Industry 4.0. *Procedia Manufacturing*, *11*, 545–554. https://doi.org/10.1016/j.promfg.2017.07.148

Ding, Y., Li, B., Wang, M., Liu, F., & He, J. (2016). Bis-GMA Free Dental Materials Based on UDMA/SR833s Dental Resin System. *Advances in Polymer Technology*, *35*(4), 396–401. https://doi.org/https://doi.org/10.1002/adv.21564

Du, M., & Zheng, Y. (2007). Modification of silica nanoparticles and their application in UDMA dental polymeric composites. *Polymer Composites*, *28*(2), 198–207. https://doi.org/https://doi.org/10.1002/pc.20377

Dubey, R. S., Rajesh, Y. B. R. D., & More, M. A. (2015). Synthesis and Characterization of SiO2 Nanoparticles via Sol-gel Method for Industrial Applications. *Materials Today: Proceedings*, *2*(4), 3575–3579. https://doi.org/https://doi.org/10.1016/j.matpr.2015.07.098

Ferracane, J. L., Berge, H. X., & Condon, J. R. (1998). In vitro aging of dental composites in water—Effect of degree of conversion, filler volume, and filler/matrix coupling. *Journal of Biomedical Materials Research*, *42*(3), 465–472. https://doi.org/https://doi.org/10.1002/(SICI)1097-4636(19981205)42:3<465::AID-JBM17>3.0.CO;2-F

Fina, F., Goyanes, A., Gaisford, S., & Basit, A. W. (2017). Selective laser sintering (SLS) 3D printing of medicines. *International Journal of Pharmaceutics*, *529*(1–2), 285–293. https://doi.org/10.1016/j.ijpharm.2017.06.082

Floyd, C. J. E., & Dickens, S. H. (2006). Network structure of Bis-GMA- and UDMA-based resin systems. *Dental Materials*, *22*(12), 1143–1149. https://doi.org/https://doi.org/10.1016/j.dental.2005.10.009

Gad, M. M. A., Abualsaud, R., Al-Thobity, A. M., Almaskin, D. F., Alzaher, Z. A., Abushowmi, T. H., Qaw, M. S., Akhtar, S., & Al-Harbi, F. A. (2020). Effect of SiO 2 Nanoparticles Addition on the Flexural Strength of Repaired Acrylic Denture Base. *European Journal of Dentistry*, *14*(1), 19–23. https://doi.org/10.1055/s-0039-1701076

Gad, M. M., Al-Thobity, A. M., Rahoma, A., Abualsaud, R., Al-Harbi, F. A., & Akhtar, S. (2019). Reinforcement of PMMA Denture Base Material with a Mixture of ZrO_2 Nanoparticles and Glass Fibers. *International Journal of Dentistry*, *2019*, 2489393. https://doi.org/10.1155/2019/2489393

Gajapriya, M., Somasundaram, J., & Geetha, R. v. (2020). Fillers in Composite Resins - Recent Advances. *European Journal of Molecular & Clinical Medicine*, *7*(1), 971–977. https://ejmcm.com/article_2263.html

Gajewski, V., Pfeifer, C., Fróes-Salgado, N., Boaro, L., & Braga, R. (2012). Monomers used in resin composites: Degree of conversion, mechanical properties and water sorption/solubility. *Brazilian Dental Journal*, *23*, 508–514. https://doi.org/10.1590/S0103-64402012000500007

Geng, L. C., Ruan, X. L., Wu, W. W., Xia, R., & Fang, D. N. (2019). Mechanical Properties of Selective Laser Sintering (SLS) Additive Manufactured Chiral Auxetic Cylindrical Stent. *Experimental Mechanics*, *59*(6), 913–925. https://doi.org/10.1007/s11340-019-00489-0

Gonçalves, F., Kawano, Y., Pfeifer, C., Stansbury, J. W., & Braga, R. R. (2009). Influence of BisGMA, TEGDMA, and BisEMA contents on viscosity, conversion, and flexural strength of experimental resins and composites. *European Journal of Oral Sciences*, *117*(4), 442–446. https://doi.org/https://doi.org/10.1111/j.1600-0722.2009.00636.x

Hari Sankar, P., Mohana Reddy, Y. V., & Hemachandra Reddy, K. (2015). Polyester/vinylester polymer hybrid blended nanocomposites: Effect of nano on mechanical and thermal properties. *Fibers and Polymers*, *16*(2), 443–448. https://doi.org/10.1007/s12221-015-0443-9

Horvath, J. (2014). A Brief History of 3D Printing. In *Mastering 3D Printing* (pp. 3–10). Apress. https://doi.org/10.1007/978-1-4842-0025-4_1

Işıtan, A. (2018). Makro, Mikro, Nano. In M. Ersöz, A. Işıtan, & M. Balaban (Eds.), *Nanoteknoloji 1: Nanoteknolojinin Temelleri* (1st ed., pp. 11–18).

Joseph, B., Sam, R. M., Tharayil, A., Sagarika, V. K., Kalarikkal, N., & Thomas, S. (2022). Chapter 13 - Photopolymers for 3D printing. In J. Izdebska-Podsiadły (Ed.), *Polymers for 3D Printing* (pp. 145–154). William Andrew Publishing. https://doi.org/https://doi.org/10.1016/B978-0-12-818311-3.00011-2

Kasapoğlu, N., Baykal, A., Toprak, M. S., Köseoğlu, Y., & Bayrakdar, H. (2007). Synthesis and characterization of NiFe2O4 nano-octahedrons by EDTA-assisted hydrothermal method. *Turkish Journal of Chemistry*, *31*(6), 659–666.

Kim, S., Seong, H., Her, Y., & Chun, J. (2019). A study of the development and improvement of fashion products using a FDM type 3D printer. *Fashion and Textiles*, *6*(1). https://doi.org/10.1186/s40691-018-0162-0

Lei, Z., Bi, J., Chen, Y., Chen, X., Tian, Z., & Qin, X. (2020). Effect of TiB2 content on microstructural features and hardness of TiB2/AA7075 composites manufactured by LMD. *Journal of Manufacturing Processes*, *53*, 283–292. https://doi.org/10.1016/j.jmapro.2020.02.036

Leitune, V. C. B., Collares, F. M., Takimi, A., Lima, G. B. de, Petzhold, C. L., Bergmann, C. P., & Samuel, S. M. W. (2013). Niobium pentoxide as a novel filler for dental adhesive resin. *Journal of Dentistry*, *41*(2), 106–113. https://doi.org/https://doi.org/10.1016/j.jdent.2012.04.022

Lemon, M. T., Jones, M. S., & Stansbury, J. W. (2007). Hydrogen bonding interactions in methacrylate monomers and polymers. *Journal of Biomedical Materials Research Part A*, *83A*(3), 734–746. https://doi.org/https://doi.org/10.1002/jbm.a.31448

Lin, C.-H., Lin, Y.-M., Lai, Y.-L., & Lee, S.-Y. (2020). Mechanical properties, accuracy, and cytotoxicity of UV-polymerized 3D printing resins composed of Bis-EMA, UDMA, and TEGDMA. *The Journal of Prosthetic Dentistry*, *123*(2), 349–354. https://doi.org/https://doi.org/10.1016/j.prosdent.2019.05.002

Liu, Y., Li, Y., Li, X.-M., & He, T. (2013). Kinetics of (3-Aminopropyl)triethoxylsilane (APTES) Silanization of Superparamagnetic Iron Oxide Nanoparticles. *Langmuir*, *29*(49), 15275–15282. https://doi.org/10.1021/la403269u

Lu, H., Stansbury, J. W., Nie, J., Berchtold, K. A., & Bowman, C. N. (2005). Development of highly reactive mono-(meth)acrylates as reactive diluents for dimethacrylate-based dental resin systems. *Biomaterials*, *26*(12), 1329–1336. https://doi.org/10.1016/j.biomaterials.2004.04.041

Lv, X., Ye, F., Cheng, L., Fan, S., & Liu, Y. (2019). Binder jetting of ceramics: Powders, binders, printing parameters, equipment, and post-treatment. In *Ceramics International* (Vol. 45, Issue 10, pp. 12609–12624). Elsevier Ltd. https://doi.org/10.1016/j.ceramint.2019.04.012

Manapat, J. Z., Chen, Q., Ye, P., & Advincula, R. C. (2017). 3D Printing of Polymer Nanocomposites via Stereolithography. *Macromolecular Materials and Engineering*, *302*(9), 1600553. https://doi.org/https://doi.org/10.1002/mame.201600553

Merad, L., Benyoucef, B., Abadie, M. J. M., & Charles, J. P. (2014). Characterization and mechanical properties of epoxy resin reinforced with TiO2 nanoparticles. *Experimental Techniques*, *38*(1), 59–66. https://doi.org/10.1111/j.1747-1567.2011.00797.x

Mohamed, O. A., Masood, S. H., & Bhowmik, J. L. (2015). Optimization of fused deposition modeling process parameters: a review of current research and future

prospects. *Advances in Manufacturing*, *3*(1), 42–53. https://doi.org/10.1007/s40436-014-0097-7

Mohsen, N. M., & Craig, R. G. (1995). Effect of silanation of fillers on their dispersability by monomer systems. *Journal of Oral Rehabilitation*, *22*(3), 183–189.

Moncada, E., Quijada, R., & Retuert, J. (2007). Nanoparticles prepared by the sol–gel method and their use in the formation of nanocomposites with polypropylene. *Nanotechnology*, *18*(33), 335606. https://doi.org/10.1088/0957-4484/18/33/335606

Moulder, J. F., Stickle, W. F., Sobol, W. M., & Bomben, K. D. (1992). *Handbook of X-Ray Photoelectron Spectroscopy*.

Mussatto, C. M. B., Oliveira, E. M. N., Subramani, K., Papaléo, R. M., & Mota, E. G. (2020). Effect of silica nanoparticles on mechanical properties of self-cured acrylic resin. *Journal of Nanoparticle Research*, *22*(11). https://doi.org/10.1007/s11051-020-05050-y

N. Bahremandi Tolou, M. H. Fathi, A. Monshi, v. S. Mortazavi, F. S., & M. Mohammadi. (2013). THE EFFECT OF ADDING TiO2 NANOPARTICLES ON DENTAL AMALGAM PROPERTIES. *IUST*, *10*(2), 46–56. http://ijmse.iust.ac.ir/article-1-565-en.html

Neibloom, D., Bevan, M. A., & Frechette, J. (2020). Surfactant-Stabilized Spontaneous 3-(Trimethoxysilyl) Propyl Methacrylate Nanoemulsions. *Langmuir*, *36*(1), 284–292. https://doi.org/10.1021/acs.langmuir.9b03412

Nguyen, T. C., Nguyen, T. D., Vu, D. T., Dinh, D. P., Nguyen, A. H., Ly, T. N. L., Dao, P. H., Nguyen, T. L., Bach, L. G., & Thai, H. (2020). Modification of Titanium Dioxide Nanoparticles with 3-(Trimethoxysilyl)propyl Methacrylate

Silane Coupling Agent. *Journal of Chemistry, 2020*. https://doi.org/10.1155/2020/1381407

Nyamukamba, P., Okoh, O., Heroe, H., Taziwa, R., & Zinya, S. (2018). *Synthetic Methods for Titanium Dioxide Nanoparticles: A Review*. https://doi.org/10.5772/intechopen.75425

Onar, V. (2018). Sol - Jel Üretimi. In M. Ersöz, A. Işıtan, & M. Balaban (Eds.), *Nanoteknoloji 1: Nanoteknolojinin Temelleri* (1st ed., pp. 102–110).

Pal, G., Rai, P., & Pandey, A. (2019). Chapter 1 - Green synthesis of nanoparticles: A greener approach for a cleaner future. In A. K. Shukla & S. Iravani (Eds.), *Green Synthesis, Characterization and Applications of Nanoparticles* (pp. 1–26). Elsevier. https://doi.org/https://doi.org/10.1016/B978-0-08-102579-6.00001-0

Partee, B., Hollister, S. J., & Das, S. (2006). Selective laser sintering process optimization for layered manufacturing of CAPA® 6501 polycaprolactone bone tissue engineering scaffolds. *Journal of Manufacturing Science and Engineering, 128*(2), 531–540. https://doi.org/10.1115/1.2162589

Pathak, G., Pandey, S., Katiyar, R., Srivastava, A., Dabrowski, R., Garbat, K., & Manohar, R. (2017). Analysis of photoluminescence, UV absorbance, optical band gap and threshold voltage of TiO2 nanoparticles dispersed in high birefringence nematic liquid crystal towards its application in display and photovoltaic devices. *Journal of Luminescence, 192*, 33–39. https://doi.org/10.1016/j.jlumin.2017.06.021

Pehlivan, N., & Karacaer, Ö. (2014). Diş hekimliğinde kullanılan kompozit rezinlerin güçlendirilmesi. In *Acta Odontologica Turcica* (Vol. 31, pp. 160–166). Gazi Üniversitesi. https://doi.org/10.17214/aot.66166

Peters, R. J. B., van Bemmel, G., Herrera-Rivera, Z., Helsper, H. P. F. G., Marvin, H. J. P., Weigel, S., Tromp, P. C., Oomen, A. G., Rietveld, A. G., & Bouwmeester, H. (2014). Characterization of Titanium Dioxide Nanoparticles in Food Products: Analytical Methods To Define Nanoparticles. *Journal of Agricultural and Food Chemistry*, *62*(27), 6285–6293. https://doi.org/10.1021/jf5011885

Pierre, A. C. (1998). The Chemistry of Precursors Solutions. In A. C. Pierre (Ed.), *Introduction to Sol-Gel Processing* (pp. 11–89). Springer US. https://doi.org/10.1007/978-1-4615-5659-6_2

Poosti, M., Ramazanzadeh, B., Zebarjad, M., Javadzadeh, P., Naderinasab, M., & Shakeri, M. T. (2013). Shear bond strength and antibacterial effects of orthodontic composite containing TiO2 nanoparticles. *European Journal of Orthodontics*, *35*(5), 676–679. https://doi.org/10.1093/ejo/cjs073

Prasanna, N., Reddy, P., Kavitha, S., & Narayanan, L. (2007). Degree of conversion and residual stress of preheated and room-temperature composites. *Indian Journal of Dental Research : Official Publication of Indian Society for Dental Research*, *18*, 173–176. https://doi.org/10.4103/0970-9290.35827

Ramaiah, G., Ramesh, K., & Bhatia, D. (2017). Structural Analysis Of Merino Wool, Pashmina And Angora Fibers Using Analytical Instruments Like Scanning Electron Microscope And Infra-Red Spectroscopy. *International Journal of Engineering Technology Science and Research 2394-3386*, *4*, 112–125.

Raval, N., Maheshwari, R., Kalyane, D., Youngren-Ortiz, S. R., Chougule, M. B., & Tekade, R. K. (2019). Chapter 10 - Importance of Physicochemical Characterization of Nanoparticles in Pharmaceutical Product Development. In R. K. Tekade (Ed.), *Basic Fundamentals of Drug Delivery* (pp. 369–400). Academic Press. https://doi.org/https://doi.org/10.1016/B978-0-12-817909-3.00010-8

Revilla-León, M., & Özcan, M. (2019). Additive Manufacturing Technologies Used for Processing Polymers: Current Status and Potential Application in Prosthetic Dentistry. In *Journal of Prosthodontics* (Vol. 28, Issue 2, pp. 146–158). Blackwell Publishing Inc. https://doi.org/10.1111/jopr.12801

Rezvani, M. B., Atai, M., Hamze, F., & Hajrezai, R. (2016). The effect of silica nanoparticles on the mechanical properties of fiber-reinforced composite resins. *Journal of Dental Research, Dental Clinics, Dental Prospects*, *10*(2), 112–117. https://doi.org/10.15171/joddd.2016.018

Rong, Y., Chen, H. Z., Wu, G., & Wang, M. (2005). Preparation and characterization of titanium dioxide nanoparticle/ polystyrene composites via radical polymerization. *Materials Chemistry and Physics*, *91*(2–3), 370–374. https://doi.org/10.1016/j.matchemphys.2004.11.042

Rossi Canuto de Menezes, B., da Graça Sampaio, A., Morais da Silva, D., Larissa do Amaral Montanheiro, T., Yumi Koga-Ito, C., & Patrocínio Thim, G. (2021). AgVO3 nanorods silanized with γ-MPS: An alternative for effective dispersion of AgVO3 in dental acrylic resins improving the mechanical properties. *Applied Surface Science*, *543*. https://doi.org/10.1016/j.apsusc.2020.148830

Schwalm, R. (2007a). CHAPTER 2 - The UV Curing Process. In R. Schwalm (Ed.), *UV Coatings* (pp. 19–61). Elsevier. https://doi.org/https://doi.org/10.1016/B978-044452979-4/50002-0

Schwalm, R. (2007b). CHAPTER 4 - Raw Materials. In R. Schwalm (Ed.), *UV Coatings* (pp. 94–139). Elsevier. https://doi.org/https://doi.org/10.1016/B978-044452979-4/50004-4

Sedlak, J., Rican, D., Piska, M., & Rozkosny, L. (2015). Study of materials produced by powder metallurgy using classical and modern additive laser technology.

Procedia Engineering, *100*(January), 1232–1241. https://doi.org/10.1016/j.proeng.2015.01.488

Siddiquey, I. A., Ukaji, E., Furusawa, T., Sato, M., & Suzuki, N. (2007). The effects of organic surface treatment by methacryloxypropyltrimethoxysilane on the photostability of TiO2. *Materials Chemistry and Physics*, *105*(2–3), 162–168. https://doi.org/10.1016/j.matchemphys.2007.04.017

Sideridou, I. D., & Achilias, D. S. (2005). Elution study of unreacted Bis-GMA, TEGDMA, UDMA, and Bis-EMA from light-cured dental resins and resin composites using HPLC. *Journal of Biomedical Materials Research - Part B Applied Biomaterials*, *74*(1), 617–626. https://doi.org/10.1002/jbm.b.30252

Siek, M. (2015). *Electrochemical preparation of Ag- and Au-based plasmonic platforms*. https://doi.org/10.13140/RG.2.2.24644.01924

Silva, A. L., Salvador, G. M. da S., Castro, S. V. F., Carvalho, N. M. F., & Munoz, R. A. A. (2021). A 3D Printer Guide for the Development and Application of Electrochemical Cells and Devices. In *Frontiers in Chemistry* (Vol. 9). Frontiers Media S.A. https://doi.org/10.3389/fchem.2021.684256

Sodagar, A., Bahador, A., Khalil, S., Saffar Shahroudi, A., & Zaman Kassaee, M. (2013). The effect of TiO2 and SiO2 nanoparticles on flexural strength of poly (methyl methacrylate) acrylic resins. *Journal of Prosthodontic Research*, *57*(1), 15–19. https://doi.org/10.1016/j.jpor.2012.05.001

Subramani, K., Dhas, M., Jose, M., & Das, S. (2020). Thermo analytical study of phase transformation of TiO 2 nanoparticles prepared using mono and di α-hydroxy acid water-soluble precursor by hydrothermal technique. *Phase Transitions*, *93*, 1–11. https://doi.org/10.1080/01411594.2020.1770756

Sun, J., Forster, A. M., Johnson, P. M., Eidelman, N., Quinn, G., Schumacher, G., Zhang, X., & Wu, W. (2011). Improving performance of dental resins by adding titanium dioxide nanoparticles. *Dental Materials*, *27*(10), 972–982. https://doi.org/https://doi.org/10.1016/j.dental.2011.06.003

Surange, V. G., & Gharat, P. v. (2016). 3D Printing Process Using Fused Deposition Modelling (FDM). *International Research Journal of Engineering and Technology*. www.irjet.net

Sürmen, H. K. (2019). Eklemeli İmalat (3B Baskı): Teknolojiler ve Uygulamalar. *Uludağ University Journal of The Faculty of Engineering*, *24*(2), 373–392. https://doi.org/10.17482/uumfd.519147

Szaloki, M., Gall, J., Bukovinszki, K., Borbely, J., & Hegedus, C. (2013). Synthesis and characterization of cross-linked polymeric nanoparticles and their composites for reinforcement of photocurable dental resin. *Reactive and Functional Polymers*, *73*(3), 465–473. https://doi.org/https://doi.org/10.1016/j.reactfunctpolym.2012.11.013

Tanimoto, Y., Hayakawa, T., & Nemoto, K. (2005). Analysis of photopolymerization behavior of UDMA/TEGDMA resin mixture and its composite by differential scanning calorimetry. *Journal of Biomedical Materials Research - Part B Applied Biomaterials*, *72*(2), 310–315. https://doi.org/10.1002/jbm.b.30151

Tham, W. L., Chow, W. S., & Ishak, Z. A. M. (2010). The effect of 3-(trimethoxysilyl) propyl methacrylate on the mechanical, thermal, and morphological properties of poly(methyl methacrylate)/ hydroxyapatite composites. *Journal of Applied Polymer Science*, *118*(1), 218–228. https://doi.org/10.1002/app.32111

Tosi, D., Sypabekova, M., Bekmurzayeva, A., Molardi, C., & Dukenbayev, K. (2022). 10 - Fiber surface modifications for biosensing. In D. Tosi, M. Sypabekova, A. Bekmurzayeva, C. Molardi, & K. Dukenbayev (Eds.), *Optical Fiber Biosensors*

(pp. 253–282). Academic Press. https://doi.org/https://doi.org/10.1016/B978-0-12-819467-6.00010-X

Toygun, Ş., Köneçoğlu, G., & Kalpaklı, Y. (2013). GENERAL PRINCIPLES OF SOL - GEL. In *Sigma Journal of Engineering and Natural Sciences* (Vol. 31, Issue 4, pp. 456–476). Yildiz Technical University.

Ulusoy, N., & Nalçacı, A. (2004). Kompozit rezinlerdeki BisGMA+TEGDMA miktarının spektroskopik yöntem ile değerlendirilmesi. *Ankara Üniversitesi Diş Hekimliği Fakültesi Dergisi*, *31*(1). http://search/yayin/detay/44706

Varshney, S., Nigam, A., Pawar, S. J., & Mishra, N. (2022). Structural, optical, cytotoxic, and anti-microbial properties of amorphous silica nanoparticles synthesised via hybrid method for biomedical applications. *Materials Technology*, *37*(10), 1504–1515. https://doi.org/10.1080/10667857.2021.1959190

Viana, M. M., Soares, V. F., & Mohallem, N. D. S. (2010). Synthesis and characterization of TiO2 nanoparticles. *Ceramics International*, *36*(7), 2047–2053. https://doi.org/10.1016/j.ceramint.2010.04.006

Walters, N. J., Xia, W., Salih, V., Ashley, P. F., & Young, A. M. (2016). Poly(propylene glycol) and urethane dimethacrylates improve conversion of dental composites and reveal complexity of cytocompatibility testing. *Dental Materials*, *32*(2), 264–277. https://doi.org/10.1016/j.dental.2015.11.017

Weng, Z., Zhou, Y., Lin, W., Senthil, T., & Wu, L. (2016). Structure-property relationship of nano enhanced stereolithography resin for desktop SLA 3D printer. *Composites Part A: Applied Science and Manufacturing*, *88*, 234–242. https://doi.org/10.1016/j.compositesa.2016.05.035

Yan, Z., & Peng, H. (2021). FabHydro: Printing Interactive Hydraulic Devices with an Affordable SLA 3D Printer. *UIST 2021 - Proceedings of the 34th Annual ACM Symposium on User Interface Software and Technology*, 298–311. https://doi.org/10.1145/3472749.3474751

Yang, H., Lim, J. C., Liu, Y., Qi, X., Yap, Y. L., Dikshit, V., Yeong, W. Y., & Wei, J. (2017). Performance evaluation of ProJet multi-material jetting 3D printer. *Virtual and Physical Prototyping*, *12*(1), 95–103. https://doi.org/10.1080/17452759.2016.1242915

Yap, Y. L., Wang, C., Sing, S. L., Dikshit, V., Yeong, W. Y., & Wei, J. (2017). Material jetting additive manufacturing: An experimental study using designed metrological benchmarks. *Precision Engineering*, *50*, 275–285. https://doi.org/10.1016/j.precisioneng.2017.05.015

Yıldırım, S. (2017). *Production and Development of Implant Dosimeters in Radiotherapy* [Ph.D.]. Graduate School of Natural and Applied Sciences.

Yu, X., Zhang, T., & Li, Y. (2020). 3D Printing and Bioprinting Nerve Conduits for Neural Tissue Engineering. *Polymers*, *12*, 1637. https://doi.org/10.3390/polym12081637

Yuran, A. F., & Yavuz, İ. (2021). ENDÜSTRİ 4.0 VE 3 BOYUTLU YAZICILARIN KARŞILAŞTIRILMASI. *Mühendis ve Makina*. https://doi.org/10.46399/muhendismakina.910501

Yurddaşkal, M. (2017). *Fabrication, Development and Industrial Applications of Flame Retardant Polymeric Nanocomposite Materials for Battery Systems* [Ph.D. Thesis]. Graduate School of Natural and Applied Sciences.

Yurddaskal, M., Dikici, T., Yildirim, S., Yurddaskal, M., Toparli, M., & Celik, E. (2015). Fabrication and characterization of nanostructured anatase TiO2 films

prepared by electrochemical anodization and their photocatalytic properties. *Journal of Alloys and Compounds*, *651*, 59–71. https://doi.org/10.1016/j.jallcom.2015.08.064

Zhang, J., & Xiao, P. (2018). 3D printing of photopolymers. *Polym. Chem.*, *9*(13), 1530–1540. https://doi.org/10.1039/C8PY00157J

Ziaee, M., & Crane, N. B. (2019). Binder jetting: A review of process, materials, and methods. In *Additive Manufacturing* (Vol. 28, pp. 781–801). Elsevier B.V. https://doi.org/10.1016/j.addma.2019.05.031

Zornoza-Indart, A., & López-Arce, P. (2015). Silica nanoparticles (SiO2): Influence of relative humidity in stone consolidation. *Journal of Cultural Heritage*. https://doi.org/10.1016/j.culher.2015.06.002